N O T I C E

THIS DOCUMENT HAS BEEN REPRODUCED FROM
MICROFICHE. ALTHOUGH IT IS RECOGNIZED THAT
CERTAIN PORTIONS ARE ILLEGIBLE, IT IS BEING RELEASED
IN THE INTEREST OF MAKING AVAILABLE AS MUCH
INFORMATION AS POSSIBLE

ORI

NOSS/ALDCS
ANALYSIS AND SYSTEM
REQUIREMENTS DEFINITION

FINAL REPORT

FEBRUARY, 1981

ORI
Silver Spring, Maryland 20910

NOSS/ALDCS
ANALYSIS AND
SYSTEM REQUIREMENTS

FINAL REPORT

FEBRUARY, 1981

TABLE OF CONTENTS

LIST OF FIGURES

LIST OF TABLES

FOREWORD

This report contains both the results of Task I, "Analysis and System Definition," of GSFC Contract No. NAS5-26164, and Task III, "NOSS/ALDCS System Requirements Definition Study" of Modification No. 1 to that contract. Task I was concerned with advanced location and data collection system (ALDCS) concepts, and was not necessarily directed at any particular application. The body of the report and Appendices A through F are the outcome of Task I. In Task III, the analysis of Task I (as well as that of Task II, contained in a separate report) was applied to the National Oceanic Satellite System (NOSS). Appendix G is the result of Task III. It describes a NOSS ALDCS employing the combined Doppler/Interferometer concept, and defines engineering design requirements for this system.

1.0 INTRODUCTION AND SUMMARY

1.1 INTRODUCTION

Spaceborne position location systems to date have employed almost exclusively Doppler processing, in which the variation in the received frequency of the ground transmitter is analyzed to estimate its position. Such Doppler systems have inherent limitations:

- The ground transmitters require highly stable oscillators to achieve the required location estimation accuracy. This requirement contributes substantially to their cost.

- The average velocity of a moving transmitter, such as one aboard a balloon, can only be estimated from frequency measurements acquired from two consecutive overpasses of a satellite. This is too coarse an estimate for many applications. Velocity errors on the order of meters/second, independent of satellite overpass geometry, based upon a single satellite overpass are highly desirable.

- The accuracy of the position estimate is dependent on the location with respect to the satellite path. In particular, the error in the direction perpendicular to the ground track is very large for platforms located near the ground track. Location errors on the order of one kilometer, relatively independent of overpass geometry are highly desirable.

An alternate satellite-based location technique, analyzed in this report, uses multiple antennas to determine the direction of arrival of a ground platform's signal. This method, known as RF interferometry, does not suffer from the drawbacks of the Doppler technique cited above. It has, in addition, the capability of estimating location on the basis of a single received pulse, while Doppler systems require several. This is a distinct advantage in some applications.

RF interferometer location systems combined with data collection capabilities have several possible application areas. In environmental monitoring and scientific data collection, the traditional domain of data collection systems, the advantage of low platform transmitter cost would allow mass deployments to study widely distributed phenomena such as ocean or air currents. The capability to estimate velocity on one overpass lends itself to meteorological balloon-tracking, as well as various vehicle-tracking applications. An RF interferometer system, because of its ability to arrive at a position estimate upon receiving a single platform transmission, is also particularly well-suited to a search and rescue application, where the number of transmissions received from an emergency locator transmitter may be limited by line-of-sight blockage by terrain and other obstructions.

An RF inteRFerometer system requires five or more antennas, arranged on two orthogonal baselines, to provide all the advantages cited. A more modest sytem, employing only two antennas, offers some of the advantages with an appreciable reduction in size, weight and complexity. This is a hybrid system that uses RF interferometry and Doppler processing in a complementary manner. It also allows platform frequency stability requirements to be relaxed, and overcomes the near-ground track resolution problems, but requires more than one transmission for a position estimate.

This report presents the results of analyses of system design and hardware implementation aspects of advanced location and data collection systems employing the RF interferometry technique. Both the dual-baseline interferometer, and the hybrid interferometer/Doppler systems were studied. Data collection capabilities were assumed in either type of system. The salient study results are given in what follows.

1.2   RF SIGNAL ANALYSIS

The mode of access assumed is random. Each platform transmits a short burst or pulse that is digitally modulated with identification and data. The transmissions occur at regular intervals, and there is no synchronization among platforms. Their transmitting frequencies are distributed over a specified band. There is a certain low probability that pulses from two or more platforms will overlap in time and frequency and thus be lost. This probability can be shown to be approximately proportional to the total number of data bits transmitted during each interval by all the platforms in the satellite's field of view. This is a well-known result for data collection systems with identical platforms all having the same pulse length and transmission interval. But this convenient estimate applies as well to systems with platforms of several different types, each with a different pulse length and transmission interval.

The selection of hardware performance parameters and signal modulation characteristics is governed by two requirements:

- to transfer data from the ground platform to the spacecraft with no more than a specified error rate

- to measure with a specified accuracy the relative phase between the signals received at the interferometer's various antennas.

Both of these can be accomplished at the same time with the proper choice of signal modulation. This is advantageous because it allows the pulse length to be limited to that required to send the data. The alternative to simultaneous data demodulation and phase measurement is to precede or follow the data-modulated portion of the pulse by a period of pure carrier and measure the relative phases during this period. An unmodulated preamble is necessary for signal acquisition, but the shorter the unmodulated part of the pulse is made, the lower is the interference probability between transmissions of different platforms. A type of modulation that lends itself to simultaneous phase measurement is phase-shift keying or a pseudo-minimal-shift keying with Manchester signalling. These produce spectra with carrier components that can be easily separated from the modulation sidebands. The peak modulation angle

determines the fraction of the signal power in the carrier. Varying this angle allows a trade-off between phase measurement accuracy and bit error rate.

Through a link analysis based on easily implemented performance parameters at 400 MHz, it was found that an adequate bit error rate (at 128 b/s) and phase measurement accuracy can be achieved with a one-watt platform transmitter and a simple omnidirectional turnstile antenna. The maximum range of received signal levels expected at the spacecraft, assuming a distribution of these platforms over the field of view and a minimum elevation angle of 20°, was estimated to be 10 dB.

1.3   POSITION AND VELOCITY ESTIMATION ANALYSIS

Three systems are evaluated in terms of the precision with which position and velocity estimates are provided for platforms. One of these is a pure interferometer system comprising two orthogonal (cross-arm) axes whose plane is maintained perpendicular to local vertical. A second system assumes frequency (Doppler) measurements are also made during the satellite overpass and are combined with the interferometer measurements. The third system comprises measurements from a signal axis interferometer oriented perpendicular to the satellite's orbital plane again combined with frequency measurements.

The cross-arm interferometer is shown to be marginally capable of meeting the performance levels of one kilometer location and one meter per second velocity estimation. For a relative phase measurement precision of 3° at 400 MHz, arm lengths approaching 100 meters are necessary while attitude errors must approach $.01^o$.

By combining cross-arm interferometer measurements with Doppler frequency measurements, considerable improvement in performance is achieved. With 20 meter arms and assuming 0.5 Hz frequency measurement errors, location estimates with errors consistently less than one kilometer are experienced while velocity estimation errors range between one and two meters per second. These analyses are based upon local platform transitters having frequencies

that are offset by an unknown amount during an overpass and also exhibit an unknown linear drift with time.

The third system, a single axis interferometer combined with frequency measurements, arises from consideration of Geometric Dilution of Precision effects experienced by an interferometer ax and a Doppler system. In particular, a single axis interferometer oriented perpendicular to the satellite's orbit plane is found to be highly complementary to a Doppler system. With an arm length of 20 meters, this system exhibits location and velocity errors only slightly larger than the 20 meter cross-arm interferometer plus Doppler system.

1.4 INTERFEROMETER AMBIGUITY RESOLUTION

An RF interferometer must determine the angle of signal arrival with respect to two (preferably orthogonal) baselines to provide a position estimate. To resolve the ambiguity that is in general always present in the angle measurement, there must be a second pair of antennas on each baseline in addition to the primary antenna pair. The spacing between the second pair of antennas is small compared with that between the primary ones. The need for two pairs of antennas on a baseline does not necessarily imply four antennas, since one antenna may belong to both pairs. Likewise, one antenna may be paired with others on both baselines. As a result of this dual use, a dual-baseline interferometer may be constructed out of from five to eight antennas. A five-antenna configuration requires the least RF circuitry, though it may not be optimum because of instrument packaging and antenna mounting considerations. At any rate, when frequency (Doppler) measurements are acquired, the location estimate obtained from them precludes the need for the additional ambiguity resolving antennas.

1.5 PHASE MEASUREMENT

A hardware technique for on-board signal processing and phase measurement was analyzed and its performance trade-offs were determined. The method consists of using a phase-locked loop to down-convert the signals from both antennas to the same frequency, offsetting one of these signals by a

small reference frequency, then mixing the two signals to produce a tone at the reference frequency. The phase of this signal is a function of the phase difference between the input signals. The bandwidth of the filter used to reject modulation sidebands and thermal noise is a critical parameter determining the achievable phase measurement resolution. It was found that a filter noise bandwidth of about 20% of the bit rate insures that phase noise contribution from the modulation sidebands does not exceed one-tenth of the contribution from thermal noise. Reducing the filter bandwidth lowers both of the phase noise contributions and increases the measurement resolution, but it also raises the response time of the circuit. The slower the response, the longer the platform pulse must be, so phase resolution may be traded off against pulse length, which in turn affects interference probability and system capacity.

The time that the phase measurement circuit takes to respond is only a part of the total pulse duration. The signal must be detected and acquired before the phase measurement can begin, and the measurement must be integrated to further decrease the error. Estimates were derived for all the required steps in the process. It was found that a total of about 360 milleseconds (ms) is sufficient for obtaining a phase measurement with a 1^O standard deviation, assuming a conservative received signal-to-noise density ratio of 40 dB-Hz for 30° PSK modulation at a 128 b/s rate.

1.6   NUMBER OF DATA EXTRACTION CHANNELS

Multiple signal processing and phase measurement channels are required to accommodate platform pulses that overlap one another in time, but which do not interfere in frequency. The parameter determining the number of channels that should be provided is the probability that all channels are occupied when a signal is received. This probability has been determined as a function of the number of channels and the average rate of arrival of transmissions. This latter parameter is equal to the duty cycle of a platform (pulse duration divided by transmission interval) times the number of platforms in the satellite's field of view. To insure that a channel is available when a signal is received, with a probability of 0.95, five channels must be provided in a system with an average arrival rate of two. For a rate of four, eight channels are needed.

1.7   CALIBRATION TECHNIQUES

Two basic methods of calibrating the interferometer are available: by injecting calibration signals on board the satellite, and by the use of ground platforms at known locations. The signal injection technique localizes corrections to the interferometer instrument itself. When calibration platforms on the ground are used, however, corrections are given for the position estimate. This includes several other error sources besides the interferometer, such as attitude determination and tropospheric and ionospheric refraction. It is difficult to allocate the position correction so determined among those sources. In an actual system implementation, both methods would probably be used.

1.8   VOLUME, MASS AND POWER ESTIMATES

Estimates were derived for the volume, mass and prime power requirements of two interferometer instruments. The first was a dual-baseline interferometer with five antennas and six signal processing channels. The second was a hybrid instrument, using a single-baseline interferometer along with Doppler processing. It also had six channels. The frequency of operation was assumed to be 400 MHz. The results of this analysis are as follows:

	Two-Baseline System	One-Baseline System plus Doppler
Volume (excluding antennas)	55.9 liters	43.1 liters
Mass (including antennas)	50.1 kilograms	32.7 kilograms
Prime Power	63.9 watts	68.8 watts

2.0   SYSTEM ANALYSIS

The analysis of satellite location and data collection systems can be divided into two broad areas:

- Radiofrequency signal aspects - link analysis, interference statistics, modulation techniques, etc.

- Position and velocity estimation aspects - processing algorithms, geometric dilution of precision, estimation error, etc.

While investigations in these areas may be carried out mostly independently, there are necessarily some trade-offs requiring consideratons from both areas. For example, the time between platform transmissions and the interference probability together determine the number of independent observations of a platform the spacecraft is likely to make during its overpass, and this is a determining factor in position and velocity estimation accuracy.

In this section, the two areas are considered separately. The signal analysis presents basic relations between signal attributes (transmission pulse length, transmission interval, data rate, etc.), and the interference probability, examines implications of the system's dual purpose (information transfer and position estimation) on signal design, and gives a link budget using parameters typical of a real system implementation. The position and velocity estimation analysis describes the operation of two possible advanced systems: one using two orthogonal RF interferometers, and one that uses a single interferometer and also performs Doppler processing. The method of operaton, processing algorithms, and inherent advantages and limitations are described for each system, along with the effects of errors from various sources on the estimation accuracy. Finally, error estimates are presented for selected system implementations.

2.1   RF SIGNAL ANALYSIS

2.1.1   Introduction

The principal behind a random access system is that a certain
fraction of the transmissions will be lost due to self-interference, but this
fraction is small enough, and the number of transmissions made by a platform
during an overpass is large enough, that there is a good change of receiving
the required number. The fraction of transmissions that overlap in time and
are close in frequency (i.e., interfere with one another) is related,
intuitively, to the number of platforms and the fraction of the available time
and spectrum each platform uses. Analysis confirms this, and produces another
interesting result: The probability of not receiving a given transmission due
to interference is approximately proportional to the total number of data bits
transmitted by all the platform during one transmission interval. This result
holds for a system in which the length of the transmissions is different for
different platforms, as well as a system using identical platform
transmissions. This approximation is useful in the preliminary sizing of a
location and data collection system.

In an RF interferometer-based location and data collection system,
the signal received from a platform contains two types of information: the
binary data modulating the carrier, and the direction of arrival. The latter
is expressed through the phase difference measurement between the antennas.
By using the proper kind of modulation, it is possible to extract both the
digital data and the phase information from the signal at the same time. This
is desirable because it allows nearly all of the transmitted pulse length to
be used to transmit platform identification and data. The modulation technique
used results in a division of the total RF power between the carrier component,
used to measure the phase difference, and the modulation sidebands. Adjust-
ment of the parameter that determines this division of power (the peak
modulation angle) allows the phase measurement accuracy to be traded off
against the bit error rate.

There is another aspect of the signal modulation used that has
system-wide impact. Different techniques of binary modulation result in

spectra with different distributions of signal power around the carrier. The technique that gives the narrowest distribution is best in the present application because the more the power is concentrated about the carrier, the closer in frequency two signals can be before there is unacceptable interference. In a random access system, using such spectrum-efficient modulation techniques results in a decreased interference probability. One such technique, minimal-shift keying, is considered in this report.

This section discusses the system-level aspects of the RF signal design, and presents an RF link budget. The questions of how the above concepts are actually used, and performance achievable using them are considered in Secton 3.

2.1.2   Random Access Considerations

The number of transmitter platforms that can be accommodated by a random access location and data collection system depends on the desired reliability, which can be measured by the probability of receiving transmission from a platform in the satellite field of view. The probability that a transmission will be lost due to interference between platforms clearly increases (the reliability decreases) with the number of platforms. It should also increase with the duty cycle (transmission length divided by transmission period). Other factors are the total bandwidth available for use by the system, and the data rate, since transmitting at a higher rate occupies a larger piece of the spectrum. The interference probability is determined later as a function of these factors, and the individual factors are examined.

A reliability measure that is perhaps better than the probability of receiving a particular transmission is the probability of receiving some minimum number of transmissions out of the total possible. The total number possible is determined by the duration of the satellite overpass, and the transmission period. The overpass duration is in turn a function of the satellite altitude and the minimum elevation angle at which communication is possible. The "minimum number of transmissions" criterion is useful because location accuracy improves with the number of independent observations. With

this criterion, the system may be designed to yield a specified location accuracy with a given probability. The probability of receiving at least 3, 4, or 5 transmissions out of six is shown in Figure 2.1-1 as a function of the probability of missing any one.

2.1.2.1 <u>Interference Probabilities</u>. In a random access location and data collection system, a transmission will not be received if it interferes both temporally and spectrally with another transmission. Temporal interference occurs when another transmission is in progress at the time a given transmission starts. Spectral interference refers to the proximity of the carrier frequencies of the transmissions received. When the frequencies are too close, their modulation sidebands overlap, and interference occurs.

Spectral interference may have several effects: the error rate in the demodulated data may increase, for example, or a phase-locked loop tracking one of the signals may break lock. The phase error in the loop may increase. The severity of the interference effects, whatever they are, depends on the difference in the amplitudes of the interfering signal and the character of their modulation sidebands, as well as their proximity in frequency. Analysis of the interference effects is involved and will not be addressed here. Instead, the problem will be simplified by assuming that there is some minimum spacing between signals that must be exceeded for interference not to occur. Whenever the spacing is less than the minimum, we assume one of the interfering transmissions is lost. This minimum carrier frequency spacing is normally taken to be some multiple of the bit rate, since the modulation sidelobes are so spaced. The multiple chosen depends on the type of modulation used, the expected dynamic range of the received signals, and how conservative one wishes to be.

With this simplified view of spectral interference, we assume a transmission is lost due to temporal and spectral interference if it starts while another transmission, within the "interference" frequency proximity, is in progress. Call the length of a transmission τ, and the frequency spacing for interference Δf. The probability of losing a given transmission due to interference is just the probability that at least one transmission started τ or less seconds in the past, in a particular frequency band of width $2\Delta f$.
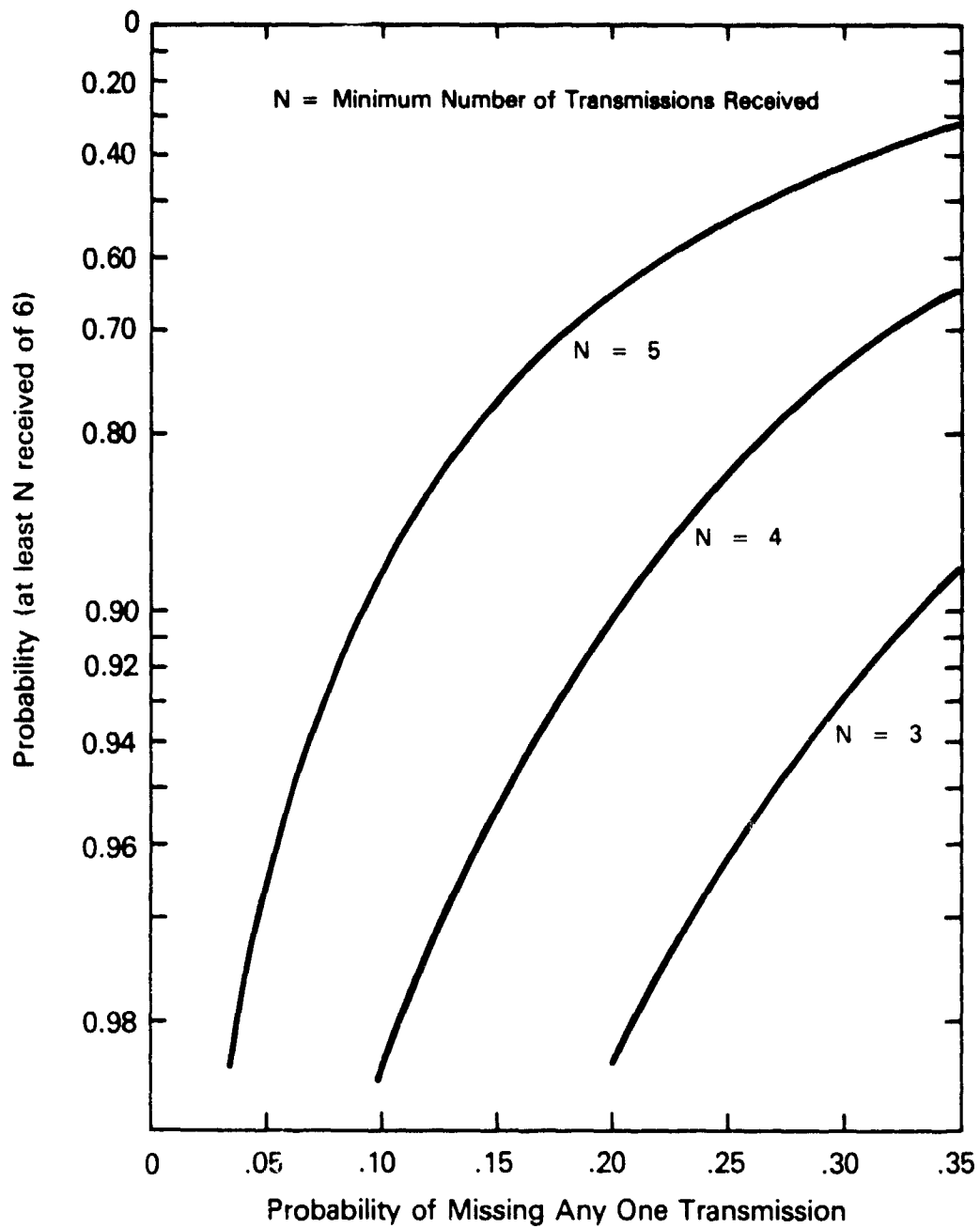
FIGURE 2.1-1. PROBABILITY OF RECEIVING AT LEAST N OUT OF 6 TRANSMISSIONS

(The factor of two arises because the frequency of an interfering transmission in progress may be within Δf on either side of the given transmission.) Say there are N transmitters, and each transmits a pulse every T seconds. If the transmitters' timers are randomly phased, we may say that the average rate of occurrence of pulses in any τ-second interval is $N\tau/T$. If we further assume that the transmit frequencies are uniformly distributed over a band F, then the average rate of occurrence of transmissions in a given τ-second time interval and a given $2\Delta f$ Hz frequency interval is $(2\Delta f/F)(N\tau/T)$. Simulations have shown that the assumption about uniform frequency distribution turns out to be surprisingly good (Ref. 1).

The occurrence of interfering transmissions in time and frequency can be modelled as a Poisson process with rate $\lambda = (2\Delta f/F)(N\tau/T)$. The probability of at least one occurrence (i.e., interference) is given by (Ref. 2)

$$P_{int} = \text{Prob(at least one)} = 1 - \text{Prob(none)} = 1 - e^{-\lambda}$$

when λ is a small number, this may be approximated by

$$P_{int} \cong \lambda = (2\Delta f/F)(N\tau/T)$$

If the interference frequency spacing is expressed as a multiple (k) of the bit rate (R), then $\Delta f = kR$, and we have

$$P_{int} \cong 2kRN\tau/FT$$

This shows that when the interference probability is small, it is directly proportional to the total number of bits transmitted every T seconds, $RN\tau$, which is a useful result.

2.1.2.2 Mixed Duty Cycles. The foregoing assumes that all the transmitters have the same duty cycle. The results may be extended to the case of mixed duty cycles, in which there are several classes of transmitter platform with different duty cycles. This would arise in a system with platforms that transmitted different amounts of data, but all with the same transmission period, to maintain the minimum number received per overpass. For such a

system, the average rate of occurrence of a transmission within the past τ_i seconds and in a frequency range of 2kR is

$$\lambda_i = (2kR)\ N_i \tau_i / FT$$

where N_i is the number of platforms in the satellite field of view in the class with duty cycle τ_i/T. The probability that no transmission from any class of platform occurs in a time and frequency interval that will cause interference is

$$\text{Prob(no transmissions)} = P_1 P_2 \cdots P_n$$

where P_i ($i = 1, 2, \ldots n$) is the probability of no transmissions from a platform with duty cycle τ_i/T and n is the number of different duty cycles. From previous discussion, we may say

$$P_i = e^{\lambda_i}$$

Therefore,

$$\text{Prob(no trans.)} = \exp\left(\sum_i \lambda_i\right)$$

$$P_{int} = 1 - \text{Prob(no trans.)}$$

$$= 1 - \exp\left[(2kR\sum_i N_i \tau_i)/FT\right]$$

Note that in the approximation for small interference probability,

$$P_{int} \cong 2kR \sum_i N_i \tau_i / FT$$

there is a direct dependence on the total number of bits transmitted each interval, as with the case of constant duty cycle.

2.1.2.3 <u>System Bandwidth</u>. The system bandwidth F in the above formulas is the frequency range over which platform transmissions are received. It is determined by the range over which the transmitter frequencies fall, or are
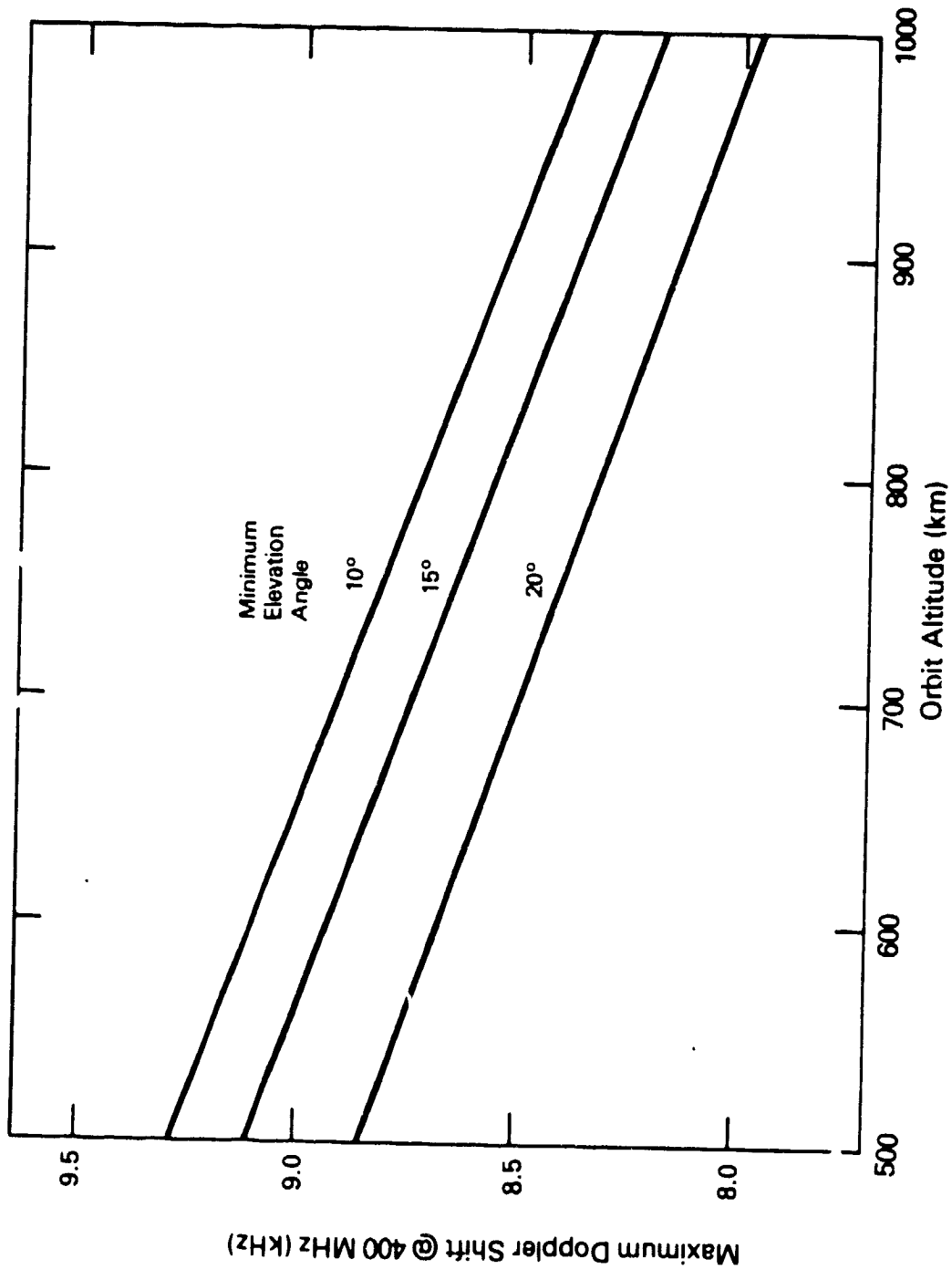
FIGURE 2.1-2.   MAXIMUM DOPPLER SHIFT AT 400 MHz

set, the amount of frequency drift to be expected of the oscillators over time, and the range of Doppler shift. The last is a function of the satellite elevation and minimum elevation angle, and is shown in Figure 2.1-2 for 400 MHz. This range applies to a transmitter directly on the satellite subtrack, so the Doppler shift for most of the platforms in the field of view will be appreciably less. Determination of the probability density of the Doppler shift, assuming a randomly placed transmitter in the satellite field of view, is a complex problem requiring computer simulation techniques. Once this density is found, it must be convolved with the probability densities of the initial oscillator frequency and of the frequency drift to yield the overall frequency density function. This has been accomplished, assuming a Gaussian density without Doppler, and it has been found that the resulting density is close to uniform (Ref. 1). This supports the assumption of a uniform density used in the interference probability model.

2.1.2.3 Dynamic Range and Modulation Effects. The simplified interference model does not consider the effects of the dynamic range of the received signals. The frequency separation at which one signal may interfere with another increases with the difference in amplitude of the signals. This is because what determines the degree of interference is essentially the amount of sideband power from one signal falling within the band occupied by a second, relative to the power of the second signal. The lower power density of the sidebands further away from the carrier is offset by the higher relative amplitude of the interfering signal.

The increased probability of interference due to this is minimized by taking measures to equalize the amplitudes of the received signals. This can be done by making the transmitted power the same for all platforms and by proper design of both the spacecraft and ground platform antennas. Ideally, the ground antenna should have uniform hemispherical coverage, and the spacecraft antenna pattern should vary with nadir angle inversely as the range to the surface varies. Both of these patterns may be approximated with a quadrifilar helix type of antenna.

The interference probability is also decreased by using a modulation technique with favorable spectral characteristics. The rate of decrease of

the sideband level with separation from the carrier should be as great as possible. Phase modulation with smoothed modulating waveforms have rapidly-decreasing sidebands. One of the best in this respect is Minimal-Shift Keying (MSK), in which the phase modulation waveform is linear. MSK sidebands decrease as the fourth power of frequency, while those of normal PSK decrease as the square of frequency.

2.1.3   RF Link Analysis

Table 2.1-1 gives a link budget for the ground platform-to-satellite channel. Assumptions made about hardware performance and other basic parameters are also given in the table. Some of these values have been taken from the link budget for the NIMBUS/RAMS system. As indicated, the satellite altitude and minimum elevation angle have been taken at 800 km and 20 degrees, respectively. This altitude is in the range required for a sun-synchronous orbit, which is probably the orbit best suited for a global-coverage location and detection system such as this. The minimum elevation angle is on one hand a function of the tolerable degree of multipath reception and tropospheric turbulence and refraction effects, and on the other hand, determined by the location accuracy desired. The location accuracy is involved because of the increase with decreasing elevation angle in the surface distance error due to a given interferometer angular error. The value chosen for the minimum elevation angle is a representative value, not based on any detailed consideration of these factors.

The antenna assumed for the spacecraft has a gain that increases with nadir angle, having a maximum near the horizon, and is constant in azimuth. The purpose of this pattern is to keep the sensitivity approximately equal over the satellite field of view. Ideally, the gain should vary exactly as the variation in range. A quadrifilar helix type of antenna can be designed to produce such a pattern with very pure circular polarization (Ref. 3). It is the degree to which the satellite antenna pattern deviates from the ideal function, along with the variation in the gain of the platform antenna, that will largely determine the range of signal levels that will be seen at the satellite. It is desirable that this range be small. The best ground platform antenna to use therefore is one with a hemispherical pattern, such as

TABLE 2.1-1

LDCS LINK CALCULATIONS

SYSTEM PARAMETERS

Frequency	400 MHz
Range	800-2000 km
Earth Surface Noise Temp	300 K
Receiver Noise Figure	3 dB
Receiver Front End Loss	1 dB
Satellite Antenna	Quadrifilar Helix, CP
Platform Antenna	Turnstile, CP

LINK CALCULATIONS

Satellite	@ Nadir	@ 57° From Nadir[1]
Noise Temperature		28.7 dBK
Gain	-4.0 dB	5.0 dB
Polarization Loss[2]	0	-0.9 dB
G/T	-31.7 dB	-23.6 dB

Path	Min Range	Max Range
Path Loss	-142.5 dB	-150.5 dB
Multipath	-0.5 dB	-1.0 dB

Platform	@ Zenith	@ 20° Elevation
Power Output (1w)		0 dBw
Coax Loss		-0.5 dB
Antenna Gain	4.0 dBi	-5.5 dBi
EIRP	3.5 dBw	-6.0 dBw
Boltzmann's Constant		-228.6 dBw/K/Hz
Carrier[3]-to- Noise Density	57.4 dB-Hz	47.5 dB-Hz

NOTES:

1. Corresponds to 20° elevation angle
2. Worst case with axial ratios: 1 dB for satellite, 3 dB for platform
3. Without modulation

a turnstile. The expected range of received signal power using a turnstile on the ground is given in the table.

The modulation used is assumed to be PSK with a peak modulation angle less than 90°. As described in Appendix A, this divides the power between the carrier and the sidebands. The interferometer accuracy varies with the amount of power in the carrier, and the bit error probability is determined by the power in the sidebands. The trade-off between the two is shown in Figure 2.1-3. One plot is the carrier power fraction, or the ratio of the carrier power to the total power, in dB. The other plot is the degradation due to the modulation angle being less than 90°. This is the amount that the total signal power would need to be increased to maintain the bit error probability at the same value it is when the angle is 90°. The basis of Figure 2.1-3 is given in Appendix A. As an example of the use of the figure, consider a signal received with a total signal power to noise density ratio of 40 dB-Hz. Suppose the modulation angle is 30° and the bit rate is 128 b/s. According to the curve, the <u>carrier</u> to noise density ratio is 1.25 dB less than the total signal-to-noise density ratio, or 38.75 dB-Hz. We also see that there is 6 dB degradation associated with a 30° modulation angle, which means that the 30°-modulated signal has the same bit error probability as a 90°-modulated signal with 6 db less power. Such a signal, at 128 b/s, would have a bit energy to noise power density ratio, E_b/N_0, of 12.9 dB. Theoretically, the bit error probability for PSK with 90° modulation and $E_b/N_0 = 9.6$ dB is 10^{-5}. It is expected that there would be about 2.5 dB degradation in implementation of the demodulator, requiring E_b/N_0 of 12.1 dB for 10^{-5} bit error probability. Thus the 30° modulation achieves 10^{-5} with a 0.8 dB margin.

The frequency range over which one signal may interfere with another is dependent on the rate that the modulation sidebands decrease with distance from the carrier. This rate can be made greater by modulating the carrier with a waveform that does not have the sharp discontinuities of PSK. One such "smoothed" modulation technique is minimal-shift keying (MSK), which uses a triangular waveform. The peak modulation angle for MSK is 90°. A triangular waveform modulation in which the peak angle can be any value, called here "pseudo-MSK," is analyzed in Appendix A. Figure 2.1-4 shows curves of the fraction of power in the carrier and the degradation, similar to those of Figure 2.1-3, for pseudo-MSK.
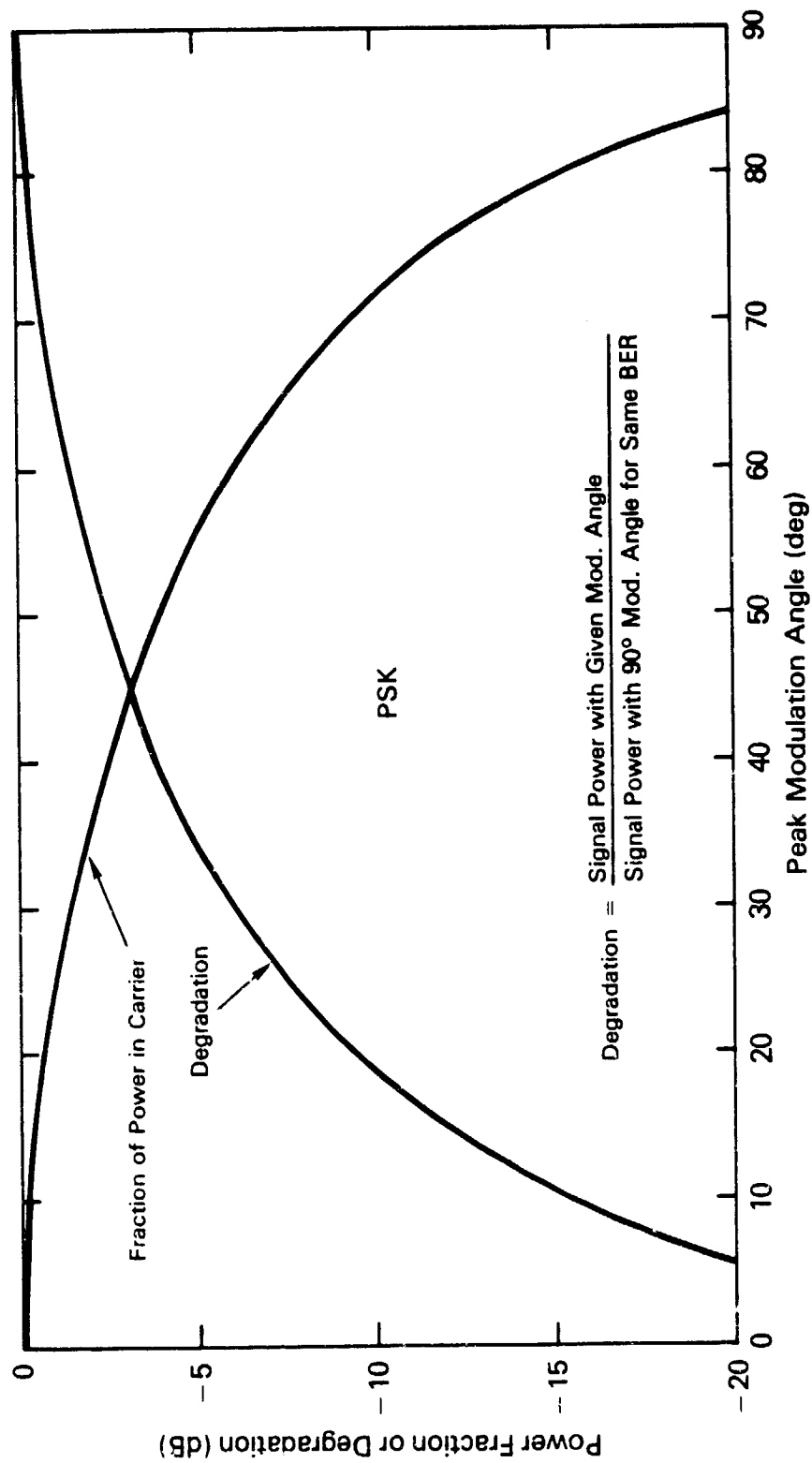
FIGURE 2.1-3. POWER IN CARRIER AND DEGRADATION FOR PSK

$$\text{Degradation} = \frac{\text{Signal Power with Given Mod. Angle}}{\text{Signal Power with 90}^\circ \text{ Mod. Angle for Same BER}}$$

PSK

Fraction of Power in Carrier

Degradation

Peak Modulation Angle (deg)

Power Fraction or Degradation (dB)
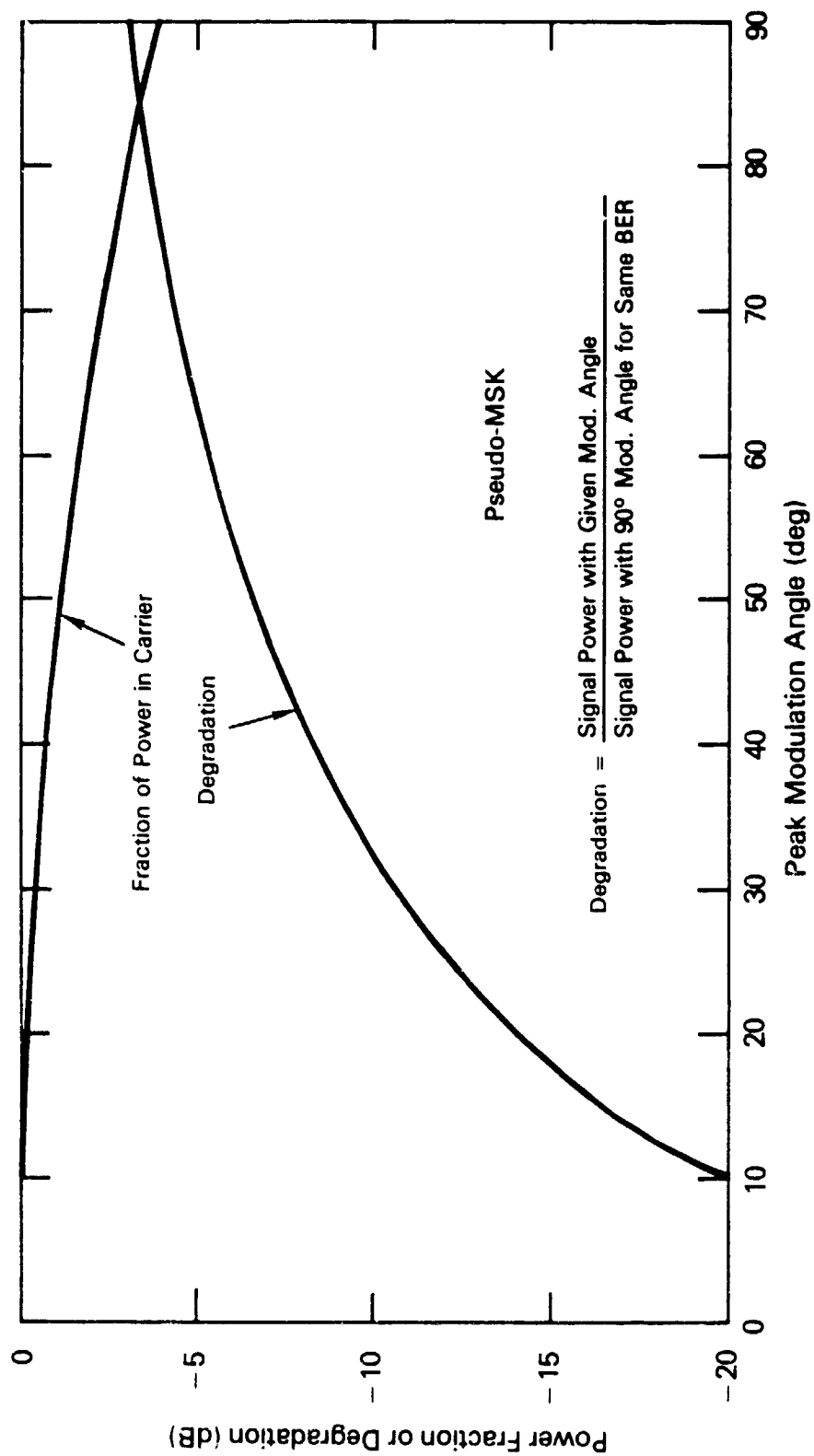
FIGURE 2.1-4. POWER IN CARRIER AND DEGRADATION FOR PSEUDO-MSK

2.2   POSITION AND VELOCITY ESTIMATION ANALYSIS

2.2.1   Geometric Concepts

The underlying basis for estimating the position and velocity of
platforms is the ability to translate RF measurements into lines on the
earth's surface along which the platform lies at the moment of a
transmission. Acquiring multiple measurements then serves to define multiple
lines-of-position (LOPs) and their point(s) of intersection identifies
latitude and longitude of the platform. This concept holds whether these RF
measurements are relative phase as derived from an interferometer or relative
frequency as employed in a Doppler location system.

In Figure 2.2-1, the LOP generated from the relative phase
measurement of an interferometer is sketched. The upper part of this figure
indicates the basis for determining the direction of a platform relative to
the axis of an interferometer. The differences between the ranges R_A and
R_B can be seen to be the relative phase or phase delay between receivers at
the ends of the interferometer axis when this relative phase is interpreted in
terms of wavelengths of the transmitted RF signal from the platform. This
geometry serves to determine the angle θ. One relative phase measurement can
be seen to define the position of the platform as being on a cone whose axis
is the interferometer axis and whose semi-apex angle is θ.

The lower sketch of Figure 2.2-1 indicates the manner in which two
cones defined by two relative phase measurements defines platform position on
the earth's surface (or at some known altitude). The interferometer is
assumed to be in earth orbit with well-defined ephemerides such that its
position relative to the earth can be established as a function of the time of
reception of a platform's transmission. Similarly, the angular orientation of
the interferometer relative to the earth is also assumed to be known. In the
sketch, the platform transmits when the satellite (interferometer) is located
at point 1. The relative phase measurement made at this point is translated
into the angle θ_1 thus establishing the vertex position, axis orientation,
and semi-vertex angle of the surface-of-position upon which the platform is

2-15
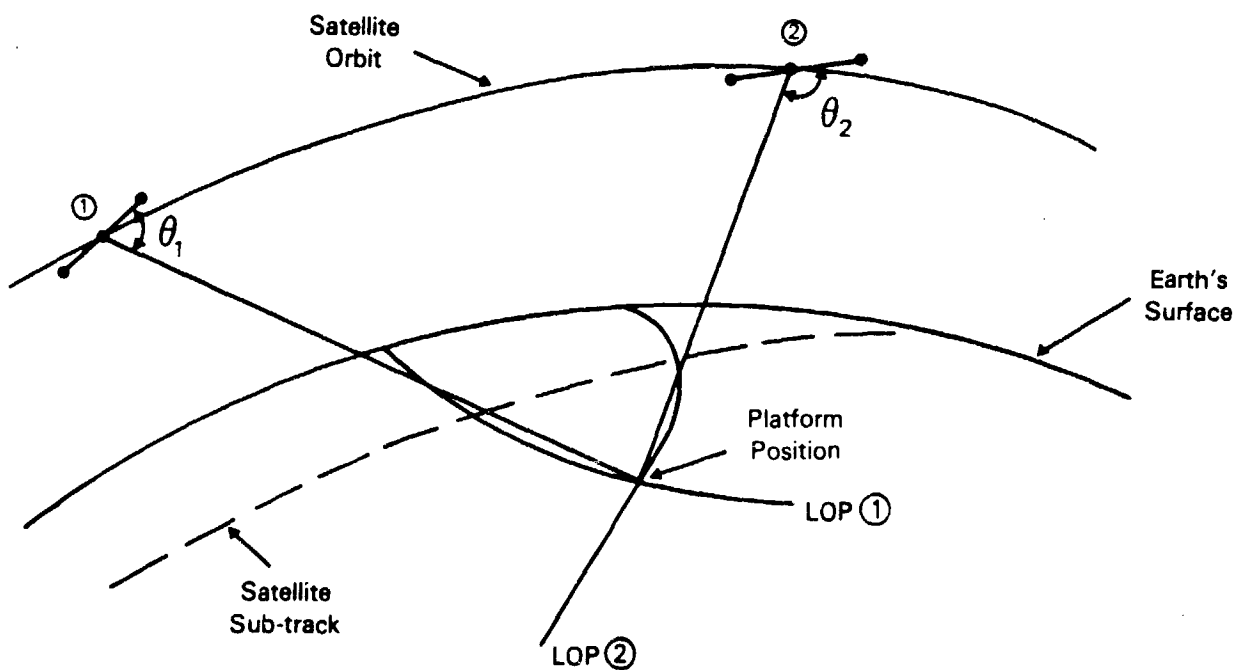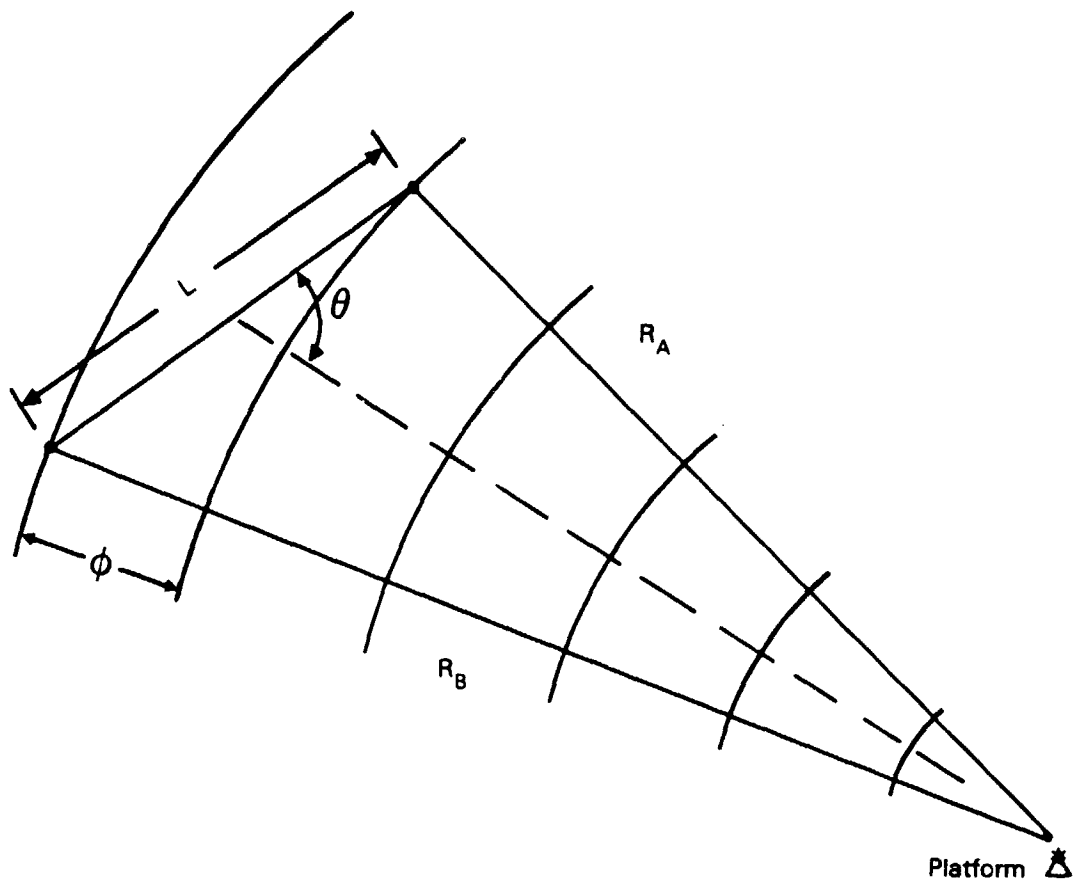
FIGURE 2.2-1. INTERFEROMETER LOP

known to be. The intersection of the conical surface-of-position with the earth's surface creates the line-of-position indicated by LOP 1. Similarly, a second platform transmission, when the satellite is positioned at point 2, generates a second line-of-position denoted by LOP 2. The intersection of these two LOPs defines the platform's position on the earth's surface.

There is an important distinction between the single and dual axis interferometers when the platform is moving with respect to the earth at some unknown velocity. In the case of the dual axis interferometer, the two surfaces-of-position are defined simultaneously. Assuming the measurement of relative phase is not affected by platform velocity (Doppler shift effects), the estimate of platform position is in turn not affected by unknown platform velocity. This is not true for the single axis interferometer.

In the case of the single axis interferometer, a basic assumption is made that the only change leading to two different lines-of-position is satellite position and angular orientation of the interferometer axis. If the platform has an unknown velocity, then the second line-of-position would reflect the platform's position at the second point of transmission which would be different, due to platform velocity, from the platform's position at the first transmission point. The intersection of the two LOPs would not then correspond to actual platform position and in fact, not necessarily to the average platform position between the two points of transmission.

The geometric concept for locating platforms using relative frequency (Doppler) measurements of platform transmissions is virtually identical to that of the interferometer. This concept is shown in Figure 2.2-2. The measurement in this concept is the Doppler frequency shift experienced by the platform RF transmission due to the relative range rate between the satellite and platform. As shown in the upper sketch of Figure 2.2-2, measurement of the Doppler frequency and therefore range rate, determines the angle θ_1 between the satellite's velocity vector relative to the earth and the line-of-sight direction to the platform under the assumption that the platform is stationary relative to the earth. This angle θ_1 is completely analogous to the θ_1 angle defined by interferometer relative phase measurement indicated in Figure 2.2-1. The surface-of-position for the

Satellite Velocity Vector

θ

Relative
Range Rate

Platform

Velocity
Vector @ ②

Satellite
Orbit

Velocity
Vector @ ①

②

θ_2

①

θ_1

Earth's
Surface

LOP ①

Satellite
Sub-Track

LOP ②
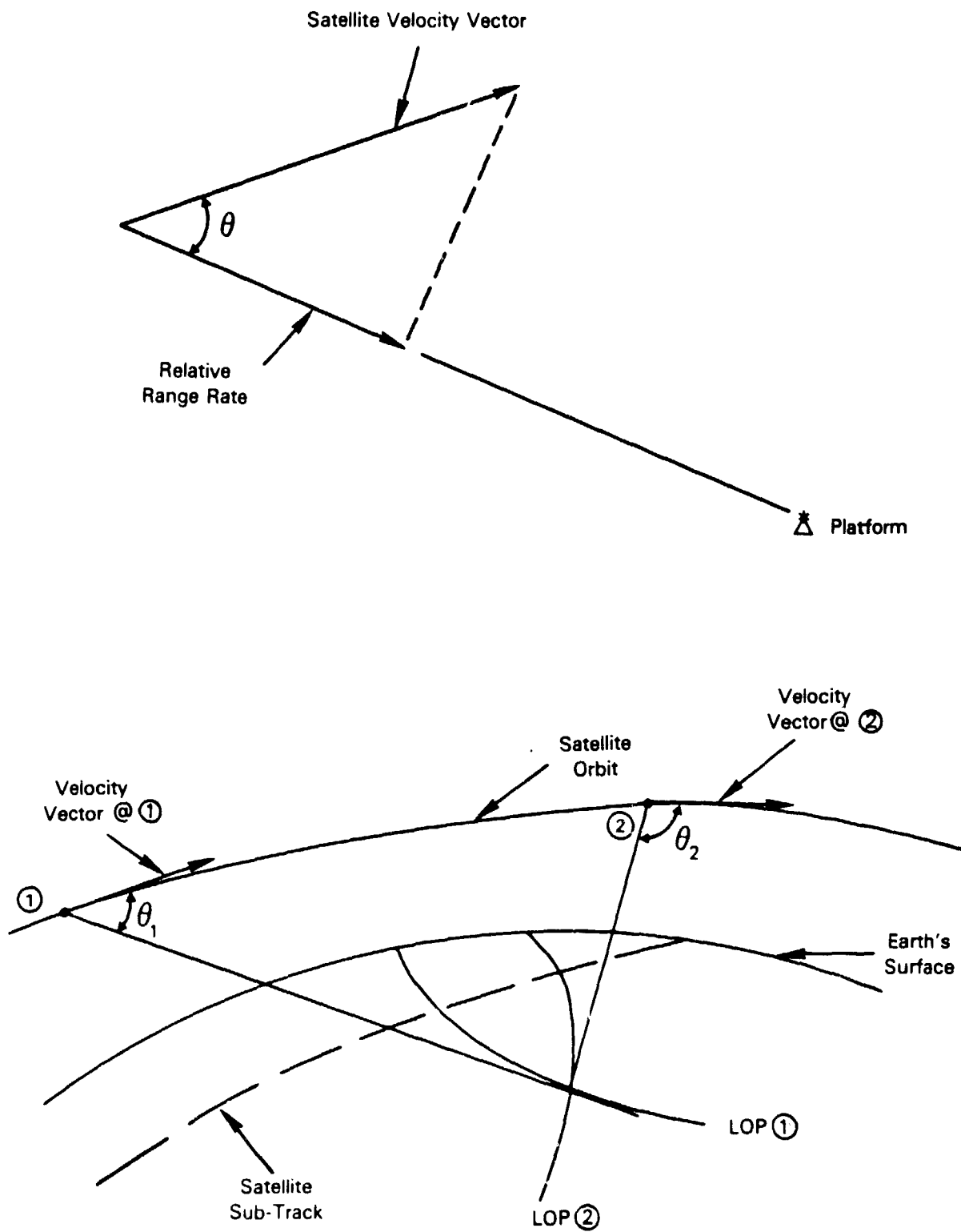
FIGURE 2.2-2.   DOPPLER LOP

2-18

platform is again a cone of semi-apex angle θ_1 but in this case the axis of
the cone is the satellite's velocity vector. With this interpretation, the
lower sketch of Figure 2.2-2 is virtually identical in concept to the
previously described lower sketch of Figure 2.2-1.

Although these discussions indicate the similarity between inter-
ferometer position location and Doppler position location from a geometric
viewpoint, an important difference between the two should be emphasized. This
difference pertains to the axes of the conical surfaces-of-position. In a
Doppler system, the axes of the cones are pre-ordained to be the satellite's
velocity vector. However, the axes of the cones for the interferometer system
can be arbitrarily oriented merely by fixing the angular motion of the
interferometer axis(es) relative to the earth. The importance of this
flexibility can be seen by considering areas on the earth's surface relative
to the satellite where Doppler and interferometer systems experience severe
geometric dilution of precision (GDOP).

2.2.2   Geometric Dilution of Precision

When consideration is given to the accuracy and precision of locating
platforms by both Doppler and interferometric techniques, two system aspects
must be evaluated. One of these is the precision with which the conical
surfaces- of-position can be determined. This precision will be the result of
the combination of all error sources peculiar to the systems such as
measurement error (frequency or phase), satellite ephemeris errors, etc. The
second consideration is the magnification of errors caused by purely geometric
effects, i.e., geometric dilution of precision (GDOP). This magnification can
be shown to be the direct result of the angle at which the lines-of-position
cross at the platform's location and the angle at which the two conical
surfaces-of-position intersect the earth's surface.

In Figure 2.2-3, two sketches are provided which indicate these GDOP
effects. The upper sketch shows two pairs of line-of-position that would be
generated by either a Doppler system or a single axis interferometer aligned
with the satellite's velocity vector. For a platform located at position 2,
slight mispositioning of the LOPs due to any combination of errors can be seen

2-19
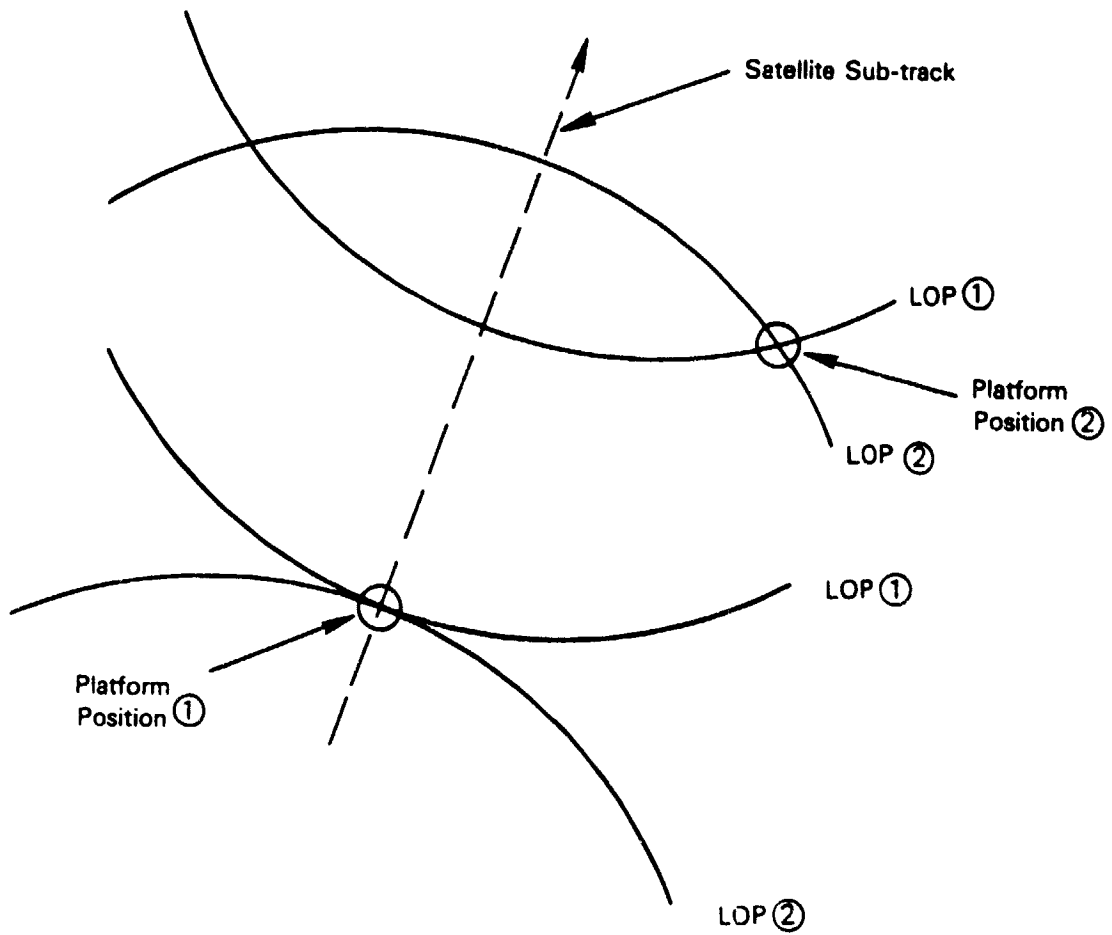
FIGURE 2.2-3. GEOMETRIC DILUTION OF PRECISION

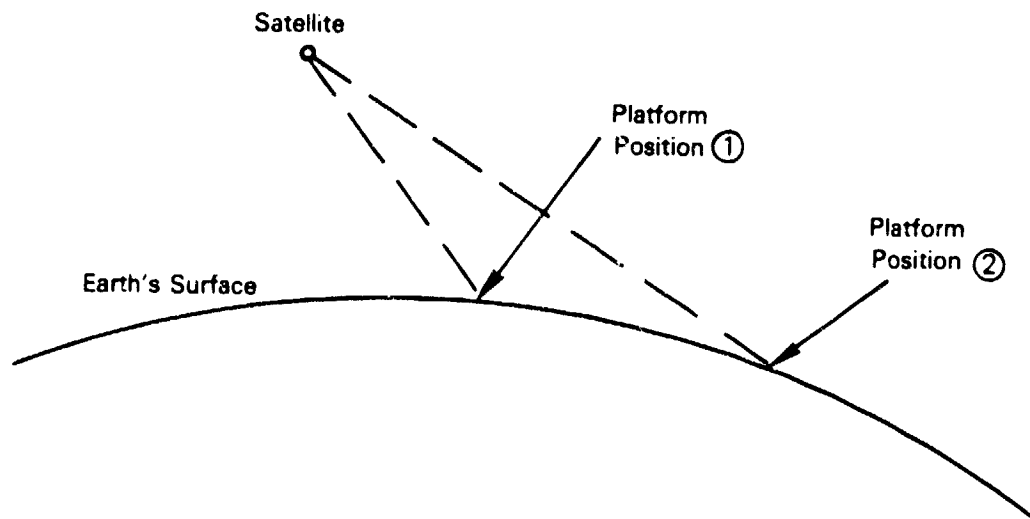to result in errors in estimating platform position that are comparable to LOP mispositioning. However, for a platform located at position 1, slight mispositioning of either or both LOP will result in very large errors in the component of platform position perpendicular to the satellite's sub-track. Because of this GDOP effect, both Doppler systems and single axis interferometers oriented parallel to a satellite's velocity vector will exhibit relatively poor position estimates for platforms located near the satellite's sub-track and rather good position estimates for platforms distant from the satellite's sub-track up to the point where the second GDOP effect becomes significant.

The second GDOP effect is indicated in the lower sketch of Figure 2.2-3. The lines from the satellite to the two platform positions represent the line-of-sight from the satellite to the platform at the moment of a platform transmission, from which the conical surfaces-of-position are defined. For a platform located at position 1, a slight mispositioning of the conical surface can be seen to create an error in platform position comparable to the mispositioning of the conical surface. However, if the platform is at position 2, a slight mispositioning of the conical surface can be seen to lead to a large error in platform position estimate on the earth's surface. This GDOP effect is, of course, common to both Doppler systems and interferometers (regardless of orientation) and leads to degradation in performance when the platform approaches the horizon as seen from the satellite.

There is one other GDOP effect which is peculiar to the interferometer, and one other that is again common to both Doppler and interferometer location. The common GDOP effect results from their both being basically angle measuring systems. The consequence of this is that for a given error in measuring the semi-vertex angle of the conical surface-of-position the resulting error in platform position must at least be proportional to line-of-sight range to the platform. This compounds the GDOP degradation of performance indicated in the lower sketch of Figure 2.2-3.

The GDOP effect peculiar to the interferometer is a result of how the relative phase or range difference is used to determine the conical angle θ. In particular, for interferometer axes much smaller than the line-of-sight range to the platform, the geometry of the upper sketch of Figure 2.2-1 gives

2-21

$$\cos \theta = \frac{R_B - R_A}{L} = \frac{\phi \lambda}{2\pi L}$$

from which

$$\Delta \theta = \frac{\lambda}{2\pi L \sin \theta} \Delta \phi$$

where

λ = Free space wavelength of received transmission

ϕ = Electrical phase difference measured by interferometer (radians)

As the angle θ becomes smaller, a fixed error in measuring relative phase, $\Delta \phi$, leads to larger errors in θ. Therefore, an interferometer oriented parallel to the earth's surface suffers this added GDOP degradation as the platform approaches the satellite's horizon.

In summary, a major consideration in formulating an interferometer-based position location system is the GDOP effects which degrade performance. These effects include

● Poor location estimates for single interferometer axes lying in the orbital plane of the satellite for platforms located near the satellite's sub-track

● Poor location estimates for platforms located near the satellite horizon compared to a Doppler system

2.2.3   Location/Velocity Algorithms*

In order to translate measured RF parameters of received platform
signals (relative phase and frequency) into estimates of platform position and
velocity, algorithms are required to establish modeling assumptions and
processing techniques. Having established these algorithms, the performance
of interferometer and combined Doppler-interferometer systems can be evaluated
in terms of errors in platform position and velocity as a function of system
error sources.

The models employed to develop these algorithms comprise the
following:

- At each point in time that a platform transmission is received
  and measured at the satellite, the satellite's position and
  velocity vectors relative to the earth can be specified.

- At each point in time that a platform transmission is received
  and measured at the satellite, the angular orientation of each
  interferometer axis can be specified relative to the earth.

- Although platform transmission frequency is set at some nominal
  frequency compatible with the satellite receiver, at the moment
  of transmission the frequency can be offset from this nominal by
  an unknown amount.

- Because of short-term transients (10 to 15 minutes), the
  platform's frequency of transmission can vary linearly with time
  during a satellite overpass at an unknown but "significant"
  rate.

---

*   Detail derivation and description of these algorithms may be found in ORI
     Technical Report 1677, "Long Baseline Interferometer," prepared under NASA
     Contract NAS5-25606, Mod 9 and NASA document X-752-70-376, "System Study
     for the Random Access System (RAMS)." A brief review of these algorithms
     is provided herein. Mathematical details are presented in Appendix F.

- The altitude of the platform above the earth's surface is known throughout the satellite overpass.

- In those cases where position-only estimates are derived, the platform's velocity is either known or assumed to be zero throughout the satellite overpass.

- In those cases wherein position and velocity estimates are derived, the velocity of the platform is assumed to be constant relative to the earth throughout the satellite overpass.

As a result of these modeling assumptions, the algorithms employed must be able to estimate as many as six parameters from the sequence of RF measurements acquired during an overpass. These parameters comprise two components of position (latitude and longitude), two components of velocity (e.g., north and east), transmission frequency offset at a specified point in time, and the time rate-of-change of frequency offset. This implies (in the case of velocity estimation) a minimum of six independent RF measurements must be acquired.

With these models, processing of the RF measurements is accomplished by means of weighted least-square techniques. At each measurement time, and for each measurement, the geometric function relating the parameters to be estimated to the measured geometric quantity (range difference for the inter-ferometer, range-rate for Doppler processing) is linearized based upon an assumed set of values for the parameters. If n measurements are acquired during an overpass, there will be n linearized equations. The left side of these equations will be a linear combination of errors in the assumed values of the parameters while the right side of these equations is set equal to the differen e between the measured geometric quantity and the computed value it would have if the assumed values for the parameters were correct.

The solution process is then one of iteratively improving the estimates of the parameters by minimizing the weighted sum of the squares of the differences between measured and computed values of the geometric

quantities. In this regard, weighting is accomplished by dividing eacn
equation by the standard deviation of the error in the measured quantity.

When these algorithms are employed, two different types of errors are
encountered. One type of error comes about when any of the modeling
assumptions are violated. These errors normally lead to bias errors in
platform position and velocity estimates. The other type of error is random.
These errors are assumed to be statistically independent from one measurement
time to another. The weighted least-square algorithm inherently provides the
covariance matrix of parameter errors as a function of the standard deviation
of random errors.

2.2.4   System Concepts

Based upon the previous discussions, two interferometer location
systems have been investigated. One of these systems is a cross-arm
interferometer with the plane of the two arms maintained perpendicular to
local vertical. The second system comprises a single axis interferometer
combined with Doppler measurements. Both of these systems are evaluated under
the following conditions:

● A 750 km altitude, circular sun-synchronous satellite orbit

● Unknown offset of the platform's transmitted frequency from its
  nominal value

● Unknown drifting of the platform's transmitted frequency during
  an overpass—this drifting assumed to be linear with time

● Nominal transmission frequency of 400 MHz

● Relative phase measurement errors are unbiased with standard
  deviation of σ_ϕ degrees

● Frequency measurement errors are biased (platform and/or
  satellite local reference offset) with standard deviation of
  σ_f Hertz

2-25

- The elevation angle of the satellite above the local horizon of the platform must be greater than 5°

- Satellite ephemeris and angular orientation of interferometer axes can be specified at each point in time with negligible error

- Platform transmissions occur at regular intervals of time.

In Figure 2.2-4, the overpass geometry is shown that results from the assumed satellite orbit. The platform to be located is arbitrarily assumed to be at zero degrees latitude and longitude. The satellite overflies the platform, as indicated by its sub-track, and the cross-track separation establishes the geometry at each point of transmission by the platform. In the figure, these points are indicated when the interval of time between transmissions is ninety seconds. For the conditions indicated, and with a five degree elevation angle limit, six platform transmissions will be received by the satellite (assuming no losses due to mutual interference with other platforms).

In the following evaluations of the two location/velocity systems, several parameters noted in Figure 2.2-4 will be investigated. One of these is the cross-track separation between the satellite sub-track and the platform. As discussed previously, variation of this parameter will allow assessment of the severity of GDOP effects. The second parameter is the time between platform transmissions. Variation of this time effectively varies the number of transmissions received during an overpass thereby asses ng the gain in performance achieved through noise filtering of the measured parameters*. The third parameter is the elevation angle. While this parameter is assumed to have a nominal value of 5°, other system considerations such as antenna patterns, multi-path suppression, etc., may point to elevation angle limits greater than 5°.

---

* This parameter is also a major consideration when mutual interference between platforms is evaluated.
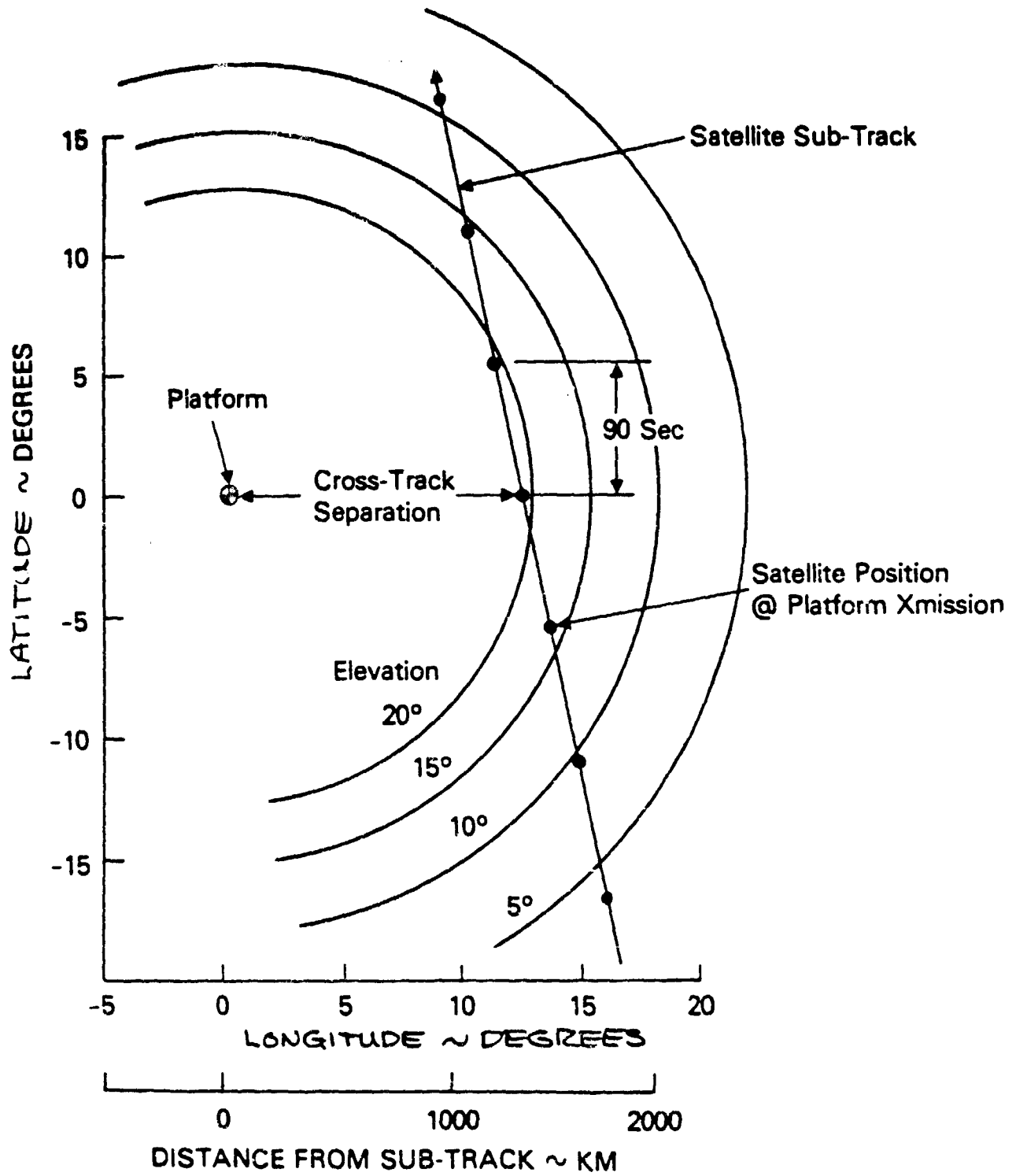
2-26

FIGURE 2.2-4. PLATFORM OVERPASS GEOMETRY

One other aspect of the overpass geometry shown in Figure 2.2-4 is the note of "maximum separation." In location and data collection systems, the maximum elapsed time between location/velocity estimates is important. Because of earth spin, this elapsed time is on the order of twelve hours under the assumption of day-night operation for satellite based systems, and under the assumption that sufficient visibility between the platform and satellite is geometrically guaranteed. For arbitrary longitudinal position of a platform at the earth's equator, the visibility requirement for the assumed orbit is satisfied if the overpass geometry of Figure 2.2-4 is tolerable, i.e., the combination of GDOP, number of transmissions, etc., allow satisfactory performance. In particular, the cross-track separation shown is the maximum separation that can occur on one of two successive overpasses of the platform twice per day or every twelve hours.

Cross-Arm Interferometer*

The concept of a cross-arm interferometer is derived from the geometric considerations discussed in Section 2.2.1. For each transmission from a platform, two lines-of-positions are derived from which a location estimate is obtained. Multiple transmission receptions during an overpass can then be used to noise filter the measurements and/or estimate platform velocity components in addition to latitude-longitude coordinates. Another important characteristic of this system is that for all practical purposes, the precision with which relative phase measurements on-board the satellite can be made is virtually independent of the stability of the reference oscillator generating the transmitted frequency from the platform**. The performance of the cross-arm interferometer is described in Figures 2.2-5 through 2.2-9.

---

* The performance of cross-arm interferometers in low earth orbit is analyzed in ORI TR 1677, "Long Baseline Interferometer."

** The basis for this statement may be found in Appendix D.

In Figure 2.2-5, the location error* of a cross-arm interferometer is shown as a function of the cross-track separation at the equator between the platform and the satellite subtrack in terms of degrees of longitude. As noted, the errors are presented for arm lengths of 5, 10, and 20 meters and the maximum longitudinal separation that can be encountered every twelve hours is shown.

The most salient feature of Figure 2.2-5 is the large increase in location error as the cross-track separation increases. This is the direct result of the GDOP degradation effects previously discussed coupled with the reduced number of platform transmissions as the satellite moves further from an overhead pass. However, the severity of these effects suggest that a pure interferometer location system would have to be augmented (e.g., through frequency measurements) if more uniform performance across the cross-track separations is required.

Another aspect of Figure 2.2-5 is that the ordinate is actually location error divided by the standard deviation of the "equivalent" relative phase measurement error. The term "equivalent" is used because this error statistic, σ_ϕ, can be interpreted as the standard deviation of all error sources of a random nature at each platform transmission time. In addition to relative phase measurement errors made on-board the satellite, this more general interpretation of σ_ϕ allows evaluation of another error source degrading interferometer performance—namely, the errors in specifying the angular orientation of interferometer axes.

In Section 2.2.2, the error in specifying the semi-apex angle, $\Delta\theta$, of the conical surface-of-position was defined as a function of interferometer length L, the nominal value of θ, and the phase measurement error $\Delta\phi$. However, an error in θ can also be approximated by an error in specifying the angular orientation of the interferometer axis (i.e., the axis of the conical

---

* The definition of location and velocity errors is provided in Appendix E.
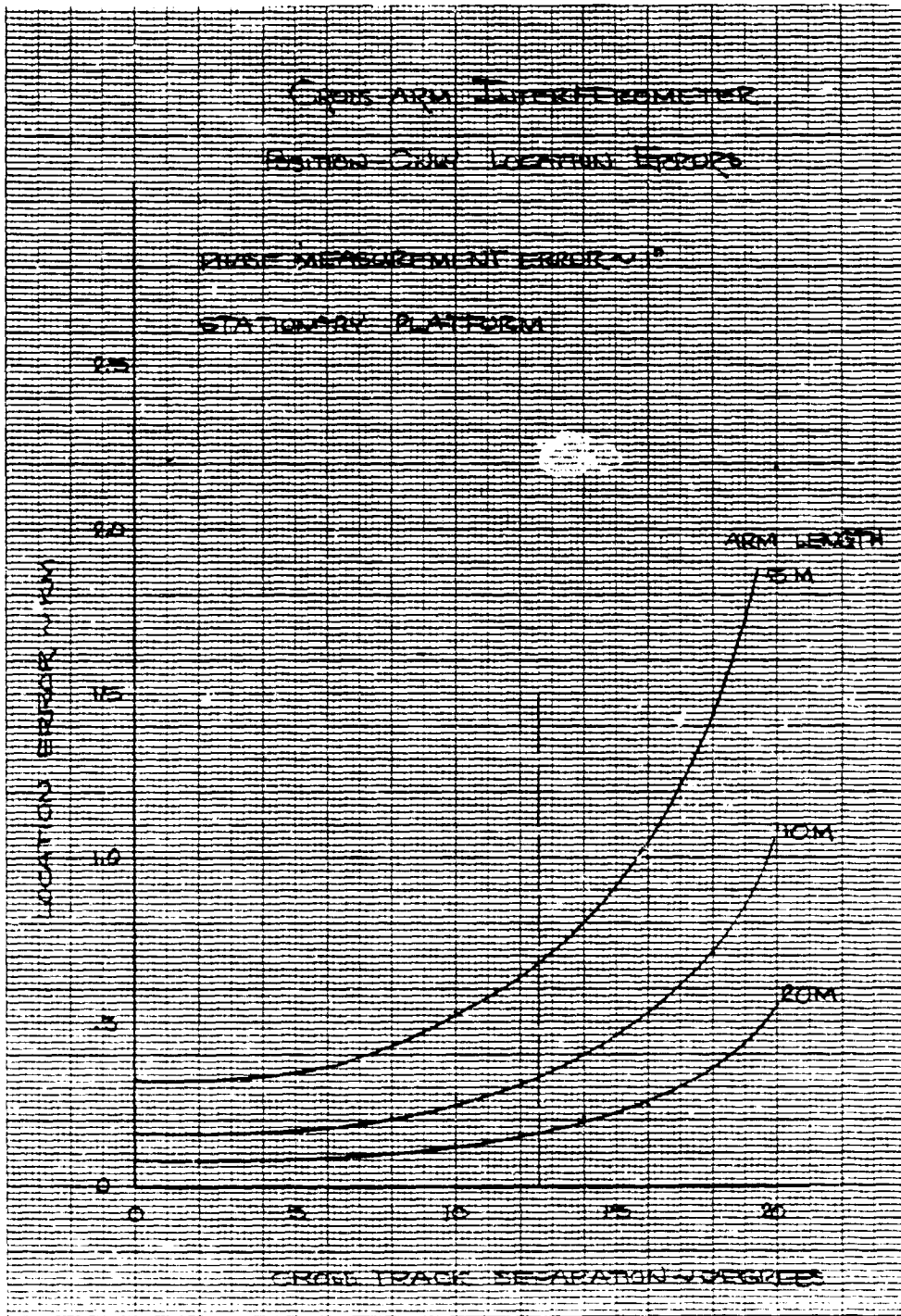
FIGURE 2.2-5. LOCATION ERRORS FOR CROSS-ARM INTERFEROMETER WITH PHASE
MEASUREMENT ERROR ONLY

2-30

surface-of-position). With this approximation, the equivalent phase error corresponding to an orientation error θ_A may be written as

$$\Delta\phi_A = \frac{2\pi L \sin\theta}{\lambda} \Delta\theta_A$$

from which

$$\sigma_{\phi_A} = \frac{2\pi L \sin\theta}{\lambda} \sigma_{\theta_A}$$

Assuming the orientation errors, $\Delta\theta_A$*, are independent of phase measurement errors, then the "equivalent" phase measurement error, σ_ϕ, that can be used in Figure 2.2-5 that includes both measurement, σ_{ϕ_M}, and orientation σ_{θ_A}, errors may be written as

$$\sigma_\phi^2 = \sigma_{\phi_M}^2 + \left(\frac{2\pi L \sin\theta}{\lambda}\right)^2 \sigma_{\theta_A}^2$$

In this expression, the nominal value of θ appears. This means that the "equivalent" standard deviation of phase measurements, σ_ϕ, is actually dependent upon the geometry existing at each platform transmission. In particular, for platforms approaching the satellite's horizon for the horizontal interferometer, the decreasing value of θ tends to suppress the degradation (increase in σ_ϕ) caused by orientation errors. This is at least one effect that counters the trend of severe GDOP degradation effects evident in Figure 2.2-5 as the platform cross-track separation increases.

---

* An inherent assumption is being made that these errors are, in fact, of a random nature from one platform transmission to another. Whether or not this is true--i.e., they may better be approximated by a bias error during an overpass--will depend upon the attitude determination system as well as the mechanical dynamics of the interferometer arms.

A quantitative presentation of the above "equivalent" σ_ϕ
relationship is shown in Figure 2.2-6. The ordinate of this figure is the
σ_ϕ as a function of the standard deviation of orientation errors, σ_{θ_A}
(abscissa). As noted, the right hand graph corresponds to an interferometer
arm length of 20 meters while the left hand graph corresponds to an arm length
of 5 meters. The values of standard deviation of measurement error σ_{ϕ_M}
are those indicated when σ_{θ_A} is zero. Nominal values of θ are 60° and 30°
which is about the minimum to be encountered.

Several conclusions can be drawn from the data of Figure 2.2-6
assuming standard deviations of phase measurement errors are in the one to
five degree range. First, for arm lengths on the order of 20 meters,
measurement errors on the order of one degree contribute little to the
"equivalent" measurement error σ_ϕ when orientation (attitude) errors,
σ_{ϕ_A}, exceed .01 to .02 degrees. For the larger values of σ_{ϕ_M}, this
dominant effect of attitude errors occurs when attitude errors approach and
exceed .04 degrees.

The second conclusion from Figure 2.2-6 is that arm lengths on the
order of 5 meters will experience a doubling of "equivalent" error, σ_ϕ, for
phase measurement errors on the order of one degree when attitude errors
approach .06 degrees. On the other hand, for measurement errors near 5
degrees, attitude errors do not have a significant effect even when they are
as large as .06 degrees.

To more accurately assess the impact of attitude errors, the location
error data presented in Figure 2.2-5 has been re-determined as follows. If
the performance of the attitude determination can be estimated, i.e., σ_{θ_A}
can be estimated, then each interferometer measurement made during an overpass
can be weighted by the "equivalent" standard deviation, σ_ϕ. The resulting
weighted least-square solutions give rise to the location error data provided
in Figures 2.2-7 and 2.2-8.

In Figure 2.2-7, the increased location errors for the cross-arm
interferometer is shown when attitude errors (standard deviations) of .03 and
.06 degrees are assumed. Comparison of these data with the data presented in
Figure 2.2-5 leads to the following conclusions.
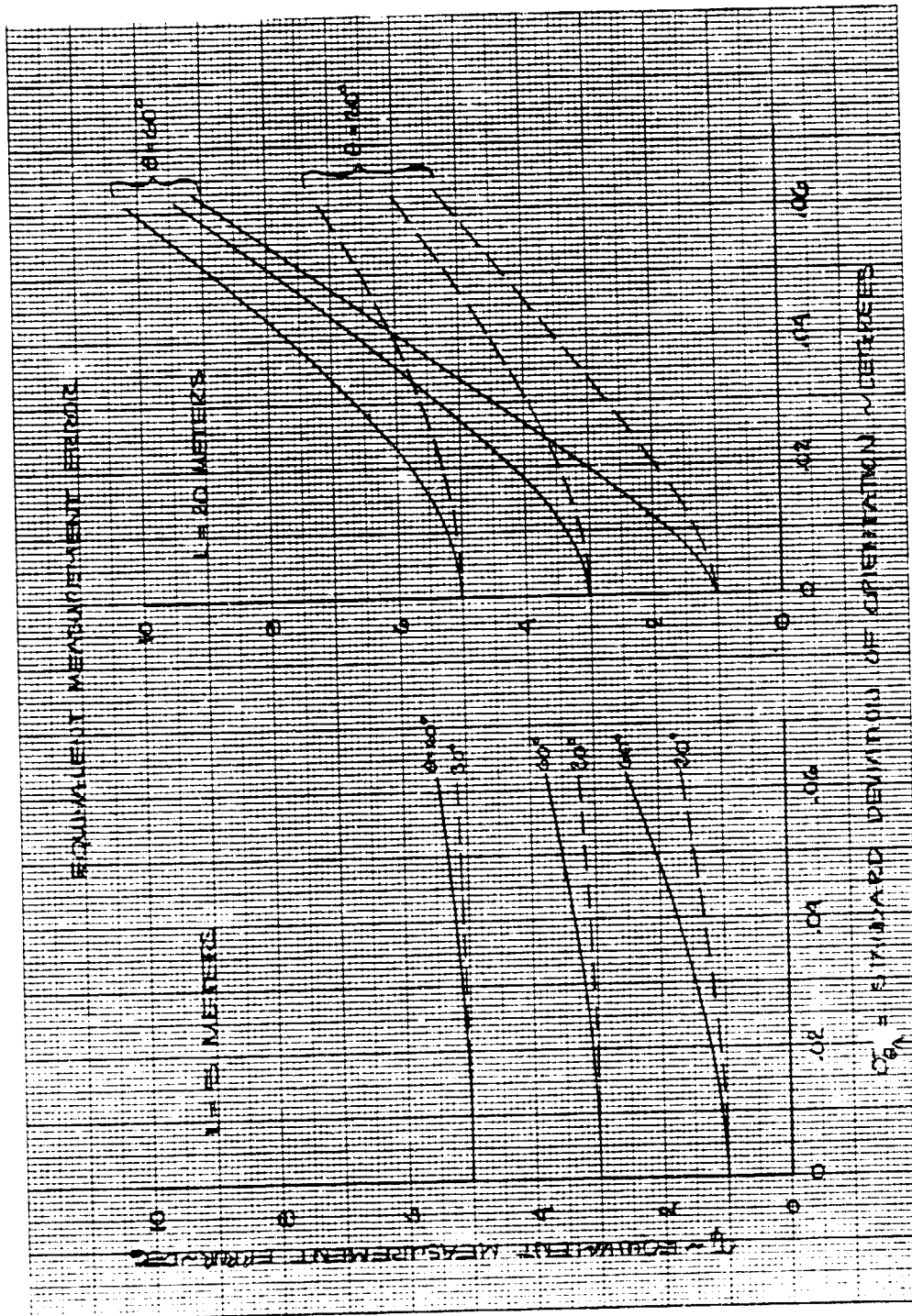
2-32

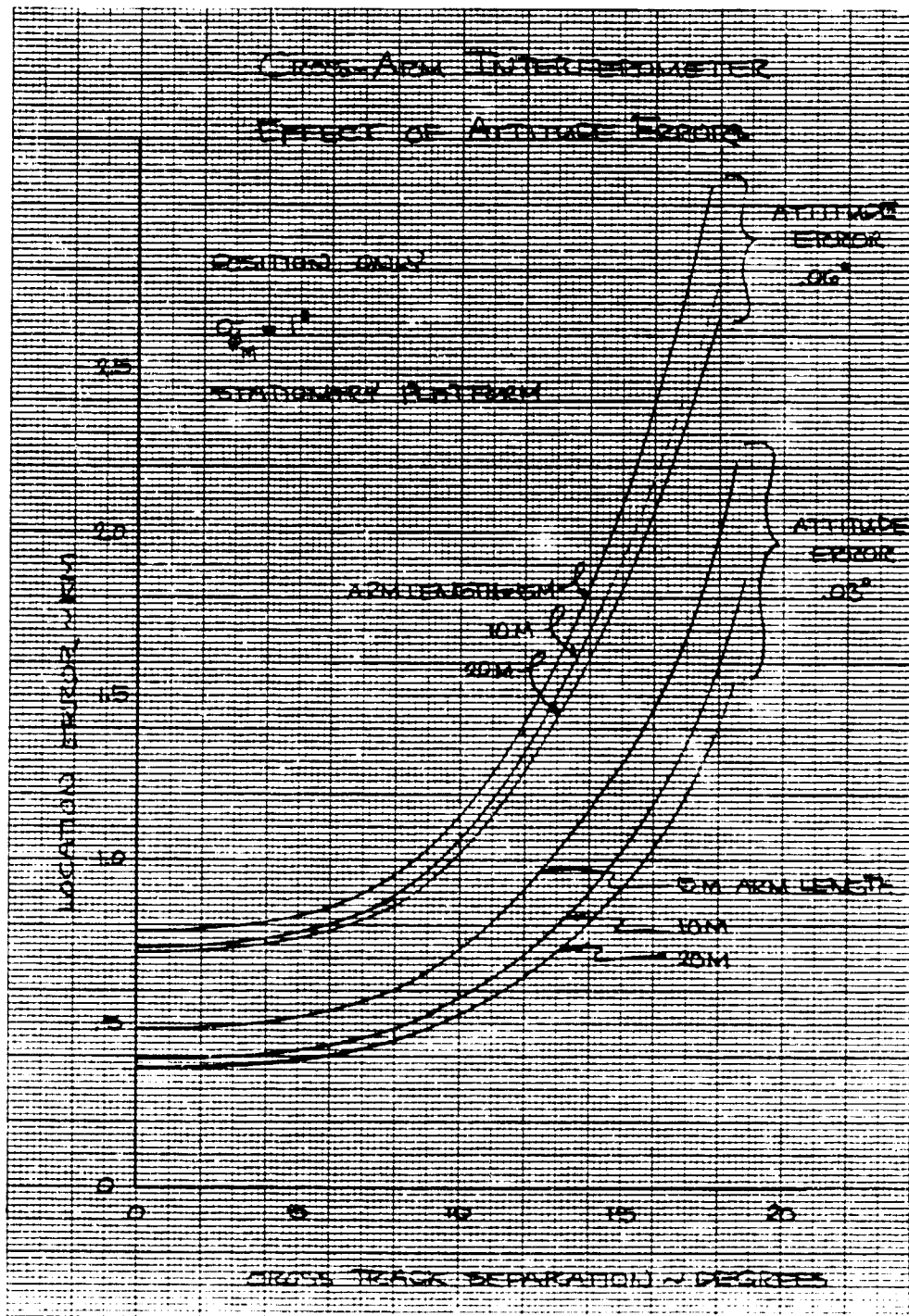FIGURE 2.2-6. EQUIVALENT PHASE MEASUREMENT ERROR INCLUDING ATTITUDE
DETERMINATION ERROR

FIGURE 2.2-7. LOCATION ERRORS FOR CROSS-ARM INTERFEROMETER WITH 1° PHASE
MEASUREMENT ERROR PLUS ATTITUDE ERROR

- For the shorter arm lengths on the order of five meters, location errors increase by 50 and 100 percent over those with no attitude error when the attitude errors are $.03°$ and $.06°$ respectively.

- For arm lengths on the order of 20 meters, the attitude errors of $.03°$ and $.06°$ lead to factors of five to ten increase in location error compared with the zero attitude error case.

These two effects combine to characterize the major overall difference between Figures 2.2-5 and 2.2-7. Namely, the inverse relationship between location error and arm length of Figure 2.2-5 disappears when attitude errors are introduced. In Figure 2.2-5, an increase in arm length from 5 meters to 20 meters decreases location error by a factor of four. However, Figure 2.2-7 indicates that the larger the attitude error, the less important arm length becomes.

While Figures 2.2-5 and 2.2-7 both assume phase measurement errors of $1°$, Figure 2.2-8 presents location errors when the phase measurement error is assumed to be $3°$. These data serve to emphasize the design trade-off of arm length versus attitude error—particularly if there is a direct relationship between arm length and attitude error. This can be seen by comparing the performance of 10 meter arms and $.03°$ attitude error with 20 meter arms and $.06°$ attitude error. For these conditions, the location errors for the 10 meter arms is better than the performance of the 20 meter arms.

In the figures discussed above, the assumption is made that the platform being located is stationary (or of known velocity) so that only position coordinates need to be estimated from the relative phase measurements. However, the performance changes considerably when both position and velocity of the platform is estimated.

In Figure 2.2-9, the errors in estimating both position and velocity of a platform are shown as a function of arm length with attitude error
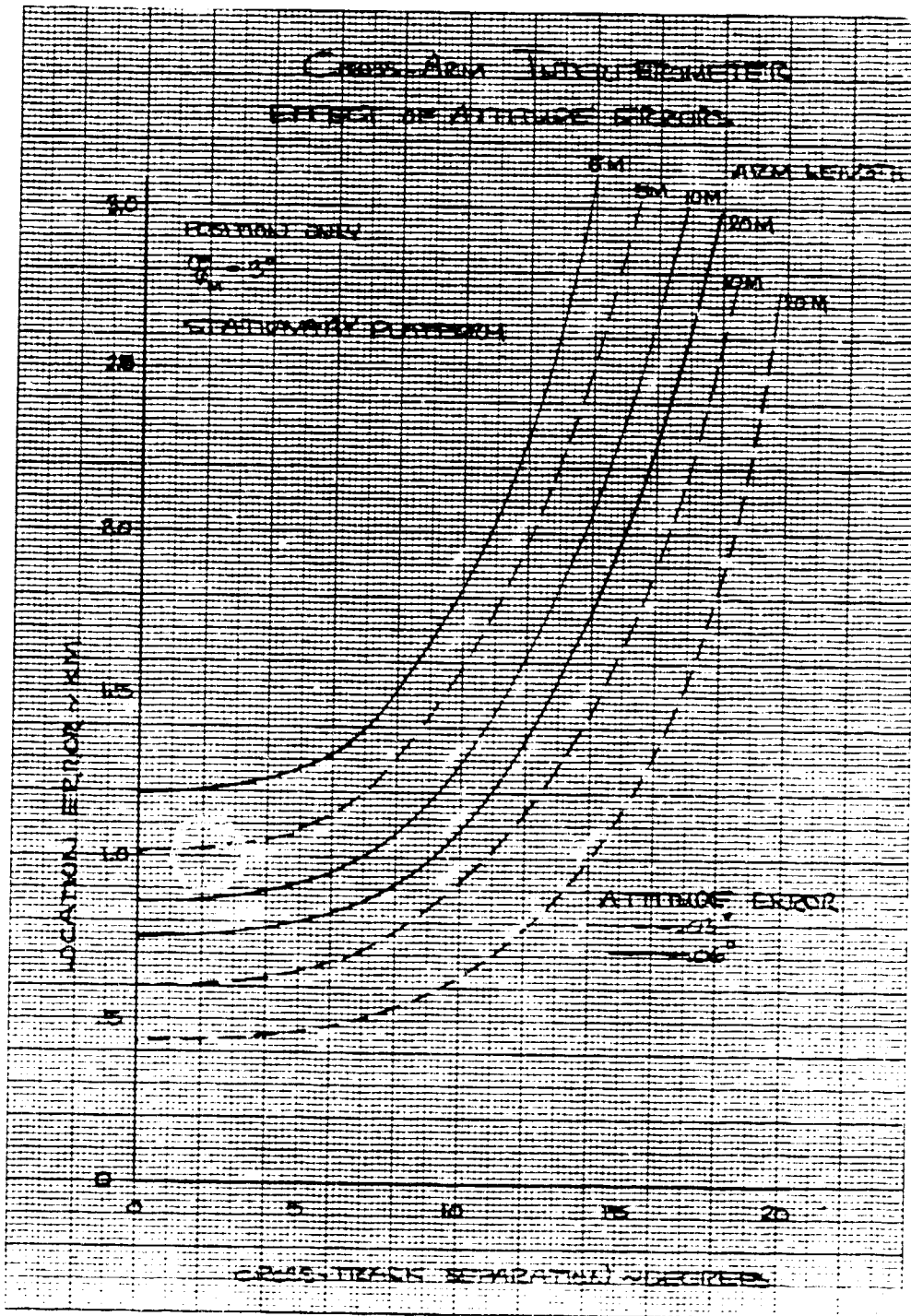
FIGURE 2.2-8. LOCATION ERRORS FOR CROSS-ARM INTERFEROMETER WITH 3° PHASE
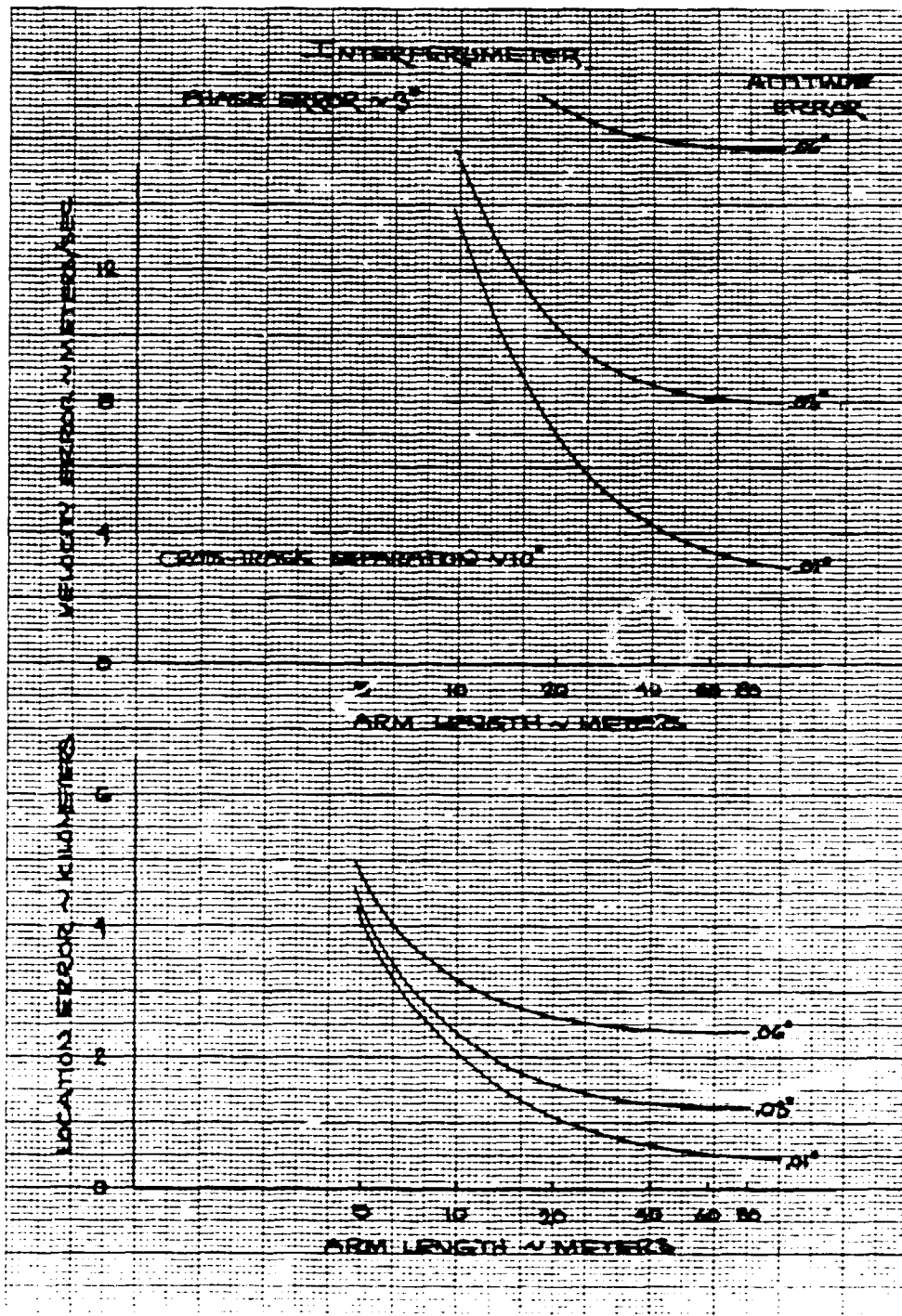MEASUREMENT ERROR PLUS ATTITUDE ERROR

FIGURE 2.2-9. LOCATION AND VELOCITY ERRORS FOR CROSS-ARM
INTERFEROMETER WITH 3° PHASE MEASUREMENT
ERROR PLUS ATTITUDE ERROR

2-37

parameter. As noted, these data correspond to a cross-track separation of 10°
which are the overpass conditions noted in Figure 2.2-4. Also a phase
measurement error of 3° has been assumed so that Figures 2.2-8 and 2.2-9 are
comparable. Note, however, that location errors of Figure 2.2-9 are greater
than those of Figure 2.2-8 for the same combination of arm length and attitude
error. This is due to the requirement to estimate both location and velocity.

The major conclusion to be drawn from Figure 2.2-9 is that the
requirement to estimate platform velocity as well as location requires both
large arm lengths and small attitude errors. If location errors in the order
of one kilometer are required, then arm lengths of 40 meters or greater are
required and attitude errors less than .03 degrees are necessary. If velocity
errors on the order of several meters per second or less are required, then
the arm lengths must approach 60 to 80 meters with attitude errors approaching
.01° or less.

In summary, a cross-arm interferometer can provide estimates of
platform location with errors on the order of one kilometer, when

- The platform is stationary (or of known velocity)

- Arm lengths of 10 to 20 meters are employed with attitude errors
  near .03 degrees.

- Phase measurement errors are on the order of 3°.

However, when both position and velocity of a platform must be
estimated, then a factor of three to four increase in arm lengths and decrease
in attitude errors is required to meet one kilometer location errors and
several meter/second velocity errors. This suggests the need to augment
interferometer measurements.

Interferometer with Doppler Processing

From Figures 2.2-5,-7 and -8, an interferometer suffers rapid
degradation in performance as the cross-track separation between the satellite
and platform increases beyond five degrees in longitude. To suppress this

degradation, frequency (Doppler) measurements of received platform transmissions can be made in addition to the relative phase measurements. The advantages accruing from these additional measurements are:

- Increased noise filtering
- Complementary performance regions

Increased noise filtering comes about merely from an increased number of independent measurements obtained during an overpass. In the case of a cross-arm interferometer, the increase will be 50 percent, i.e., three measurements per platform transmission versus two. The second advantage of complementary performance, however, is more important.

In Section 2.2.2, the degradations of interferometer and Doppler systems due to GDOP effects were discussed. These qualitative discussions led to the suspicion of severe GDOP effects for an interferometer when the platform approached the satellite horizon. This suspicion was confirmed by the variation of location/velocity errors for the cross-arm interferometer. Similarly, the good performance of the interferometer for near-overhead satellite passes was also confirmed. In contrast, a Doppler system experiences GDOP degradation that is severe for near-overhead passes of the satellite while performance is relatively stable as a platform approaches the satellite horizon. A system comprising both Doppler and interferometer measurements should therefore be highly complementary.

Before an assessment of a combined Doppler-interferometer system can be made, an important advantage of the interferometer must be considered. Namely, the interferometer relative phase measurement is virtually immune to instabilities of local platform oscillators. A Doppler system is not. A change in a platform's transmitted frequency away from an assumed or nominal value will rapidly degrade performance unless compensated for. This compensation is part of the RAMS and ARGOS systems. However, this compensation assumes the transmitted frequency will be virtually constant, although offset, throughout the satellite overpass to the extent that oscillators with short-term (10 to 20 minute) stability near one part in 10^9 are required.

In order for a Doppler system to function with platform oscillators of stabilities less than one part in 10^9, compensation must be provided for changes in platform oscillator frequency during a satellite overpass. To evaluate such compensation, the following assumption will be made.

> The time constant of a platform oscillator as may be caused by thermal or aging effects is sufficiently large so that during any 10 to 20 minute period of time its variation of frequency with time is essentially linear.

With this assumption, frequency measurements acquired during an overpass will, in addition to estimating platform position and velocity, also be used to estimate frequency offset and drift rate of the platform oscillator.

In Figures 2.2-10 through -20, the performance of Doppler and Doppler plus interferometer systems are compared. However, before discussing the indivudal figures, a brief description of the objectives is appropriate. These are phrased as the following questions.

- What degradation in performance is experienced when frequency drift of platform oscillators must be estimated

- What degradation in location performance results when platform velocity is estimated

- What performance improvements result from combining cross-arm interferometer measurements with frequency measurements

- What arm length will be necessary to achieve one kilometer location and meter/second velocity errors

- What precision in measuring frequency, relative phase, and attitude is necessary to achieve the one kilometer location and meter/second velocit errors

- Can the desired performance levels be achieved by using a single axis interferometer in combination with Doppler measurements

- How does the ability to estimate both position and velocity from a single satellite overpass impact system design and capacity

To answer these questions, Figures 2.2-10 through -20 present location and velocity errors as functions of cross-track separation between the platform and the satellite sub-track in degrees of longitude assuming the platform is located at the equator. In the case of location errors, four sets of data are presented:

- Location errors when platform position and velocity are estimated and the platform oscillator offset and drift rate must also be estimated.

- Location errors when platform position and velocity are estimated and only the offset of the platform oscillator need be estimated--i.e., the stability of platform oscillators during an overpass are on the order of one part in 10^a

- Location errors when only platform position is estimated but both oscillator offset and drift rate must be estimated.

- Location errors when only platform position and oscillator offset are estimated.

In the case of velocity errors, two sets of data are presented:

- Velocity errors when both oscillator offset and drift rate are estimated

- Velocity errors when only oscillator offset is estimated.

For Figures 2.2-10 through -18, which are directed to the comparison of the different location/velocity estimation systems, the precision with which measurements are made are fixed at the following values:

- Frequency measurement errors have a standard deviation of 0.5 Hz at 400 MHz

- Relative phase measurement errors have a standard deviation of 3° at 400 MHz.

- Attitude errors have a standard deviation of .03°.

The two other system parameters common to these figures are that platform transmissions are separated in time by 90 seconds and the satellite must be 5° above the local horizon of the platform in order to receive a transmission. These two parameters serve to fix the number of transmissions received at the satellite during an overpass as a function of the cross-track separation between the platform and satellite sub-track. This number of transmissions is noted in Figure 2.2-10 only but is the same for the other figures.

Some general comments regarding the data of Figures 2.2-10 through -20 are necessary. As described in Appendix E, location and velocity errors are actually two-dimensional errors in that both should be represented by error distributions as a function of direction (e.g., north, northeast, south, etc.). To simplify presentation, however, the direction resulting in maximum error is determined and this maximum error is presented in the figures.

Another characteristic of the figures is caused by the number of transmissions received and more particularly, the discontinuous change in errors with cross-track separation when the number of transmissions changes. This effect is particularly pronounced when velocity errors are presented. However, in most instances, some poetic license has been taken and smoothed curves are shown.

2-42

A second effect of the number of transmissions is more important from a system viewpoint. The combinations of position, velocity, offset and drift estimates determine the number of parameters estimated. With position and velocity, each having two components, this number of parameters can be as high as six or as low as three. In the case of a Doppler system, one measurement is made for each transmission received. From the number of transmissions indicated in Figure 2.2-10, a Doppler system will then not have many redundant measurements from an overpass to effect noise filtering. To increase redundant measurements, a Doppler system is therefore forced to decrease the time between platform transmissions. This directly reduces system capacity as discussed in Section 2.1.2.

A Doppler plus interferometer system exhibits a significant advantage over the Doppler system in terms of the number of redundant measurements available for noise filtering purposes. For a cross-arm interferometer plus Doppler, each platform transmission results in three independent measurements. This means that even with a cross-track separation of 16 degrees where six transmissions are received, eighteen independent measurements are acquired which is a factor of three in redundancy for the case where the maximum number of six parameters is estimated. Should such redundancy not be necessary, the option is then available to increase the time between platform transmissions thereby increasing system capacity.

One further general comment concerning Figures 2.2-10 through -20. The location and velocity errors presented represent the consequences of the standard deviations of the measurement and attitude errors only. In particular, modeling errors are inherently assumed to be negligible. For example, location errors corresponding to those curves which do not indicate velocity estimation represent the location of platforms that are in fact either stationary or of known velocity. Similarly, when only oscillator offset is estimated, no allowance is made for errors resulting from oscillator drifting during an overpass. Because of this, the magnitudes of the errors presented in Figures 2.2-10 through -20 should be viewed as the minimum errors to be anticipated.

With these general comments, Figure 2.2-10 indicates the degradation in location errors for a Doppler-only system as a result of the requirement to estimate oscillator drift during an overpass. The lower curve represents the errors for a Doppler system wherein only frequency offset is estimated. This curve is representative of present Doppler systems typified by RAMS and ARGOS. The upper curve is the consequence of having to estimate oscillator drift rate also. As can be seen, for cross-track separations greater than 8° to 10°, location errors become considerably larger; i.e., nominally double the "offset only" estimates at 10° separation. For Doppler-only systems, the system/cost trade-off between higher location errors versus lower platform cost implied by the necessity to estimate oscillator drift is important.

It should be emphasized that the location errors of Figure 2.2-10 correspond to either stationary platforms or platforms of known velocity. A Doppler-only system is not able, from a single satellite overpass, to estimate platform velocity without significant error (hundreds of meters/second and or tens of kilometers). The ability of Doppler plus interferometer systems to provide reasonable location and velocity errors from a single overpass of the satellite therefore represents a very significant improvement in capability.

In Figures 2.2-11 and -12, the location and velocity errors of a 5 meter cross-arm interferometer augmented by frequency measurements of a Doppler system are shown for the four different parameter sets (algorithms). While the location errors are comparable to the Doppler-only, position-only performance of Figure 2.2-10, the location errors when velocity is estimated can be seen to be reasonable numbers. However, the increase in errors associated with the requirement to estimate oscillator drift compared with offset only should be noted. Also, there is a rapid divergence of errors as cross-track separations greater than 8° to 10° are encountered. It is important that this divergence does not occur for smaller cross-track separations. As discussed previously, if location/velocity estimates are required at least once every twelve hours and these can be obtained from a single overpass of a satellite, then 10° is about the maximum cross-track separation that needs to be coped with.
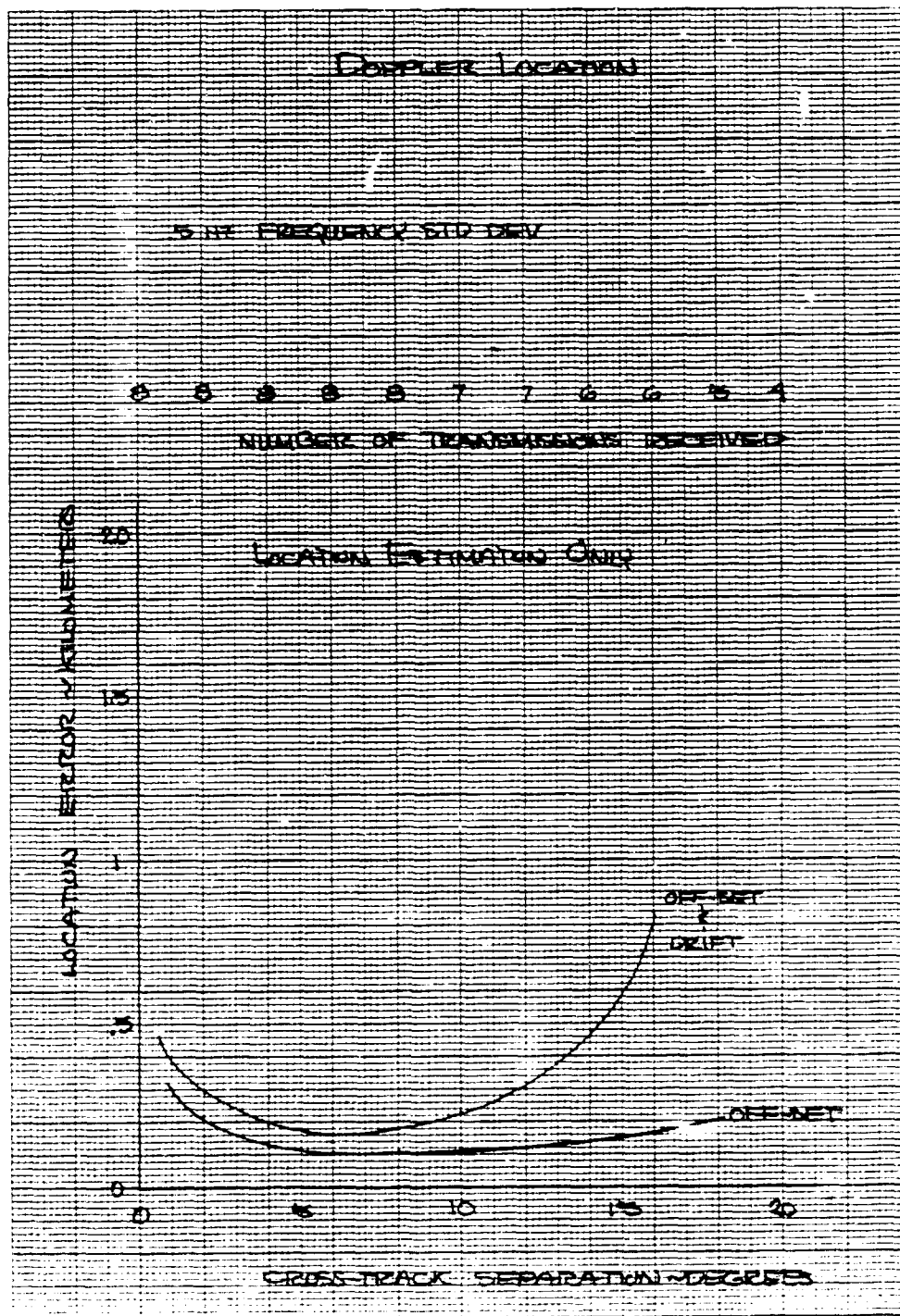
FIGURE 2.2-10. LOCATION ERRORS FOR DOPPLER SYSTEM ESTIMATING LOCATION, OFFSET AND DRIFT
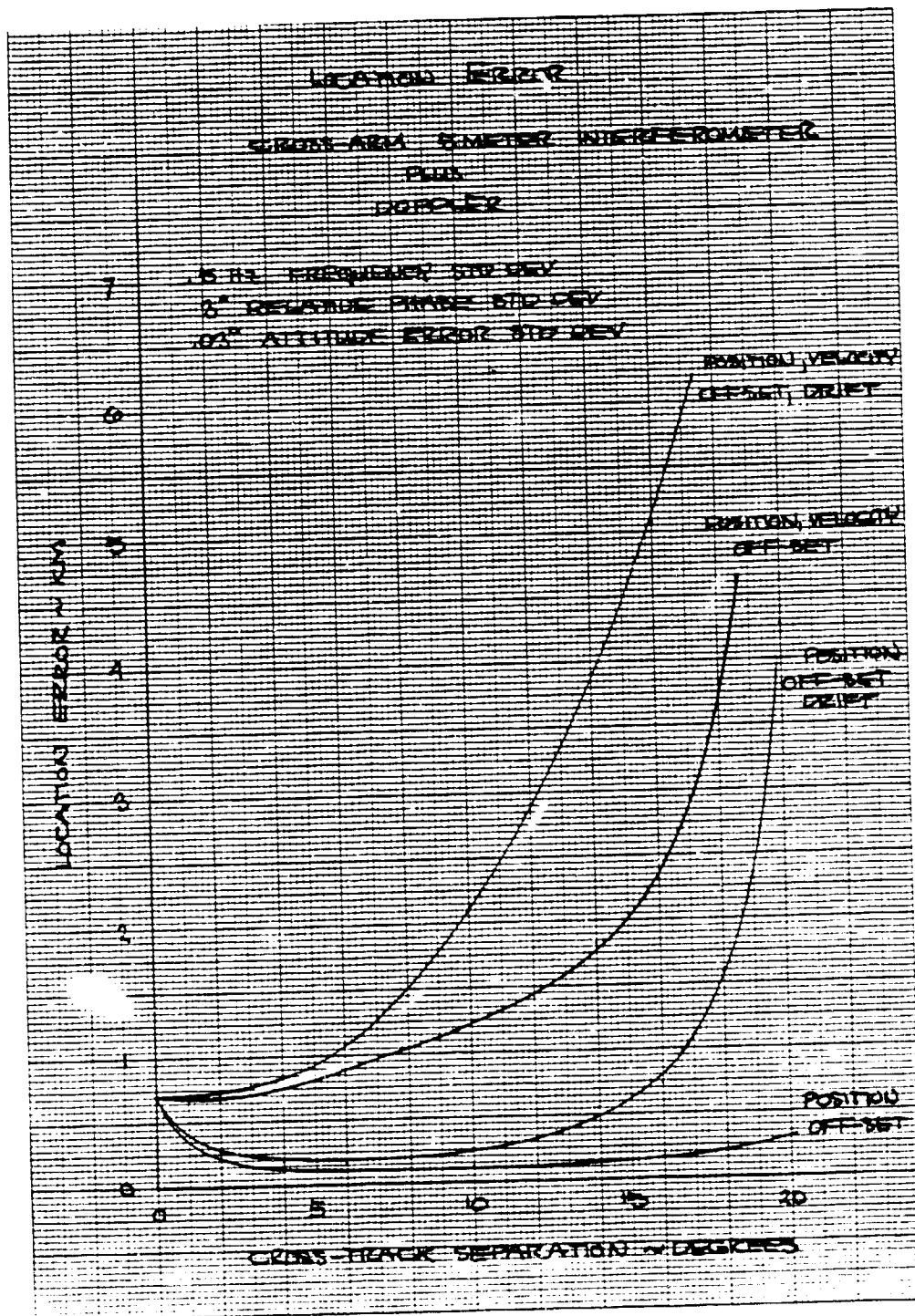
FIGURE 2.2-11. LOCATION ERRORS FOR FIVE-METER CROSS-ARM INTERFEROMETER
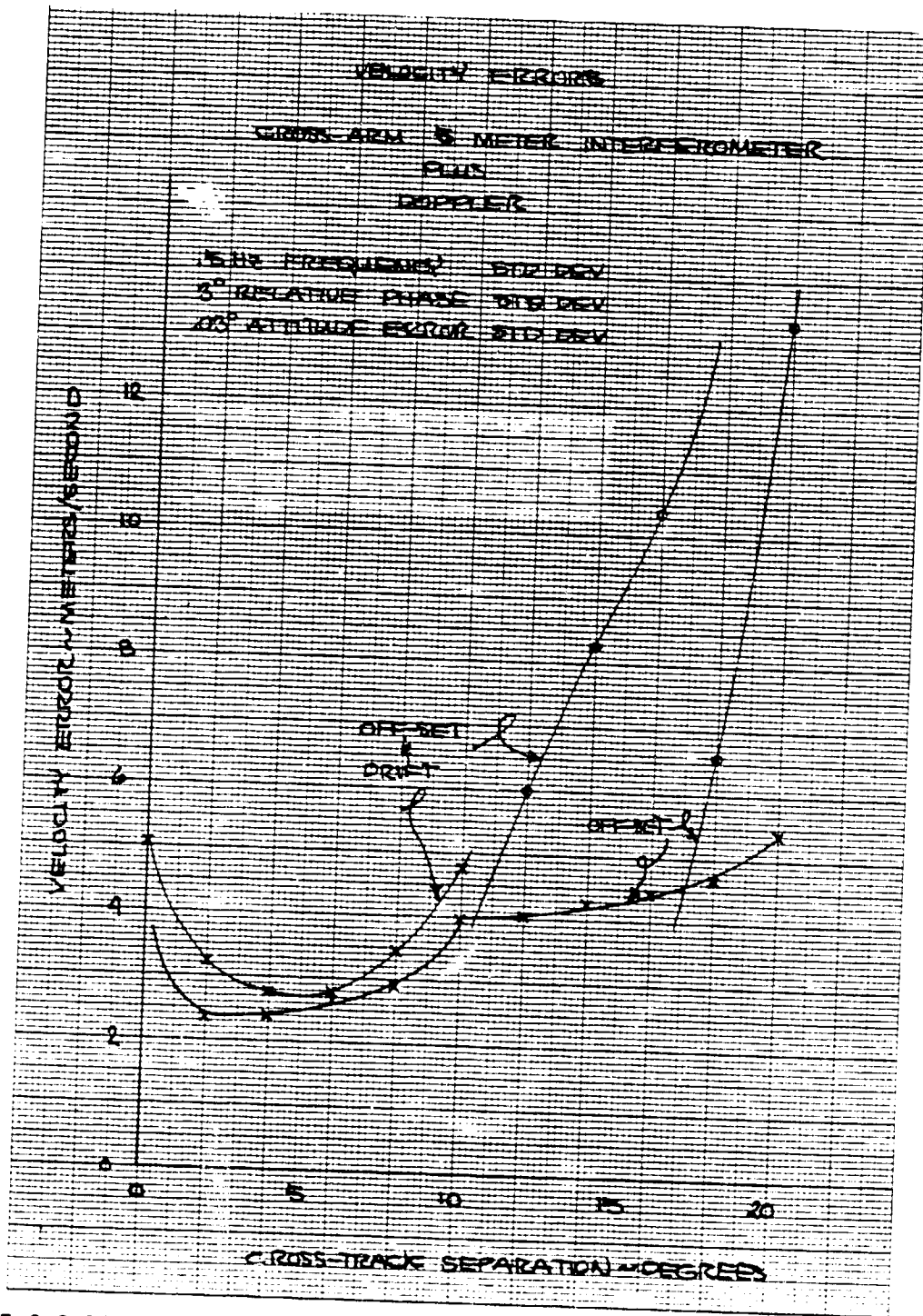PLUS DOPPLER SYSTEM

FIGURE 2.2-12.   VELOCITY ERRORS FOR FIVE-METER CROSS-ARM INTERFEROMETER
PLUS DOPPLER SYSTEM

Figure 2.2-12 presents the errors in estimates of velocity for the "offset and drift" and "offset only" algorithms. The 10° cross-track separation is seen to be particularly important. At separation values less than 10°, velocity errors range between 2 and 4 meters per second with small differences between the two algorithms; i.e., the drifting oscillator does not significantly degrade performance. However, for separations greater than 10°, the velocity errors can be seen to be significantly greater for the drifting oscillator cases.

The only difference between Figures 2.2-11 and -12 and Figures 2.2-13 and -14 is that the cross-arm interferometer arm lengths are assumed to be 20 instead of 5 meters. However, a comparison of the two pairs of figures shows a considerable improvement for the 20 meter arms. Location errors out to cross-track separations of 10° are consistently less than one kilometer even for the case of velocity estimation coupled with drifting oscillators. Similarly, velocity errors are now in the regime of one to two meters per second as opposed to two to four meters per second. Comparison of these data with the performance of a cross-arm interferometer by itself or with a Doppler-only system, serves to emphasize the complementary nature of Doppler plus interferometry.

The next two pairs of figures represent the performance of a single-axis interferometer coupled with Doppler. As noted, the single axis is oriented perpendicular to the satellite orbit plane, i.e., cross-track. The justification for considering a single axis interferometer as well as this orientation is based upon the previous discussions of geometric concepts and GDOP effects. Briefly, one of the greatest deficiencies of a Doppler system is the poor GDOP effects that occur when the satellite approaches an overhead pass and the relatively poor definition of cross-trace platform position and velocity components. By orienting an interferometer cross-track, the lines-of-position it creates tends to be perpendicular to Doppler lines-of-position.
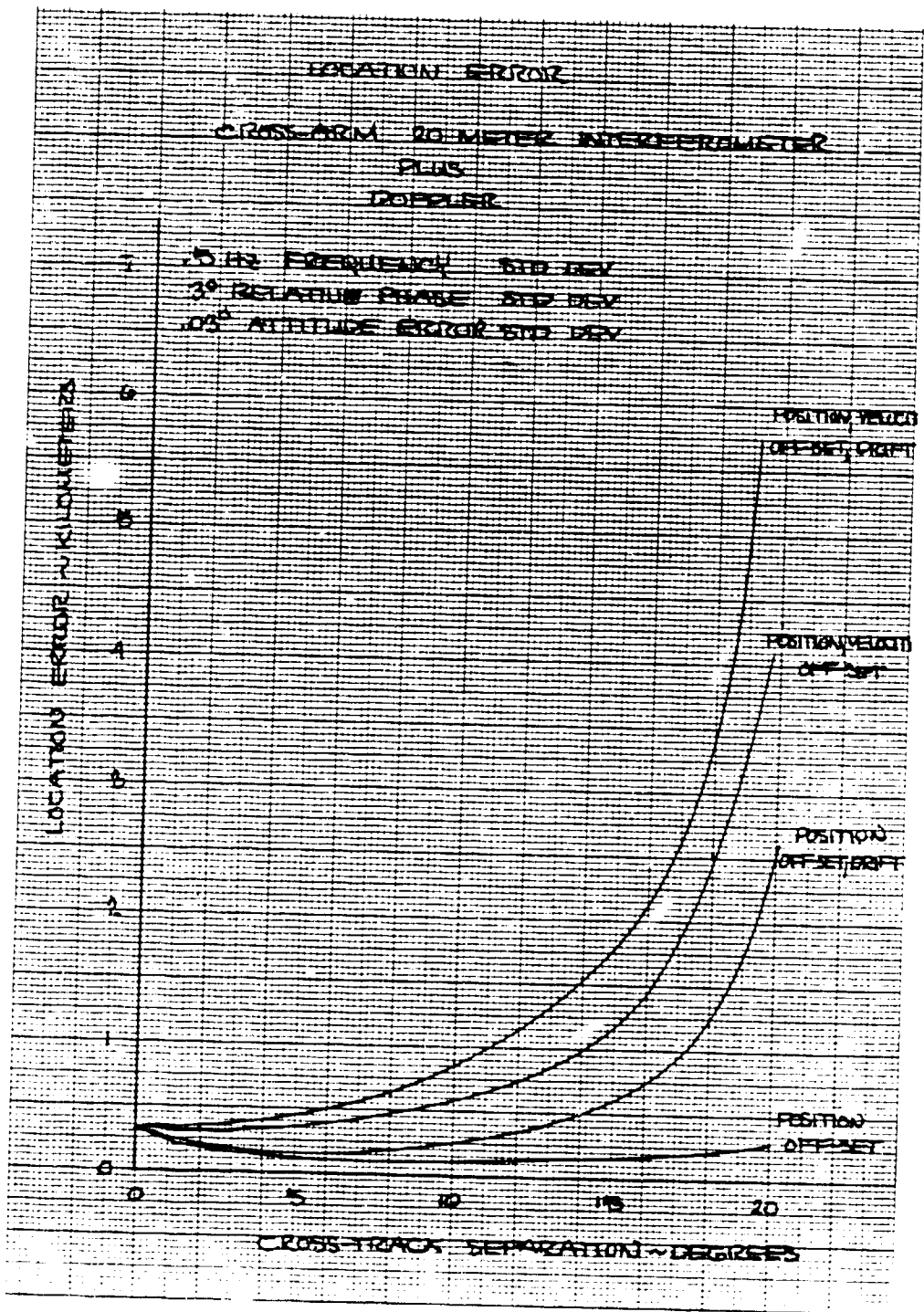
FIGURE 2.2-13. LOCATION ERRORS FOR TWENTY-METER INTERFEROMETER PLUS DOPPLER SYSTEM
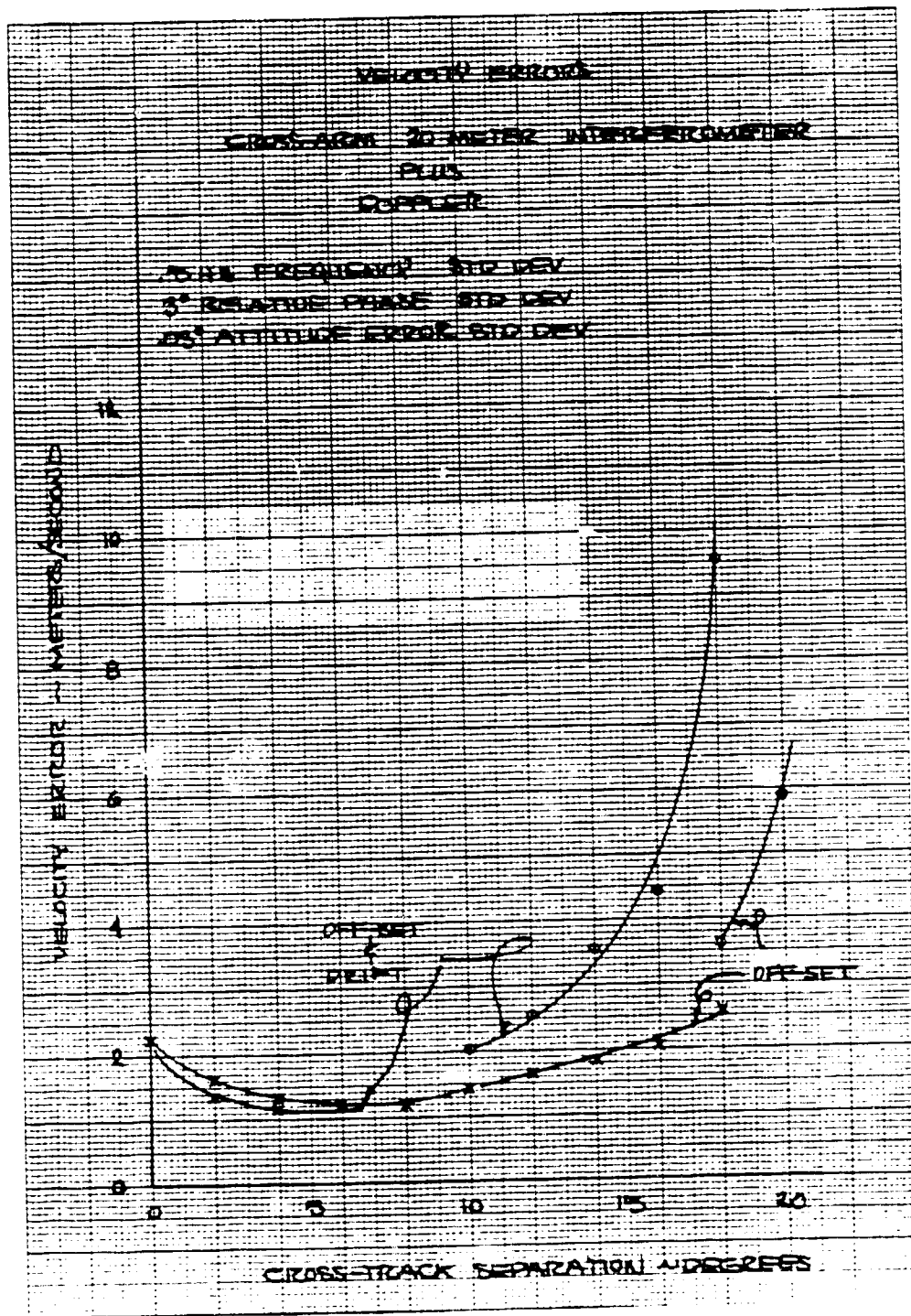
FIGURE 2.2-14. VELOCITY ERRORS FOR TWENTY-METER CROSS-ARM INTERFEROMETER
PLUS DOPPLER SYSTEM

In Figures 2.2-15 and -16, the location and velocity errors for the cross-track 5 meter interferometer plus Doppler are shown. A comparison between these data with those of the cross-arm 5 meter interferometer-plus-Doppler (Figures 2.2-11 and -12) shows that the in-track axis of the cross-arm interferometer does not significantly improve either location or velocity errors. The in-track axis is essentially aligned with the velocity vector of the satellite which means the lines-of- position it creates from each transmission are duplicates of those created by frequency measurements except for differences in orientation and measurement errors. Therefore, the basic contribution of the in-track axis is to add additional measurements for purposes of noise filtering rather than suppressing any GDOP effects.

Figure 2.2-17 and -18 present location and velocity errors for a 20 meter cross-track interferometer plus Doppler. The increased arm length can be seen to essentially halve both location and velocity errors to values of approximately one kilometer and two meters per second at the maximum cross-track separation of 10°. Again, little degratation is seen in performance compared with the 20-meter cross-arm interferometer plus Doppler system. (Compare Figures 2.2-13 and -14 with Figures 2.2-17 and -18.)

In the previous presentations of location and velocity errors, their variation with cross-track separation was shown. These variations indicated that errors generally increase with cross-track separation. Additionally, if the errors at a 10° cross-track separation are acceptable, then at least one estimate of position and velocity can be acquired every twelve hours. For this reason, subsequent location and velocity error presentations correspond to those occurring at the cross-track separation of 10°. This also enables an assessment of some of the assumptions made in the previous figures.

To this end, Figures 2.2-19 and -20 show the effects of variations in phase measurement error and attitude error as a function of cross-arm interferometer arm length. From these figures, the following conclusions can be drawn.

- For phase measurement errors on the order of 3° (Figure 19), arm lengths greater than about 20 meters do not significantly improve performance

2-51
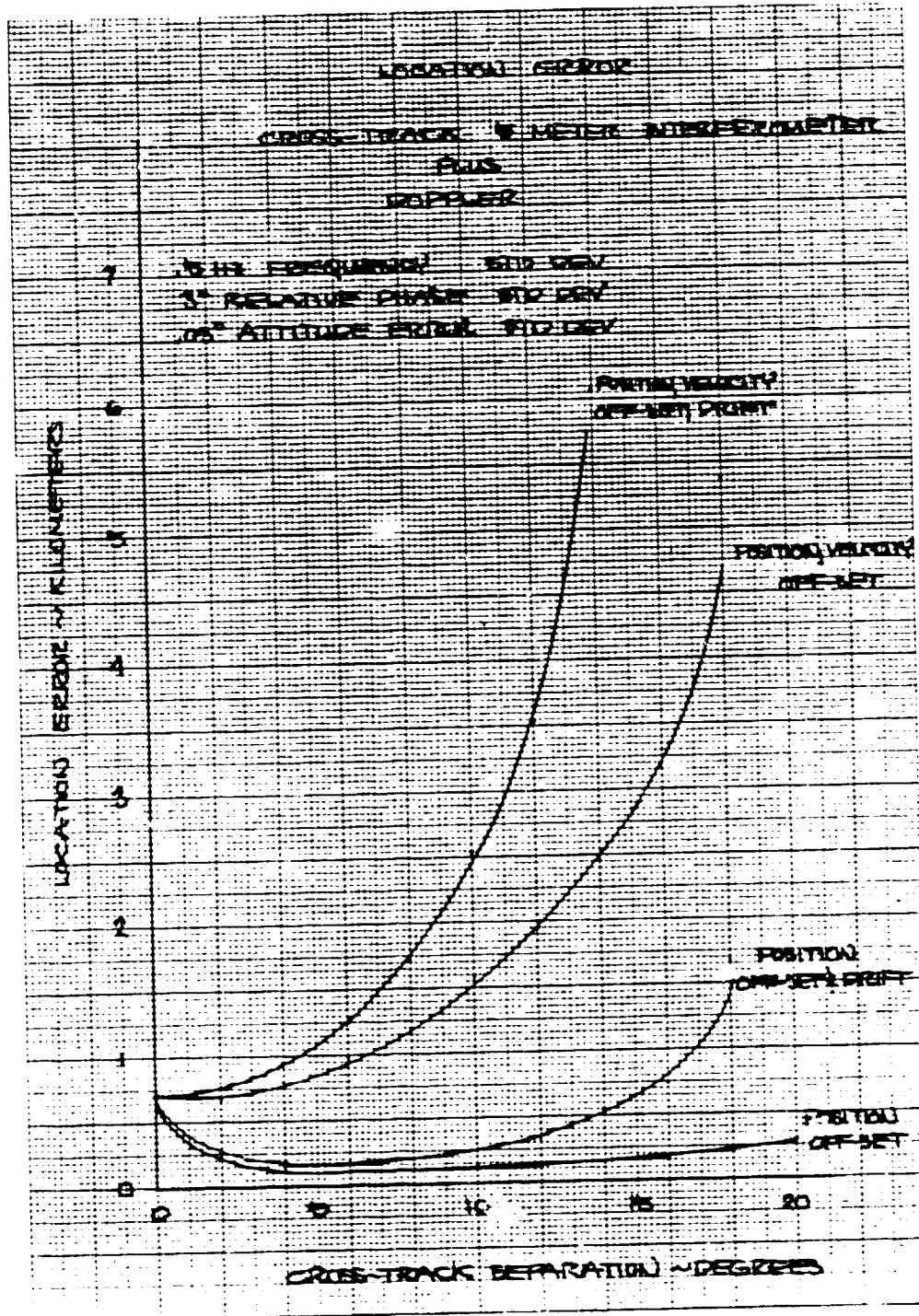
FIGURE 2.2-15.   LOCATION ERRORS FOR FIVE-METER SINGLE-ARM INTERFEROMETER
PLUS DOPPLER SYSTEM

2-52
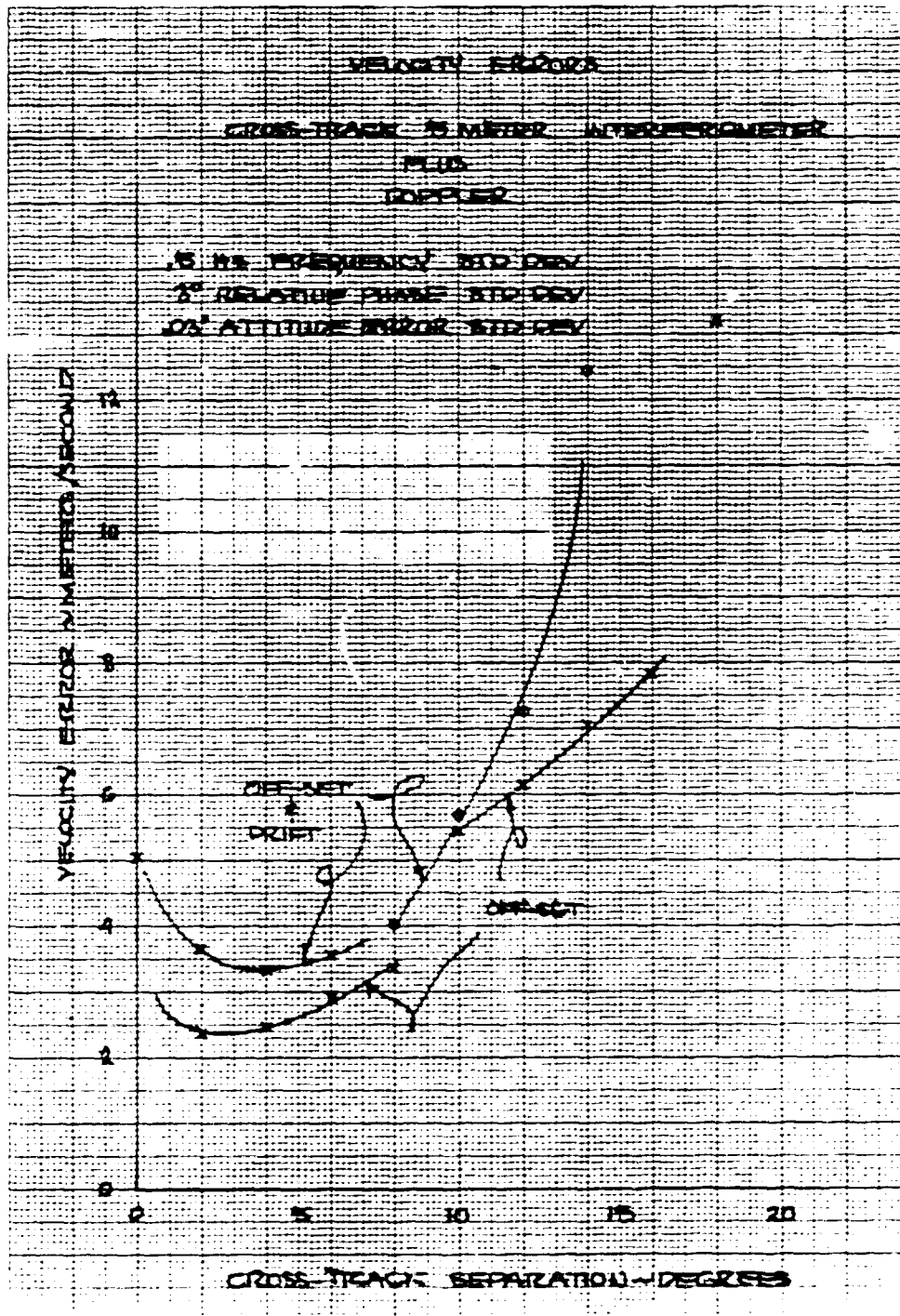
FIGURE 2.2-16.   VELOCITY ERRORS FOR FIVE-METER SINGLE-ARM INTERFEROMETER
PLUS DOPPLER SYSTEM

FIGURE 2.2-17. LOCATION ERRORS FOR TWENTY-METER SINGLE-ARM INTERFEROMETER
PLUS DOPPLER SYSTEM

FIGURE 2.2-18.   VELOCITY ERRORS FOR TWENTY-METER SINGLE-ARM INTERFEROMETER
PLUS DOPPLER SYSTEM

FIGURE 2.2-19. LOCATION AND VELOCITY ERRORS FOR CROSS-ARM INTERFEROMETER
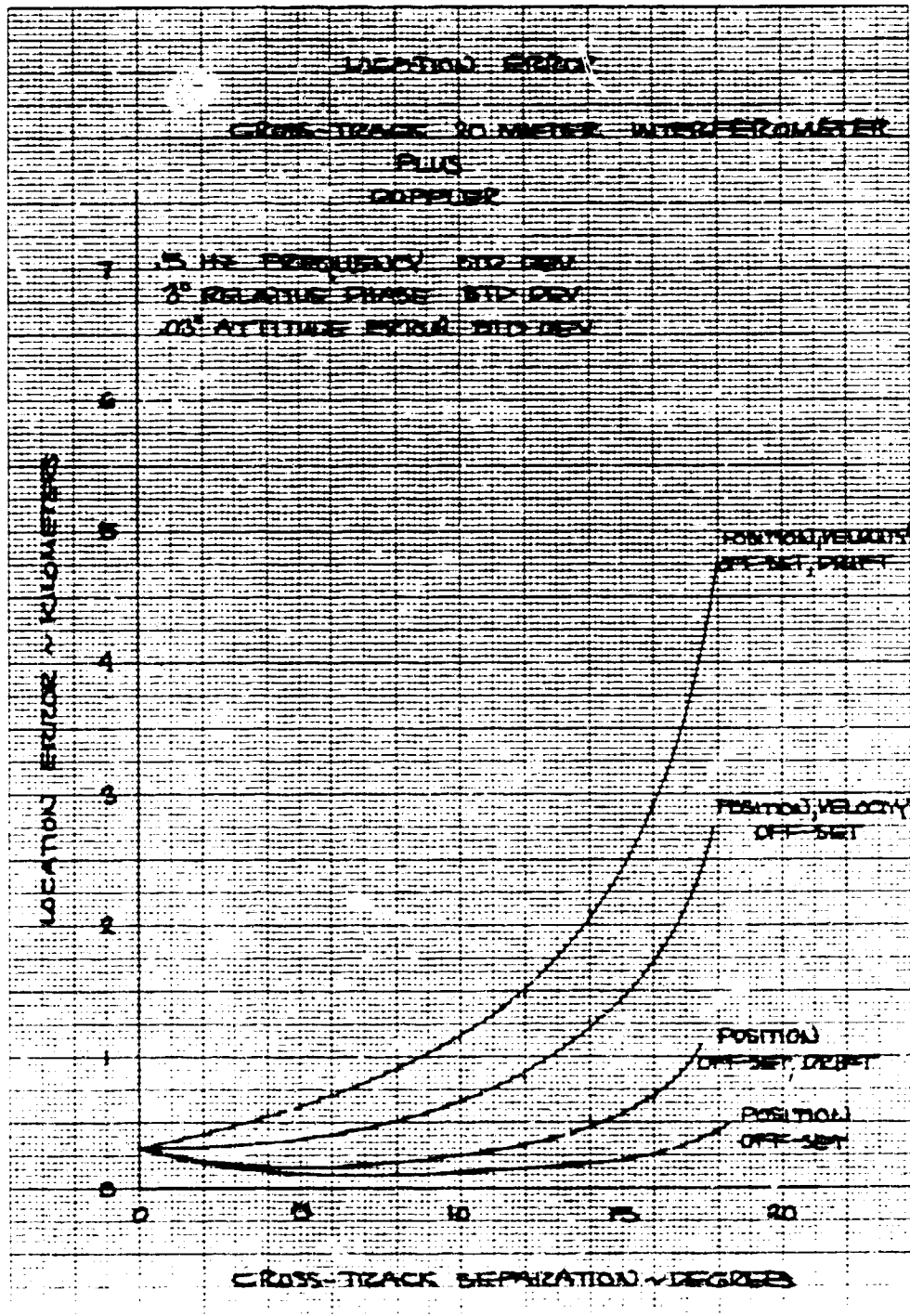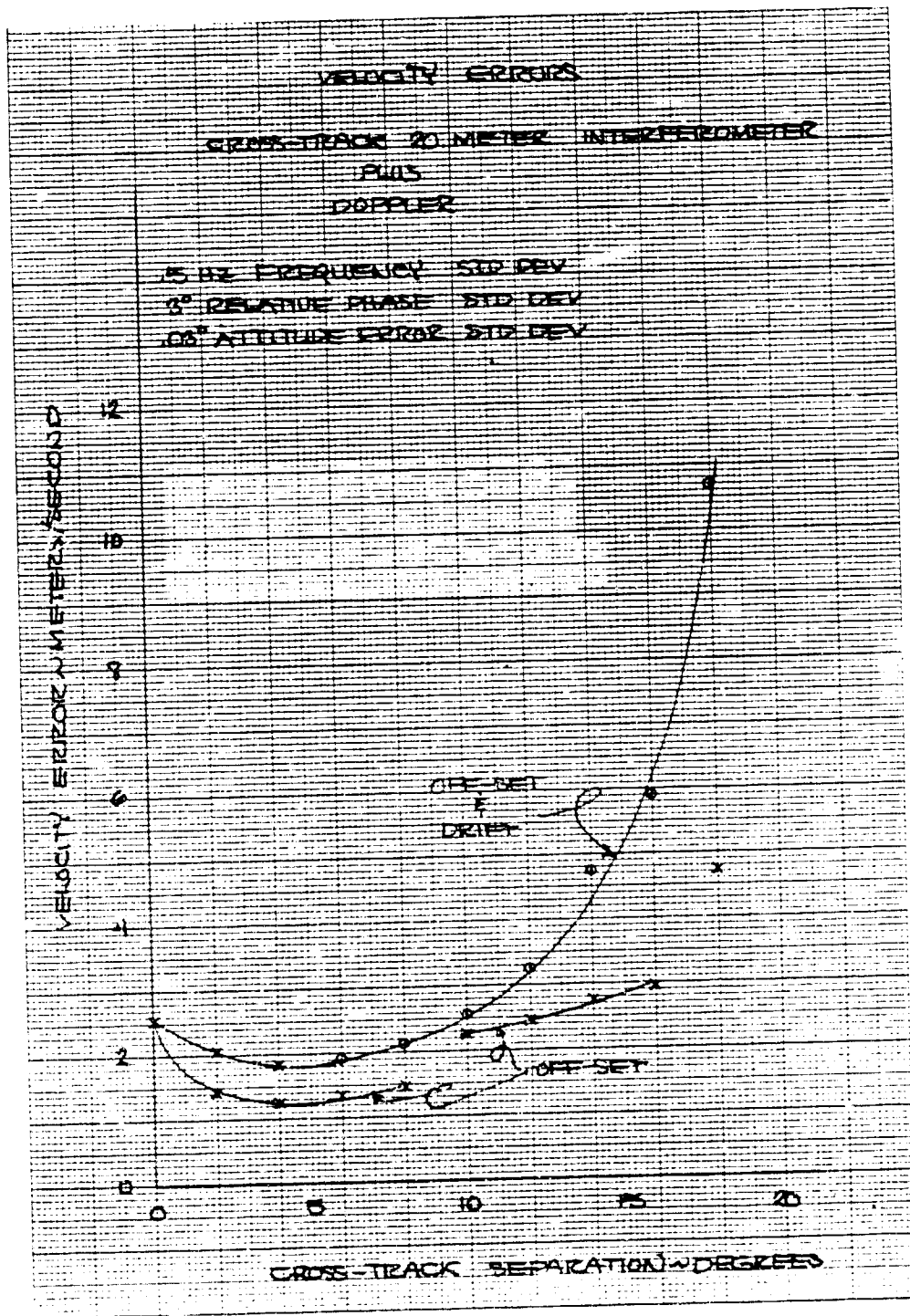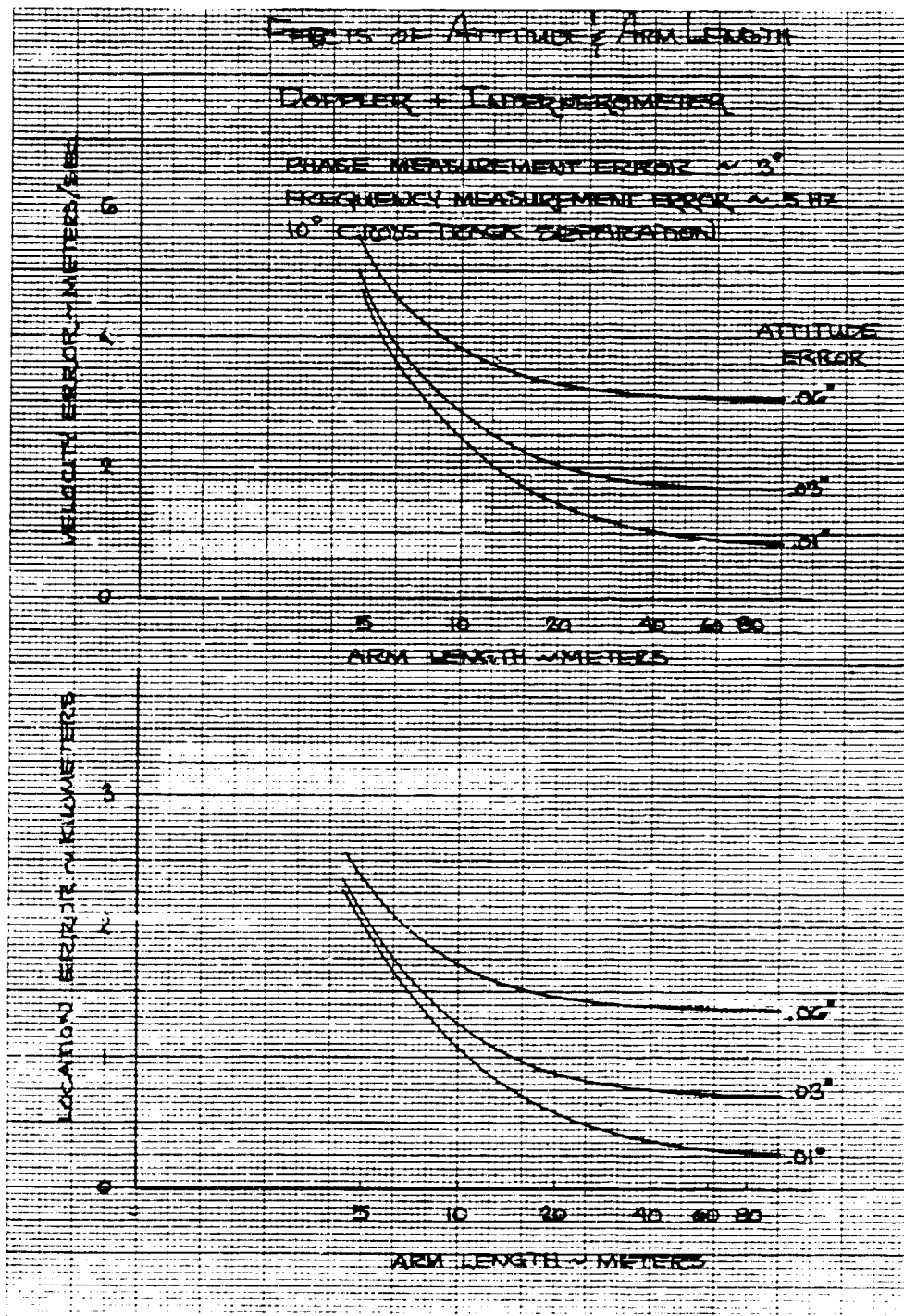PLUS DOPPLER SYSTEM WITH 3° PHASE
MEASUREMENT ERROR WITH VARYING ARM LENGTH

2-56
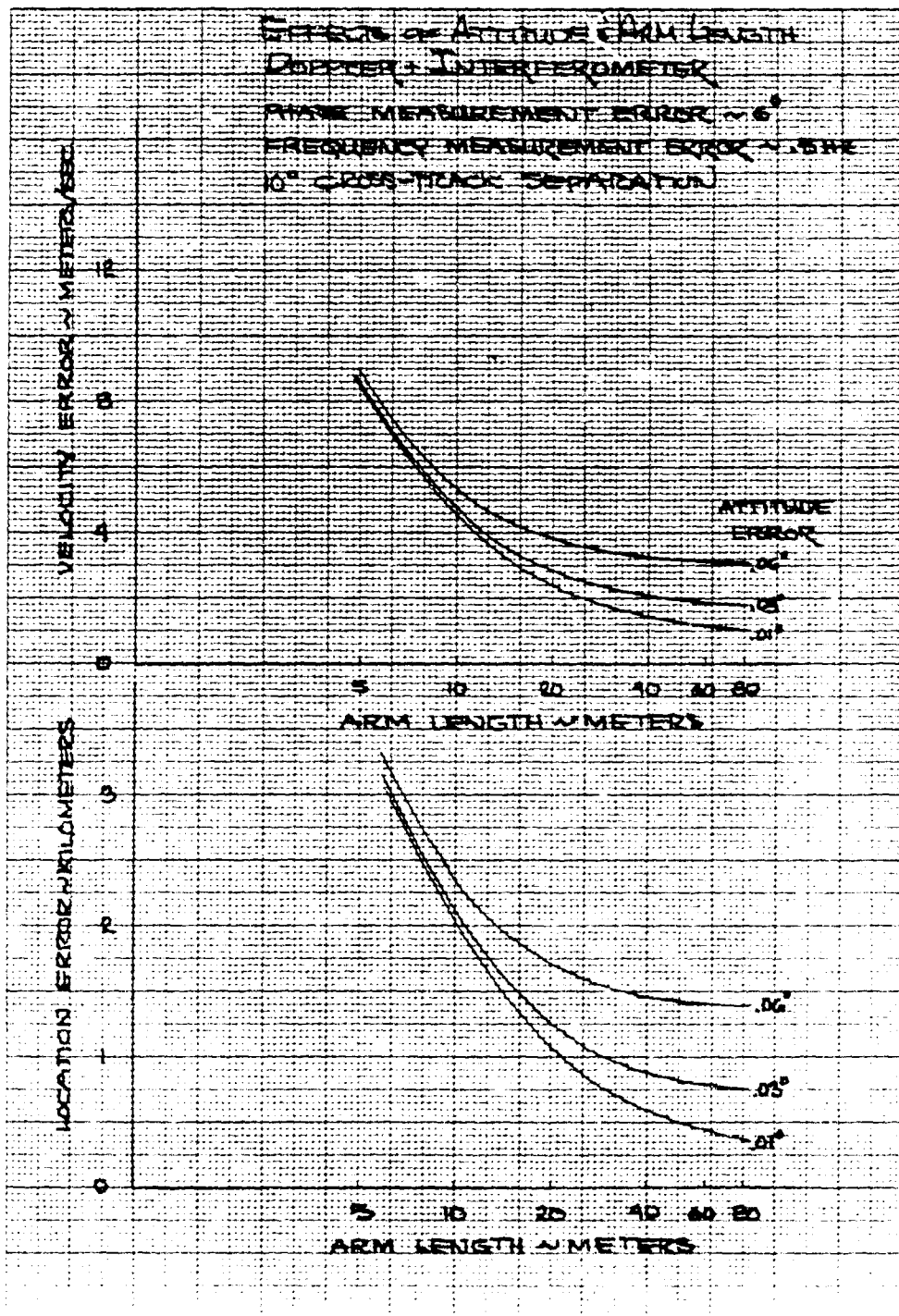
FIGURE 2.2-20.   LOCATION AND VELOCITY ERRORS FOR CROSS-ARM INTERFEROMETER
PLUS DOPPLER SYSTEM WITH 6⁰ PHASE
MEASUREMENT ERROR WITH VARYING ARM LENGTH

- For phase measurement errors on the order of 6° (Figure 20), significant performance improvements accrue until arm lengths near 40 meters are reached.

- In order to achieve location errors of one kilometer or less, attitude errors must approach .03° to .04° with arm lengths of 15 or 30 meters for 3° or 6° phase measurement errors.

- In order to achieve velocity errors of one meter per second or less, phase measurement errors less than 3° will be required along with attitude errors less than .01°. Even with these error levels, arm lengths near 40 meters will be required.

Another important system parameter which has been held fixed at 90 seconds is the interval of time between platform transmissions. As shown in Section 2.2.2, the capacity of random access systems is approximately proportional to this parameter, i.e., doubling or halving the 90 seconds will double or halve system capacity if all other parameters remain the same. However, there will be an inverse effect on location and velocity errors due to the consequent increase or decrease in the number of platform transmissions received during an overpass. Figure 2.2-21 indicates the sensitivity of location and velocity errors to the time between platform transmissions.

In Figure 2.2-21, a single-arm cross-track interferometer combined with Doppler of noted arm lengths is assumed, with a cross-track separation and the errors noted. Both location and velocity errors are shown versus the time between platform transmissions and as a consequence, the number of transmissions received is noted. The major conclusion from the data presented is that at specified levels of location and velocity errors, larger arm lengths will significantly increase the allowable time between transmissions thereby significantly increasing system capacity. For example, at a two kilometer location error, a five meter arm length requires sixty seconds between platform transmissions while a ten meter arm achieves two kilometer error at about 115 seconds. In this case, doubling the arm length essentially doubles system capacity.

2-58
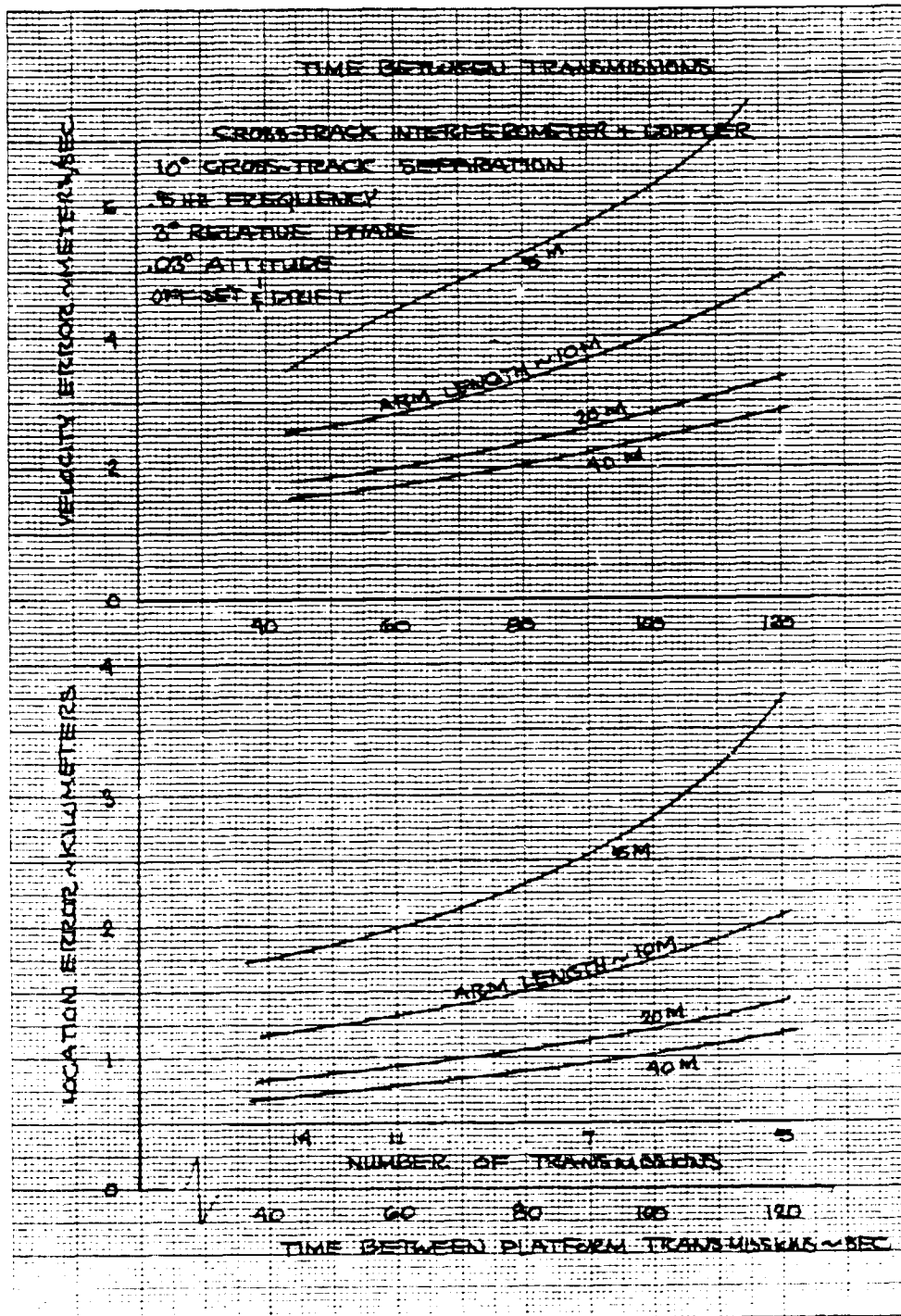
FIGURE 2.2-21.   LOCATION AND VELOCITY ERRORS FOR SINGLE-ARM INTERFEROMETER
PLUS DOPPLER SYSTEM WITH VARYING
TIME BETWEEN TRANSMISSIONS

3.0   IMPLEMENTATION STUDIES

3.1   INTRODUCTION

Implementation studies are necessary to insure that the system concepts are sound, identify critical subsystem performance requirements, and arrive at an estimate of the volume, mass and power consumption burdens the hardware will place on a host spacecraft. The objective is not to design the optimum system but only to derive a possible way of applying the advanced concepts to accomplish the desired system performance. Through this, the trade-offs possible between subsystem parameters are established, and a basis is provided for more detailed study or experimentation.

The following aspects of system implementation were studies and are described in this section.

- Interferometer Ambiguity Resolution. The required placement of the third, ambiguity-resolution, antenna with respect to the two primary antennas. Ways of configuring antennas to give two orthogonal-baseline interferometers.

- Phase Measurement. Hardware techniques for determing phase difference. Achievable precision of phase measurement during modulation and time required to achieve it.

- Number of Data Extraction Channels. Required number of signal processing channels for a given probability of receiving too many simultaneous transmissions for the system to accommodate.

- Calibration Techniques. Methods of calibrating the position and velocity determination function using on-board signal injection and platforms at know locations.

The results from the above are used to postulate possible hardware configurations. Estimates of the volume, mass and electrical power requirements are made on the basis of these candidate systems.

3.2   INTERFEROMETER AMBIGUITY RESOLUTION

The phase measurement obtained from the interferometer is only
correct to within a multiple of 360°. Multiple sources, located so that they
produce phase differences differing by 360°, cannot therefore be
distinguished. Alternately, a given phase measurement indicates that the
source is at one of several possible physical angles off the baseline axis.
The number of possible angles is roughly twice the number of wavelengths in
the baseline. A means of identifying which of the several possible angles is
the true one is with an ambiguity-resolving antenna. This is a third antenna,
placed on the same baseline as the primary interferometer antennas, that forms
a second interferometer with one of the primary antennas. This auxiliary
interferometer has a short baseline and much lower resolution.

The ambiguity-resolving interferometer need only resolve the angle to
the source to within an interval smaller than the spacing between two of the
ambiguous angles. This and the electrical angle resolution impose an antenna
spacing requirement on the auxiliary interferometer. A second constraint on
the antenna spacing is that there be no ambiguity in the indication of the
auxiliary interferometer. To achieve this, the spacing must be such that the
angle between ambiguities is greater than the angle subtended by the Earth.
In this way, only one of the ambiguous angles corresponds to a possible
platform location, and the ones that do not can be eliminated.

3.2.1   Antenna Spacing Relations

The required spacing for the primary and auxiliary antennas will now
be found. for simplicity, we assume the interferometer baseline is oriented
perpendicular to the orbit plane, and restrict our attention to platforms
located along the line perpendicular to the sub-track, intersecting at the
sub-satellite point. For this simplified geometry, the physical angle
resolution, $\delta\eta$, at a given nadir angle, η, is proportional to the electrical
phase angle resolution, $\delta\phi$, and the baseline length, L:

$$\delta\phi = (2\pi L/\lambda) \cos \eta \; \delta\eta$$

where λ is the wavelength. Note that as the nadir angle increases, for fixed baseline length and phase resolution, the physical angle resolution becomes worse ($\delta\eta$ increases).

As an example of the application of this relation, the baseline length required for 1 km ground resolution will be found for the case of an interferometer in a 750 km orbit receiving from a platform located 1300 km from the sub-track. This is the situation depicted in Figure 2.2-4. Electrical phase resolution is assumed to be $1°$. The nadir angle, η, for this geometry is $55.7°$, and the angle $\delta\eta$ corresponding to 1 km on the ground is $0.014°$. The above formula results in L = 15 m for λ = 0.75 m (400 MHz).

Given a phase measurement ϕ, the platform could be located at any of n ambiguous nadir angles. The number of these is given by

$$n = \left\lfloor L/\lambda - \phi/2\pi \right\rfloor + \left\lfloor L/\lambda + \phi/2\pi \right\rfloor + 1$$

where the notation $\lfloor \cdot \rfloor$ means the largest integer less than the quantity in the brackets. For the above case (λ = 0.75 m, L = 15 m), n = 40 or 41. Figure 3.2-1 shows the ambiguous angles for a case where n = 11. The ambiguity-resolving (auxiliary) interferometer must have a resolution of at least the spacing between the ambiguous angles. This spacing is close to λ/L radians at nadir and increases with increasing nadir angle. Applying the earlier formula to the auxiliary interferometer, the relation between L' and $\delta\phi'$, the auxiliary interferometer baseline length and phase resolution, is found to be

$$\delta\phi' < (2\pi L'/\lambda)(\lambda/L) = 2\pi L'/L$$

at nadir (η = 0). The degradation in angular resolution with increasing nadir angle noted earlier turns out to be exactly cancelled by the increase in the spacing between ambiguous angles, so the above insures sufficient resolution for any η. A second condition must be satisfied by the auxiliary interferometer antenna spacing: The physical angle indicated by the auxiliary interferometer cannot itself be ambiguous. This effectively restricts the
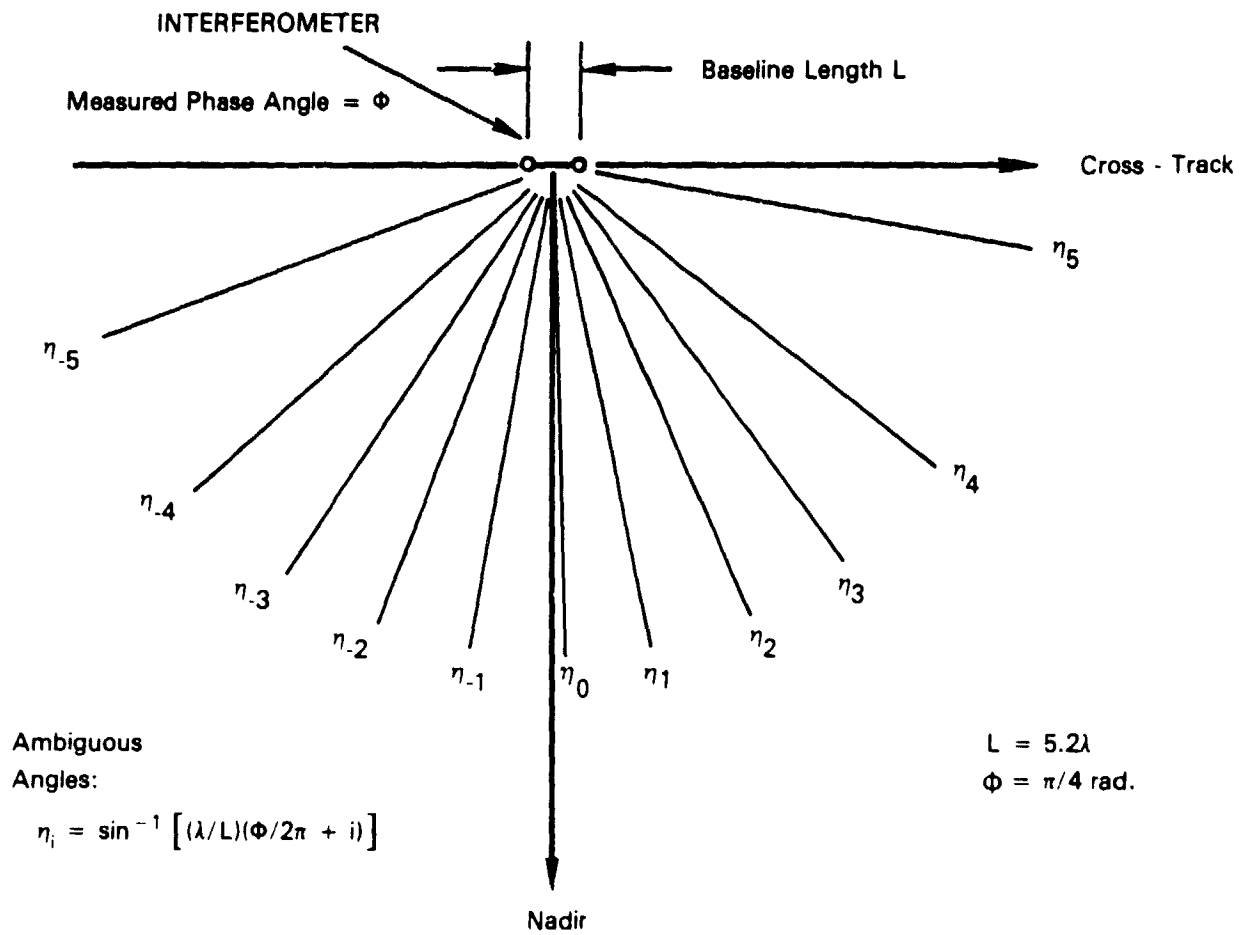
FIGURE 3.2-1.   INTERFEROMETER AMBIGUITIES

maximum baseline length to about one wavelength. The limits on the baseline
length are then

$$(\delta\phi'/2\pi) \, L < L' < \lambda$$

This also puts a limit on the phase resolution of the auxiliary
interferometer. For the example, $\delta\phi'$ must be less than $\pi/10$ radians, or $18°$,
and L' must be less than about 0.75 m.

3.2.2   Two-Baseline Interferometer Configurations

A complete RF interferometer position-location system requires two
baselines. Each baseline must have two pairs of antennas, one for the primary
and one for the auxiliary interferometer. Eight antennas might be arranged as
shown in Figure 3.2-1a to realize the two complete baselines.

It is desirable to minimize the number of antennas, since each
antenna in the system adds cost, complexity, and calibration requirements.
This can be done by sharing one or more antennas between different functions.
Since the system needs only phase differences between antenna pairs, a given
antenna may serve in more than one pair. Figure 3.2-1b through d show various
configurations made possible by combining antenna functions. The most
desirable configuration to use may depend on other factors than simply the
number of antennas. For example, the central location of the ambiguity
resolution antennas in configuration (b) might allow them to be mounted
rigidly on the body of the spacecraft while the primary antennas may require
booms. Configuration (c) uses one less antenna than (b) but two additional
antennas may need to be mounted on booms. Finally, with configuration (d),
three antennas could be mounted on the spacecraft body, with only two on
booms. However, the booms need to be longer than with the other
configurations.

The necessity of making two phase measurements for each baseline has
implications in the configuration of the signal processor as well as the
antenna system. The phase measurements could be simultaneous or consecutive.
If the primary and auxiliary phase measurements proceed simultaneously, then

3-5
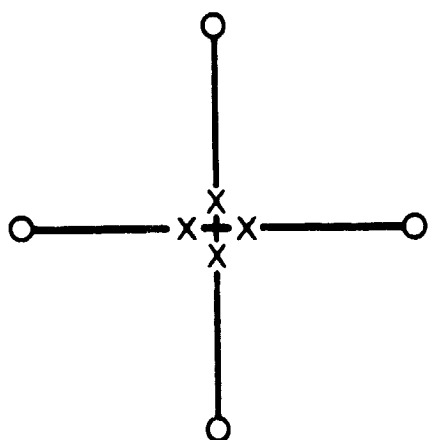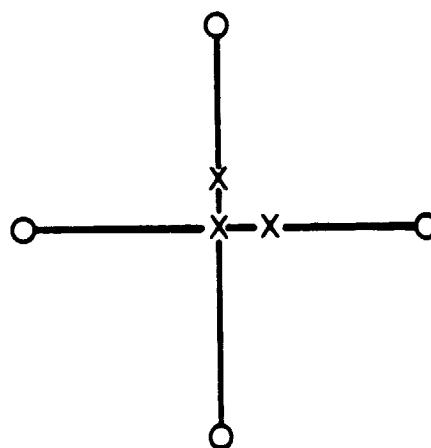
(a) 8 Antennas

(b) 7 Antennas
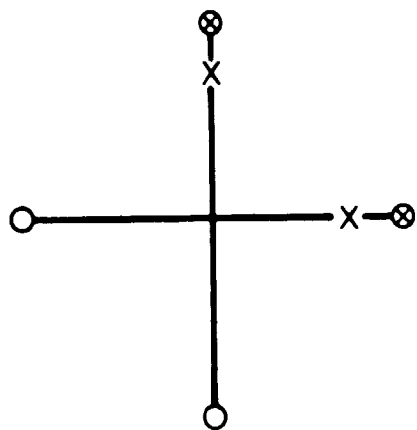
(c) 6 Antennas
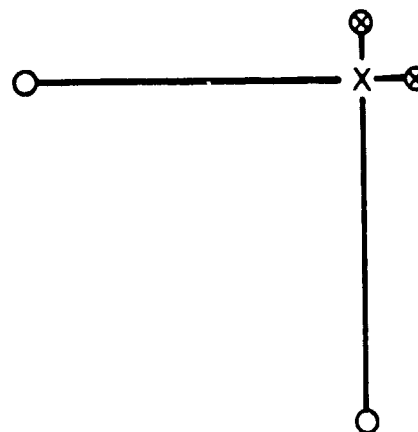
(d) 5 Antennas

o primary interferometer antenna

x auxiliary (ambiguity-resolution)
    interferometer antenna

FIGURE 3.2-2.   INTERFEROMETER ANTENNA CONFIGURATIONS

the phase measurement circuitry of the data extraction unit must be
duplicated. This implies greater volume, mass and power consumption for the
flight system. On the other hand, if the phases between the antenna pairs are
measured in sequence, more time must be allowed for the phase measurement, so
the minimum duration of the platform transmission must be greater. This
affects the self-interference probability and thus the system capacity.

3.3 PHASE MEASUREMENT

3.3.1 Basic Interferometer LDCS Operation

The surface transmitters that the LDCS is to locate each periodically
emit a short burst of power at a very low duty factor. The frequency of the
transmission is located at some point in the system bandwidth determined by
the initial setting combined with Doppler shift. The distribution of
transmitting frequencies can be considered as random. The relative phasing of
the transmission cycles of the transmitters is also random. It is the task of
the LDCS, during each random burst, to identify the platform transmission,
measure the relative phase angles between the interferometer antennas, and
extract the digital information modulating the carrier. Further, it should be
capable of doing this for a number of bursts that happen to overlap or
coincide in time, but are separated in frequency. This can be accomplished
with a measurement system of the type shown in Figure 3.3-1. (For a combined
interferometer/Doppler LDCS, the frequency of the signal must be measured and
reported as well. In this and subsequent discussion, a pure interferometer
system is presumed.)

The system works as follows. The Signal Detection Unit identifies a
possible platform transmission and quickly determines the frequency at which
it is being received. The frequency measurement is passed to the control
unit, which commands a data extraction unit that is not in use to tune to the
signal. After the signal has been acquired by the phase-lock loop of the data
extraction unit, the phase differences between the antennas are found, and the
signal is demodulated. The measured phase differences are converted into
binary form and are transmitted to the ground along with the platform
identification code and data, if any. The phase measurement must be done in

3-7
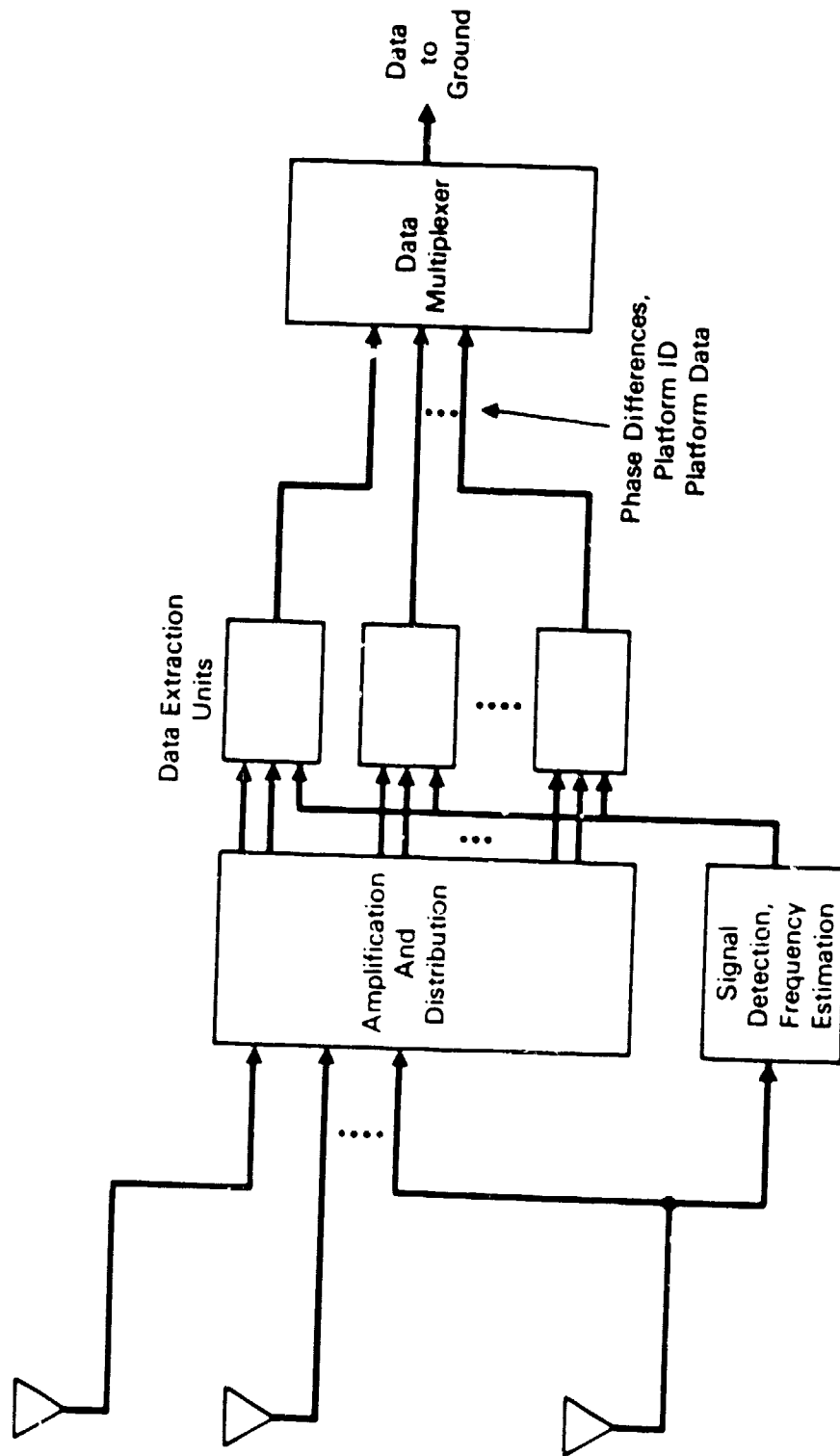
FIGURE 3.3-1. INTERFEROMETER LOCATION AND DATA COLLECTION SYSTEM

the face of rapidly changing signal frequency, due to Doppler shift, and it needs to be done as quickly as possible consistent with the required measurement accuracy. We now consider techniques to accomplish this.

3.3.2   Phase Measurement Techniques

The signals to be compared in phase are all accompanied by thermal noise, and they are all at the same, varying, frequency. Phase comparators normally require at least one input signal to have a high amplitude and low noise content. This suggests the use of a tracking filter (implemented, naturally, as a phase-locked loop) on one or more of the signals before the phase comparison. Figure 3.3-2 shows two alternate applications of this technique. In one case, both inputs to the phase detector are filtered. In the other case, only one signal is filtered, and the phase comparator output is low-pass filtered, to reduce the noise passed on from the unfiltered input. These two approaches are theoretically equivalent, but one may be preferred over the other due to practical considerations. Both of the techniques have a drawback, however, that arises from the frequency dynamics of the Doppler-shifted signals received.

The problem with using phase-locked loops in the phase measurement circuit as described is excessive phase error in the loop as it tracks signals at their highest Doppler rate. The phase error in a second order loop tracking a signal with a linearly varying frequency is proportional to the rate of frequency change (Ref. 4). A platform signal received on a satellite will have a linearly decreasing component proportional to the range acceleration, which reaches its maximum at the time of closest approach. For satellites in the 500 to 1000 km altitude range, the maximum Doppler rate is from 62 to 144 Hz/s at 400 MHz.

The proportionality constant between Doppler rate and phase error involves the square of the loop natural frequency. This means that the VCO phase, which is used to determine the relative phase between antennas, is itself different from the received signal phase by an amount depending on the loop natural frequency and the Doppler rate. Thus these parameters must be known to find the relative signal phase from the VCO phase comparison. Any
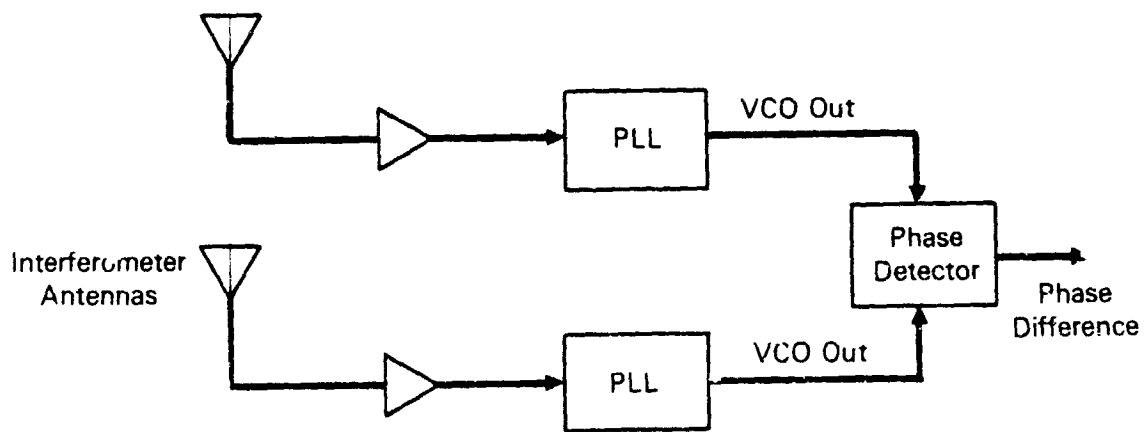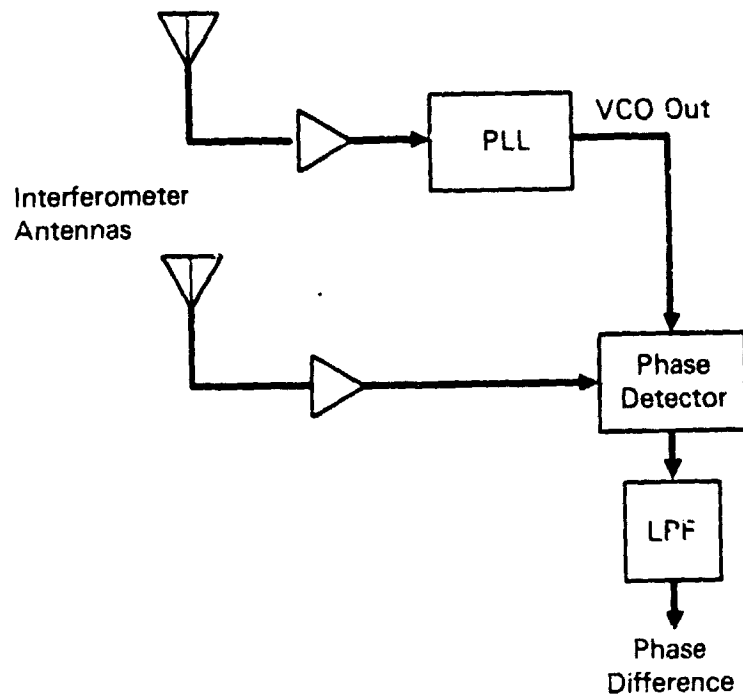
FIGURE 3.3-2. CANDIDATE PHASE MEASUREMENT TECHNIQUES

errors in the knowledge of these parameters, of course, contribute to the relative phase measurement error. Unfortunately, the loop natural frequency is a function of the input signal amplitude (or signal to noise ratio, when a limiter or AGC is used), so it may be difficult to know exactly.

It is desirable to keep the phase error small so that its error contributions to the measured phase difference are also small. Furthermore, it is always desirable to operate a phase-locked loop in its "linear" region, and this also places a limit on the allowable phase error. Given a maximum Doppler rate, established by operating frequency and orbit dynamics, the only ways available to reduce the phase error are to use a third-order loop or to use a second order loop with a greater natural frequency. Third-order loops exhibit no phase error when tracking a linearly changing frequency, so are very promising for this application and will be considered in future work. At present, we confine ourselves to second order loops. Increasing the natural frequency of a loop reduces the phase error, but at the same time it increases the noise bandwidth which results in increased phase jitter. The selected natural frequency must then be a compromise between the phase error, which gives an approximately-known bias to the relative phase measurement, and the phase jitter, which produces a zero-mean random error. Figure 3.3-3 shows the trade-off between the standard deviation of the phase jitter and the phase error for a Doppler rate of 100 Hz/s and expected values of C/N_o.

An alternate technique of making the phase measurement that eliminates all effects of Doppler-induced loop phase error is illustrated in Figure 3.3-4. This method also uses a phase-locked loop, which is locked to the signal received in one of the interferometer antennas. But instead of using the VCO output directly in the phase comparison, as with the other methods described, the VCO is used as a local oscillator to heterodyne all the interferometer channels down to an intermediate frequency. In this way, whatever jitter and phase error that are present in the VCO output are impressed on all the channels, so the relative phase between the channels is unaffected.

After the signals are down-converted to a constant intermediate frequency (call it f_1), they undergo another down-conversion. In each pair of channels to be compared, one channel is mixed with a local oscillator

3-11
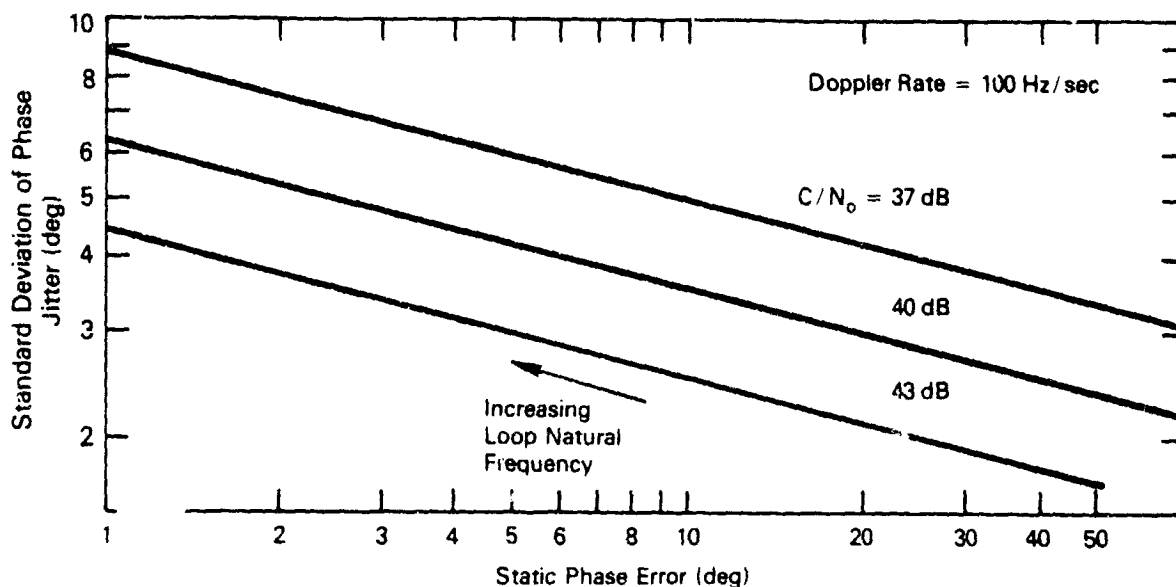
FIGURE 3.3-3.   PHASE ERROR VERSUS JITTER WHEN TRACKING
LINEAR FREQUENCY VARIATION

signal at frequency $f_1 + f_2$, and the second channel is mixed with a signal
at a slightly different frequency, $f_1 + f_2 + f_0$. After filtering to
remove the upper sideband, we have second IF channels centered at f_2 and
$f_2 + f_0$. These are then mixed, producing an output centered at the low
frequency f_0 that contains the phase difference information. This is then
put through a narrow-band bandpass filter that removes most of the noise. The
phase of this signal is then extracted by comparing it with a locally-
generated constant-phase signal at frequency f_0. This f_0 signal, as well
as the other local oscillator signals at $f_1 + f_2$ and $f_1 + f_2 + f_0$
are coherently generated in a frequency synthesizer.

The error in phase measurement due to loop error and jitter are
eliminated by the technique just described, but other sources of error
remain. The largest source is probably variation in the phase delay along the
separate paths the signals follow before being combined. This matter is
addressed later in the discussion of calibration techniques in Section 3.5.

3.3.3   Phase Measurement During Modulation

The pulse transmitted by a platform has a dual purpose: to provide
the data necessary to locate the platform and to convey digitally encoded

3-12
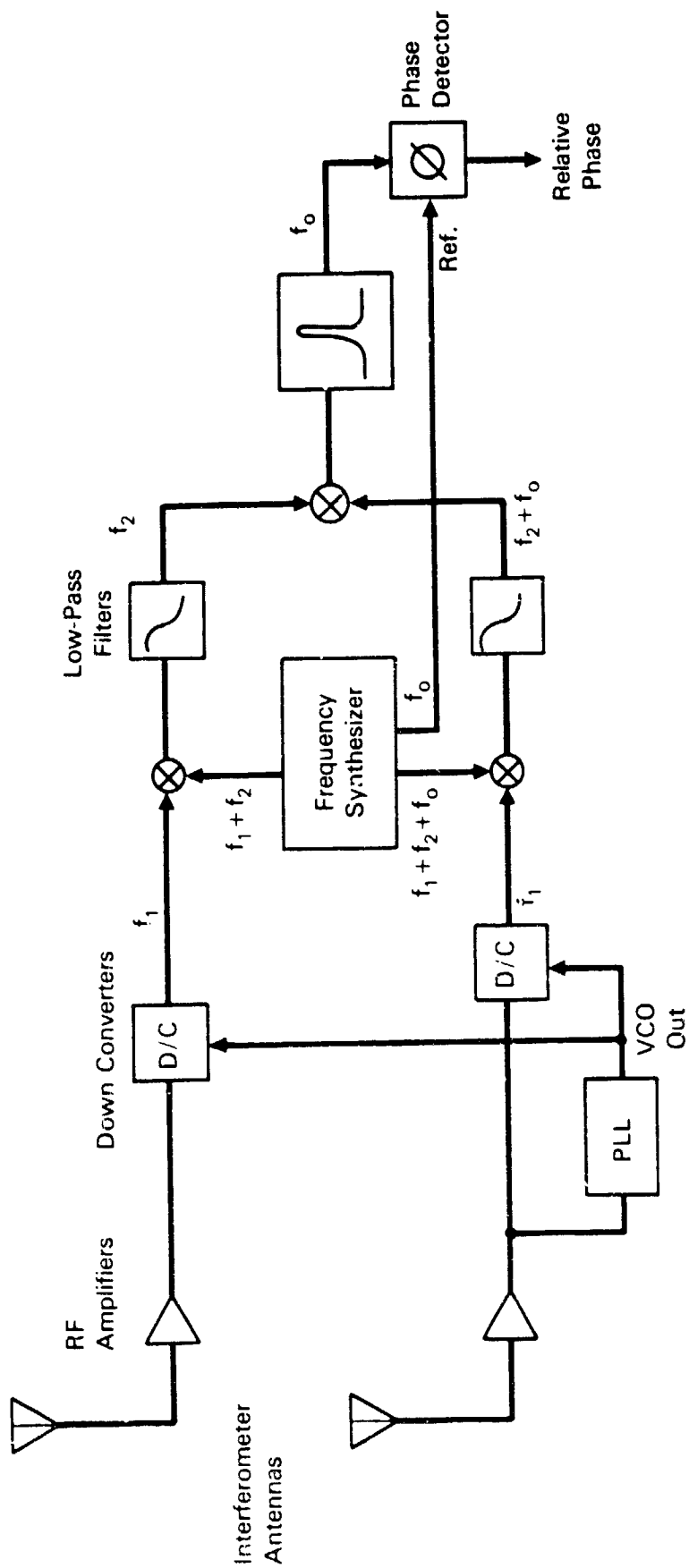
FIGURE 3.3-4. LOOP-ERROR-INDEPENDENT PHASE MEASUREMENT

information. Both of these naturally take a certain amount of time, and in the interest of maximizing system capacity by minimizing the pulse length, it is desirable that the two activities be concurrent. This reduces to making relative phase measurements at the same time as receiving the digital information impressed on the platform signal. It woul: be desirable to use phase modulaticn to transmit the digital information, due to its interference resistance and efficiency advantage, but it appears that modulating the phase would tend to degrade the measurement of relative phase. This is true to some degree, but by using the proper signalling format and modulation technique, trade-offs are possible that lead to negligible phase measurement error.

The type of modulation to use to allow simultan· jus relative phase measurement and modulation has been described above in Section 2.1.3. It has two essential features: the peak modulation angle is less than $90°$ to place part of the power into a discrete line at the carrier frequency, and Manchester signalling is used so that the spectral density falls to zero in the vicinity of the carrier. In this way, a spectral line is provided for phase comparison, and the modulation sidebands surrounding it are amenable to removal by filtering.

The degree of degradation of the phase measurement can be estimated by comparing the phase ncise on the received carrier due to thermal noise with the phase noise due to modulation. As illustrated in Figure 3.3-5, the carrier, accompanied by thermal noise and modulation sidebands, is assumed to be filtered with an infinitely-sharp cutoff bandpass filter for simplicity. The thermal noise passed by the filter under high signal-to-noise conditions produces an equivalent phase noise on the carrier with a variance equal to the noise power divided by twice the carrier power. The noise power is the integral of the thermal noise spectral density over the filter bandwidth. Likewise, the carrier phase variance due to modulation can be approximated by the modulation power passed by the filter (the integral of the modulation spectral density) divided by twice the carrier power. These phase variances have been calculated as functions of the filter bandwidth, and the peak modulation angle. (See Appendix A.) Figure 3.3-6 shows the results for normal PSK modulation with Mancheste· signalling. Figure 3.3-7 are the results for pseudo-MSK modulation with Manchester signalling. The modulation

Carrier
Power = P_c

Modulation
Spectral Density

Thermal Noise
Spectral Density

Filter
Bandwidth

//// Area = P_{th} = Thermal Noise Power

\\\\ Area = P_m = Modulation Power

$\sigma_{\phi t}^2$ = Phase Variance Due to Thermal Noise $\cong \dfrac{P_{th}}{2P_c}$

$\sigma_{\phi m}^2$ = Phase Variance Due to Modulation $\cong \dfrac{P_m}{2P_c}$
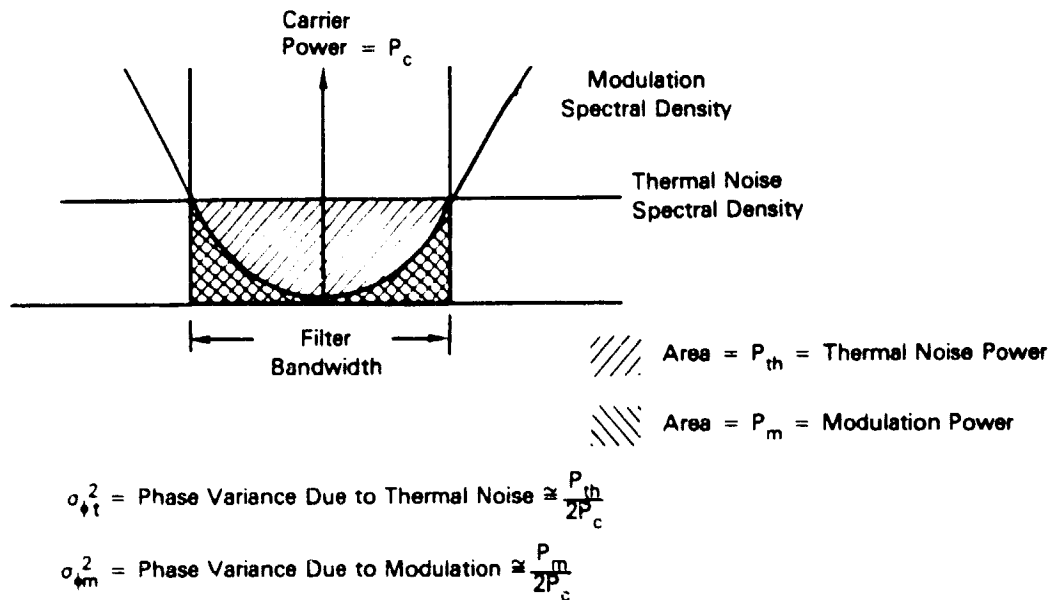
FIGURE 3.3-5. DETERMINATION OF THERMAL AND MODULATION
PHASE VARIANCE CONTRIBUTIONS

waveforms are shown on the plots. The phase variance due to thermal noise is
a function of both the modulation angle and the bit energy to noise density
ratio, E_b/N_0. The curves in the figures assume a particular value of
E_b/N_0 for each modulation angle. The E_b/N_0 values are chosen to give
a constant bit error rate of 10^{-5}, assuming a 2.5 dB degradation due to
demodulation. This corresponds to an E_b/N_0 of 12 dB for PSK with a 90°
modulation angle.

The plots show that, except for small values of modulation angle (and
corresponding large values of E_b/N_0), the phase noise due to thermal noise
dominates over that due to modulation. If we select as a criterion that the
phase variance due to modulation be one-tenth that due to thermal noise, the
curves give an optimum measurement bandwidth. As shown, this is about 0.175 R
for PSK and 0.20 R for MSK, and is independent of modulation angle.

3.3.4 Time Required to Measure Phase

The spacecraft signal acquisition and measurement system described in
section 3.3.1 goes through the following sequence of operations when a
platform transmission is received.
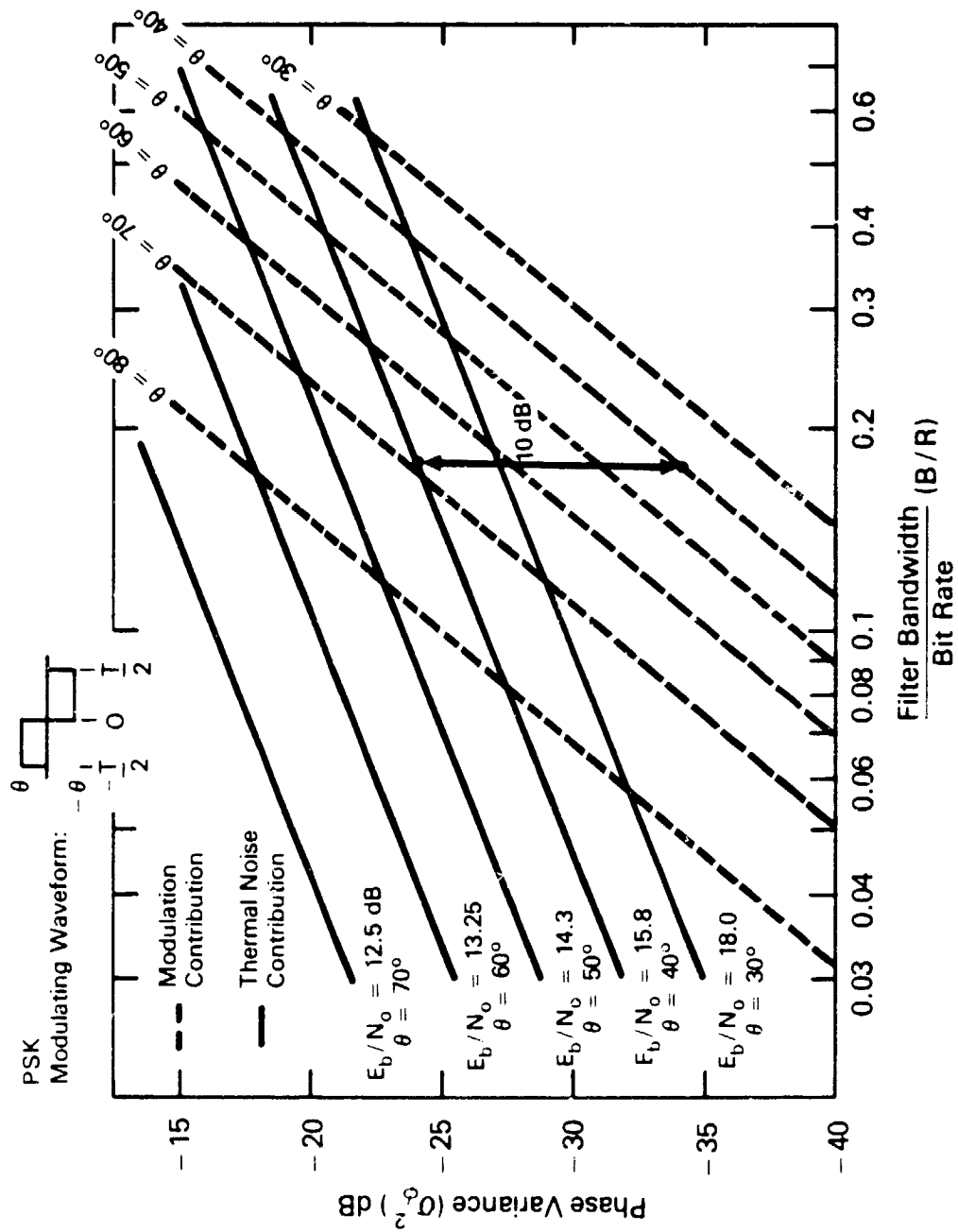
FIGURE 3.3-6. PHASE VARIANCE CONTRIBUTIONS VERSUS FILTER BANDWIDTH - PSK
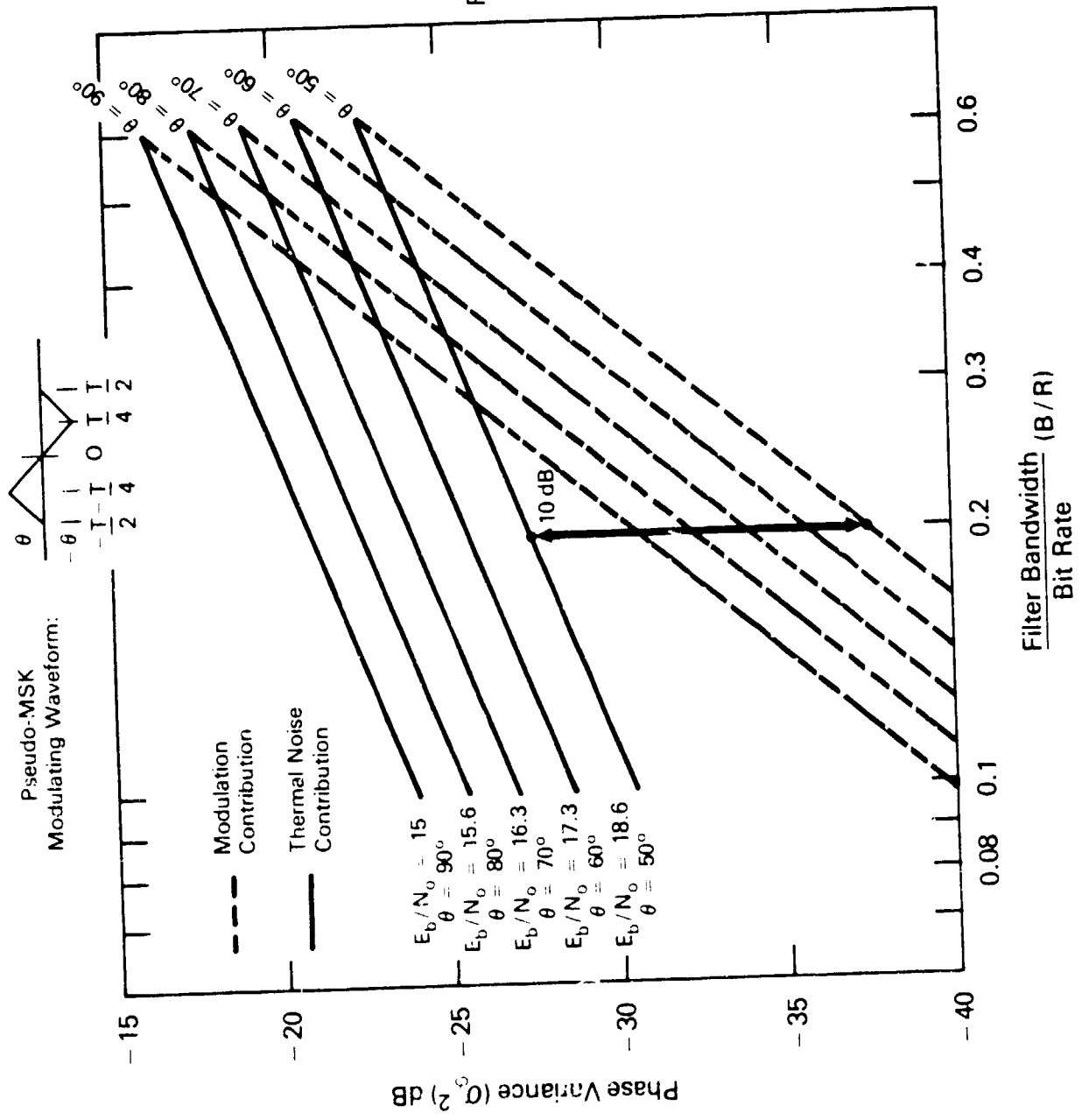
FIGURE 3.3-7. PHASE VARIANCE CONTRIBUTIONS VERSUS FILTER BANDWIDTH - PMSK

1. The signal detection unit detects the presence of a signal, estimates its frequency, and supplies this frequency to the control unit.

2. The control unit commits a data extraction unit to the signal by commanding the unit's VCO to the specified frequency. Frequency acquisition is accomplished with the loop filter set to a wide acquisition bandwidth.

3. The signal phase settles in the acquisition bandwidth (i.e., the transients die out) the loop is switched to a narrow tracking bandwidth.

4. Phase lock is achieved in the narrow bandwidth.

5. The data detector is enabled, and it begins to look for the bit synchronization pattern.

6. The phase difference signal settles in the phase measurement bandwidth, and phase integration begins.

7. The phase difference is integrated for a period sufficient to yield the desired measurement precision.

Figure 3.3-8 shows the time-line for these steps and gives estimates of the time required for them, based on the parameters given. The remainder of this section describes the steps and the factors determining the time required to perform them. Appendix B develops the mathematical basis of the estimated times.

3.3.4.1 Signal Detection and Frequency Estimation. It is assumed that this is accomplished by a modern instantaneous frequency measurement (IFM) system employing SAW and/or CCD technology and fast-Fourier Transform or Chirp-Z Transform techniques. IFM developments from the electronic countermeasures field can probably be applied to the signal detection problem without appreciable modification. The operation and design of such systems are

3-18
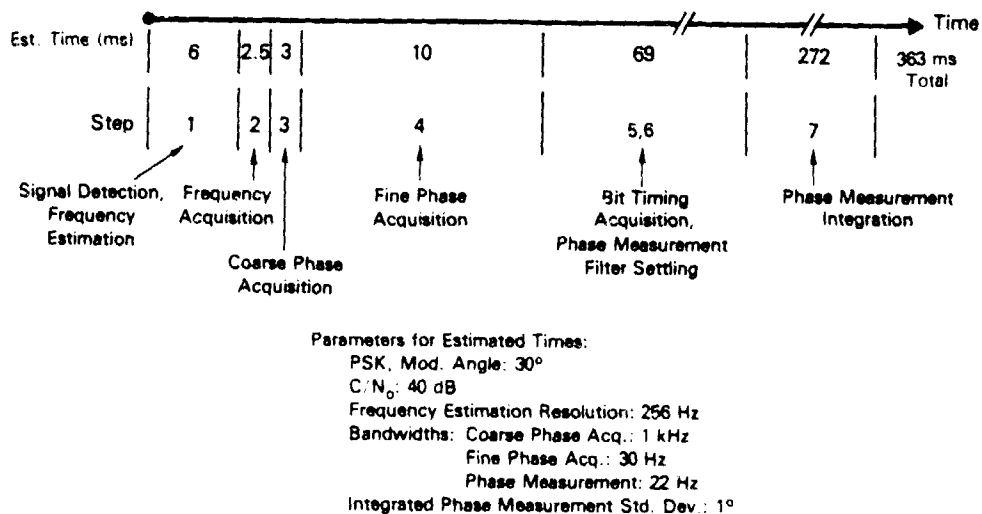
FIGURE 3.3-8. ACQUISITION AND MEASUREMENT SEQUENCE

covered well in manufacturers' literature and will not be discussed further here. The detection and frequency measurement time estimate of 6 ms is based on one manufacterer's data. The output of the detection unit is assumed to be an estimate of signal frequency to a precision of $\pm$ 256 Hz and an indication of signal strength. The width of the frequency resolution cell is twice the chosen bit rate of 128 b/s. This is judged to be fine enough so that the control unit will be able to use the information to determine if signals are too close to make an acquisition attempt worthwhile. The availability of data extraction units is improved if acquisition of signals that are obviously being interfered with is not attempted.

3.3.4.2 Frequency Acquisition. To achieve phase lock in a narrow loop in a minimum amount of time, it is common to use a loop with two bandwidths. A wide bandwidth is used for initial frequency acquisition and coarse phase acquisition, and then the bandwidth is narrowed for fine phase acquisition and tracking. We use this technique here, and select 1 kHz as the acquisition bandwidth. With an initial frequency error of up to 256 Hz, this bandwidth gives 2.5 ms as the expected time to achieve phase lock. (See Appendix B.) A wider bandwidth gives a shorter acquisition time, since the time varies

inversely as the cube of bandwidth. A wider bandwidth also admits more thermal noise, however, increasing the phase jitter. The choice of bandwidth is compromise between acquisition time and phase jitter.

3.3.4.3 Coarse Phase Acquisition. Once phase lock is achieved, time must be allowed for the transient component of the static phase error to decrease to some suitably small value. The time for the phase error to fall to $5°$ is estimated to be about 3 ms with the 1 kHz bandwidth. Together with this $5°$ static error is a jitter component, which in the steady state has a variance (σ_ϕ^2) of 0.05 rad^2 (standard deviation of $12.8°$), assuming a 40 dB C/N_0. The variance also has a transient component, but it is expected that this will become small in the 3 ms it takes the static phase error to settle to $5°$. The total expected phase error after this settling time, then, should not exceed about $5° + 2\sigma_\phi \cong 30°$.

3.3.4.4 Fine Phase Acquisition. Now the loop filter is changed to narrow the loop bandwidth to its final value. The bandwidth is selected to produce a phase jitter that will have negligible effect on the bit error probability. With C/N_0 of 40 dB, a bandwidth of 30 Hz gives a phase standard deviation of about $2°$, which is acceptable as long as the settling time is also. The settling time for the static error can be estimated, as described in Appendix B, to be about 10 ms. This is not excessive.

3.3.4.5 Bit Timing Acquisition. Up to this point, the platform signal has been unmodulated. Now that the phase is being tracked in the narrowband loop, the modulation can be applied and the data detector can start processing the phase error, which is now a filtered version of the modulation waveform. The first task, once the modulation has started, is to acquire the bit timing. This requires another loop, operating at the bit rate, optimized to the modulating waveform. The time to acquire bit timing synchronization is not of concern here, except that it should be such that sufficient time is left to transmit the platform identification code while the phase measurement is still in progress.

3.3.4.6 Phase Measurement Filter Settling. We must wait an interval for the transients in the phase measurement filter to die out before we may begin

3-20

integrating the phase. Appendix B gives the transient in the tone containing the phase information and in the variance of the thermal noise accompanying the tone. From these, the variance of the phase of the tone is estimated as a function of time. The time for this variance to become approximately equal to its steady state value, which is the settling time, is dependent on the filter bandwidth. The filter bandwidth, selected on the basis of keeping the phase variance due to modulation 10 dB less than that due to thermal noise, is $(0.175)(128) = 22$ Hz for the bit rate selected. With this bandwidth, the settling time becomes about 70 ms.

3.3.4.7 <u>Integration Time</u>. The phase variance of the filtered tone after settling is about 1.8×10^{-3} rad^2. The desired variance is 3×10^{-4} rad^2, corresponding to a 1° standard deviation. This is accomplished by integrating the output of the phase detector for a period. The variance reduction factor achieved by integration is, as shown in Appendix B, about equal to the integration time times the measurement filter bandwidth. To achieve a factor of six reduction, then, the signal must be integrated for $6/22 = 273$ ms.

3.4   NUMBER OF DATA EXTRACTION CHANNELS

The number of parallel data extraction channels (DECs) needed to accommodate transmissions overlapping in time can have a significant effect on the weight and power consumption of the spacecraft electronics. The factor determining the number of data extraction channels is the probability of missing a transmission due to all the channels being in use when a transmission is received. The sum of this probability and probability of interference is the total probability of missing a transmission.

Figure 3.4-1 shows the probability that the number of transmissions being received simultaneously is more than the number of processors. This is the probability that a transmission will be missed because a processor is not available when it is received. The parameter r is the rate of arrival of transmissions,

$$r = N\tau/T$$

Probability (Number of Simultaneous Signals > M)
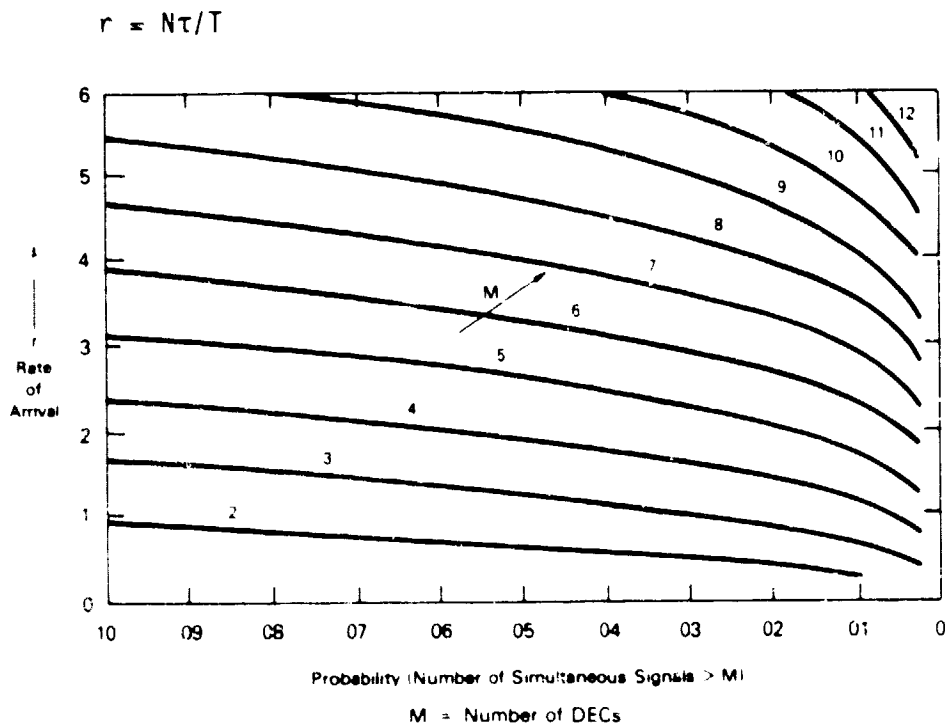
M = Number of DECs

FIGURE 3.4-1.   PROBABILITY OF NUMBER OF SIGNALS EXCEEDING NUMBER OF DECs

where N is the number of platforms in the field of view, τ is the duration of the transmitted pulse, and T is the period between pulses. Appendix C gives the mathematical basis of the figure. The figure says, for example, that making the probability of missing a transmission due to all the channels being busy no more than 0.05 requires 5 channels with $r = 2$, 6 channels with $r = 3$, and 8 channels for $r = 4$.

3.5   CALIBRATION TECHNIQUES

A means must be provided to periodically measure the "constant" parameters of the system that are involved in making the position estimate on the basis of the measured phase value. These recalibrations are necessary because many of these parameters are unpredictable functions of time and/or temperature and cannot be estimated with sufficient accuracy. The parameters used to determine position that are completely internal to the interferometer system are the location of the effective phase centers of the antennas with respect to the spacecraft reference frame, the phase delay between the antennas and the phase comparison circuit, and the transfer function of the phase measurement circuit. These parameters may be measured by injecting RF calibration signals directly into the antennas or RF lines. Other position-location parameters, external to the interferometer, include the spacecraft attitude and location, and ionospheric and tropospheric propagation effects. To include these in the calibration process, platform transmitters at known surface locations may be used.

3.5.1   Signal Injection

Injection of test signals into each antenna from a source on board the satellite is a straightforward calibration technique that takes into account the phase delays through the signal processing chain, as well as the phase comparator response. The point of signal injection determines how much of the signal processing chain is included in the calibration. Injection into the antennas themselves by a single source fixed to the satellite, would be desirable, since the phase delays would include the antenna spacing. However, near-field effects and reflections from the spacecraft structures may make it difficult to implement this. The alternative is to inject signals into the RF lines coming from the antennas. This does not take antenna spacing into account, and uncertainties in the phase delays from the source to the injection points cannot be removed. These uncertainties are likely to be more when cables are used to distribute the calibration signal than when it is radiated through space.

The calibration provisions aboard the spacecraft can be limited to the calibration signal source, and its means of distribution, by making the calibration signal appear as if it were a platform signal. In this way, it would be processed on board in exactly the same way as all the other transmissions received from the ground, and no special equipment would be nessary in the receiving, signal processing and data handling subsystems. The calibration signal would carry a special identification code which would indicate to the ground processor that special processing was required. The ground processor would then use the phase measurements of the calibration signal to calculate phase delays, etc., and with this update the position estimation algorithms.

3.5.2   Platforms With Known Location

Calibration can also be performed by comparing the known position of a surface transmitter with the position estimate determined by the system. This method takes into consideration all possible sources of error, but presents a problem of interpretation. The direct comparison of a known and estimated position yields an error, but it does not tell what the component errors are that make it up. Corrections must be allocated to the proper parameters. This overall location error must therefore be interpreted using a suitable error model in combination with other independent error indications, the geometry at the time of measurement, and other factors. One of the independent error indications may well be the phase delay values determined using the on-board signal injector.

3.6   VOLUME, MASS AND POWER ESTIMATES

Possible hardware configurations were postulated for location and
data collection systems employing (1) dual interferometers, and (2) a single
interferometer plus Doppler. Using these configurations and current
spacecraft electronics packaging concepts, it was possible to derive estimates
of the volume, mass and power requirements of the payload. These indicate the
magnitude of the burden one of these systems would place on a host
spacecraft.

The estimates assume systems with six data extraction channels.
Antennas are assumed to be of a two-turn quadrifilar helix design, with
dimensions necessary to give a pattern approximating the range-compensating
pattern desired. The windings of such an antenna for 400 MHz turn out to be
on a cylinder 7.5 cm in diameter and 93 cm long (Ref. 3). It is likely that
booms or at least some kind of support structure will be required to hold the
antennas, but no allowance has been made for these structures in the estimates
that follow. No redundancy has been assumed in the estimates.

3.6.1   Dual-Interferometer System

Figure 3.6-1 shows the hardware configuration, and Table 3.6-1 gives
the estimates. As shown, a five-antenna orthogonal-baseline interferometer
arrangement is assumed. The inputs from the five antennas are arranged into
four pairs of inputs, and each pair goes to a separate phase comparator
assembly. The four pairs correspond to the two primary (long baseline)
antenna pairs, and the two ambiguity-resolution (short-baseline) pairs.
Within a phase comparator assembly, there is assumed to be six phase
comparator units each capable of independent operation. The signal examined
by a phase comparator unit is determined by the LO input to the unit, which is
the VCO output of a phase-locked loop tracking the signal. One of the four
phase comparator units assigned to a particular signal provides a sample of
the IF to the loop. The phase-locked loop and phase comparator unit together
comprise the circuit shown in Figure 3.3-4.
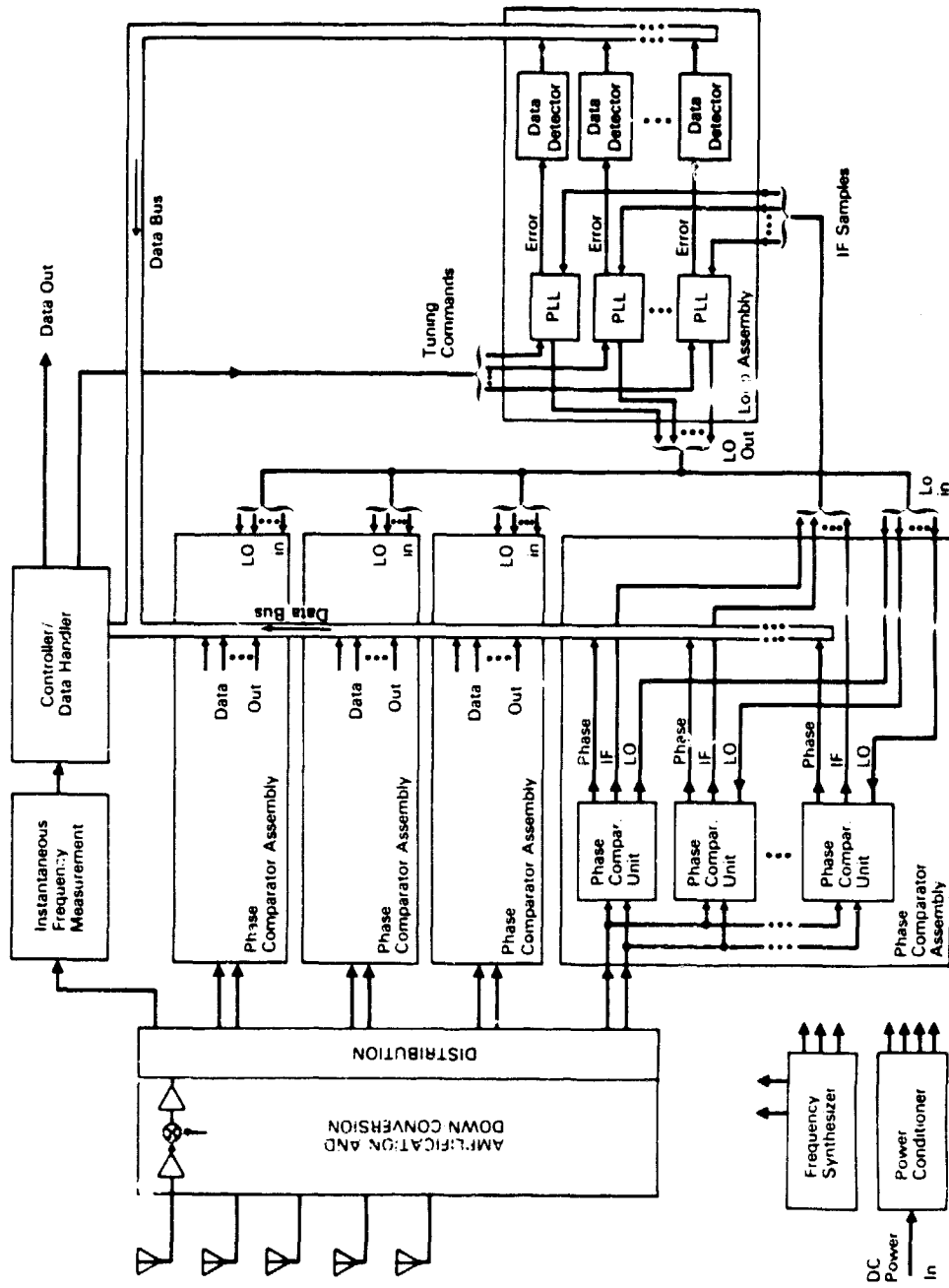
FIGURE 3.6-1. DUAL INTERFEROMETER SYSTEM HARDWARE CONFIGURATION

TABLE 3.6-1
MASS, VOLUME AND POWER ESTIMATES
SIX-CHANNEL DUAL BASELINE INTERFEROMETER

Quantity	Unit Description	Individual			Total		
		vol (ℓ)	mass (kg)	pwr (W)	vol (ℓ)	mass (kg)	pwr (W)
1	5 channel RF Amplifier, Downconverter, Distributor				1.8	3	3
1	Signal Detector, IFM				1.6	2	7
1	Controller				5.0	4	15
5	Antenna	(7.5	4	-)	(37.5	20	-)
4	Phase comparator Assembly	3.6	2.4	0.6	14.4	9.6	2.4
6	Phase comparator Unit	(0.6	0.4	0.1)	3.6	2.4	0.6
1	Loop Assembly				7.3	2.0	16.5
2	Power Divider	(0.05	0.1	-)	(0.1	0.2	-)
6	Loop	(0.6	0.3	1.5)	(3.6	1.8	7.5)
6	Data Detector	(0.6	0.25	1.5)	(3.6	1.5	9.0)
1	Frequency Synthesizer				4.0	3.5	10.0
1	Power Conditioner (80% eff.)				5.0	6.0	10.0
	Totals – electronics				39.1ℓ	30.1kg	63.9W
	– antennas				37.5ℓ	20. kg	
	Electronics Volume Assuming 70% packing Density				55.9ℓ (38 cm cube)		

The volume estimates are given in the table in thousands of cubic centimeters (or liters). The total volume has been increased to allow for a 70 percent packaging density. This is to allow for cabling between subassemblies and for access in assembling and testing.

3.6.2   Single Interferometer plus Doppler System

The configuration of this system is very similar to that shown in Figure 3.6-1. The differences are;

- Two antennas instead of five
- One phase comparator instead of four
- A new unit, a frequency counter, associated with each phase-locked loop to periodically measure the VCO frequency and send this out on the data bus.

The single interferometer system needs no ambiguity resolving antenna because Doppler processing of two or more transmissions gives a position estimate with only a single ambiguity. This ambiguity may be resolved with interferometer information.

Table 3.6-2 gives the estimates for the volume, mass and power requirements of the single-interferometer plus Doppler system.

TABLE 3.6-2
MASS, VOLUME AND POWER ESTIMATES
SIX-CHANNEL SINGLE BASELINE INTERFEROMETER PLUS DOPPLER

Quantity	Unit Description	Individual			Total		
		vol (ℓ)	mass (kg)	pwr (W)	vol (ℓ)	mass (kg)	pwr (W)
1	2 channel RF Amplifier, Downconverter, Distributor				0.9	1.5	1.5
1	Signal Detector, IFM				1.6	2	7
1	Controller				5.0	4	15
2	Antenna	(7.5	4	-)	(15.0	8	-)
1	Phase comparator Assembly				3.6	2.4	0.6
6	Phase comparator Unit	(0.6	0.4	0.1)	3.6	2.4	0.6
1	Loop Assembly				10.1	5.3	25.2
2	power divider	(0.05	0.1	-)	(0.1	0.2	-)
6	Loop	(0.6	0.3	1.2)	(3.6	1.8	7.2)
6	Data Detector	(0.6	0.25	1.5)	(3.6	1.5	9.0)
6	Frequency Counter	(0.5	0.3	1.5)	(3.0	1.8	9.0)
1	Frequency Synthesizer				4.0	3.5	8.0
1	Power Conditioner (80% eff.)				5.0	6.0	11.5

Totals - electronics   30.2ℓ   24.7kg   68.8W

        - antennas   15.0ℓ   8.0kg

Electronics Volume Assuming 70% Packing Density   43.1ℓ (35 cm cube)

APPENDIX A
SIGNAL ANALYSIS

1.0   INTRODUCTION

Properties of the modulated RF signals used in the body of this report are derived in this appendix. The signal considered has unit power, constant amplitude, and modulated phase. It is represented by

$$s(t) = \sqrt{2} \cos\left[2\pi f_c t + m(t)\right]$$

where f_c is the carrier frequency and $m(t)$ is the modulating waveform. Two types of modulation are considered, phase shift keying (PSK) using a bipolar modulating waveform, and pseudo-MSK (pMSK), which uses a triangular modulating waveform. For both cases, Manchester signaling is used to spread the spectral energy away from the carrier. The elemental modulating waveforms, corresponding to a single bit, are given by the following

PSK

$$m(t) = \begin{cases} +\theta & -\frac{T}{2} < t < 0 \\ \\ -\theta & 0 < t < \frac{T}{2} \end{cases}$$

pMSK

$$m(t) = \begin{cases} 2\theta\left(\frac{2t}{T}+1\right) & -\frac{T}{2} \le t \le -\frac{T}{4} \\ \\ -4\frac{\theta}{T} & -\frac{T}{4} \le t \le \frac{T}{4} \\ \\ 2\theta\left(\frac{2t}{T}-1\right) & \frac{T}{4} \le t \le \frac{T}{2} \end{cases}$$

These waveforms are sketched in Figures 3.3-6 and 3.3-7.

2.0   SPECTRA

The spectral density for the two types of signals, assuming random data with 0.5 "1" and "0" probability, are given by the following, with $\alpha = (\pi/2) T(f - f_c)$,

PSK

$$S(f) = T \frac{\sin^4 \alpha}{\alpha^2} \sin^2 \theta + \delta(f - f_c) \cos^2 \theta$$

pMSK

$$S(f) = \frac{T}{\theta^2} \left[\frac{\sin \alpha (\cos \alpha - \cos \theta)}{(\alpha/\theta)^2 - 1} \right]^2$$

$$+ \left(\frac{\sin \theta}{\theta} \right)^2 \sum_{n=-\infty}^{\infty} \frac{\delta[f - (f_c - \frac{2n}{T})]}{[(n\pi/\theta)^2 - 1]^2}$$

The first of these results is well-known. The second was derived using standard analysis procedures (Ref. 5). For PSK, we note that the power divides between the modulation sidebands and the discrete carrier component, denoted by $\delta(f - f_c)$, according to the peak modulation angle. When this angle is 90°, the carrier component disappears and all the power is contained in the sidebands. For pMSK, discrete lines appear at the carrier and at frequencies offset from the carrier by even multiples of the reciprocal of the bit period. The carrier amplitude is seen to decrease smoothly with modulation angle and fall to zero when the angle is 180°. The rate at which the sidelobes of the spectrum decrease with distance from the carrier is an important characteristic of the spectra. It is seen to be on the order of the square of the distance for PSK and the fourth power of the distance for pMSK. Thus the smoothed pMSK modulating waveform results in lower sidelobes, which should be expected.

3.0   MODULATION POWER IN FILTER BANDWIDTH

The amount of modulation power, P_m, passed by a perfect bandpass filter is just the integral of the spectrum over the filter bandwidth B:

$$P_m = \int_{-B/2}^{B/2} S_c(f)\, df$$

where $S_c(f)$ is the continuous portion of the power spectral density. This integral is evaluated by first finding approximations of the spectral densities at small values of frequency offset from the carrier. The filter bandwidths considered are always less than about half the bit rate. This is a small enough offset that each of the spectra may be accurately represented by a single quadratic term. The approximations turn out to be

PSK

$$S_c(f) \cong T^3 \left(\frac{\pi}{2}\right)^2 \sin^2\theta\, (f-f_c)^2$$

pMSK

$$S_c(f) \cong T^3 \left(\frac{\pi}{2}\right)^2 \left(\frac{1-\cos\theta}{\theta}\right)^2 (f-f_c)^2$$

Integrating these over the bandwidth B results in

PSK

$$\int_{-B/2}^{B/2} S_c(f)\, df \cong (BT)^3 \frac{\pi^2}{48} \sin^2\theta$$

pMSK

$$\int_{-B/2}^{B/2} S_c(f)\, df \cong (BT)^3 \frac{\pi^2}{48} \left(\frac{1-\cos\theta}{\theta}\right)^2$$

4.0 PHASE VARIANCE DUE TO MODULATION

The remnants of the modulation sidebands that pass through the filter with the carrier, as long as their power is small compared to the carrier, can be viewed as an equivalent phase modulation on the carrier. The variance of this phase modulation is given by

$$\sigma_\varphi^2 = \frac{P_m}{2 P_c}$$

where P_m is the modulation power, calculated above, and P_c is the carrier power. For the unit power signals being considered, the spectral density expressions give

PSK

$$P_c = \cos^2 \theta$$

pMSK

$$P_c = \left(\frac{\sin \theta}{\theta}\right)^2$$

Combining these with the integral approximations, we have

PSK

$$\sigma_\varphi^2 \cong (\beta T)^3 \frac{\pi^2}{96} \tan^2 \theta$$

pMSK

$$\sigma_\varphi^2 \cong (\beta T)^3 \frac{\pi^2}{96} \left(\frac{1 - \cos \theta}{\sin \theta}\right)^2$$

which are plotted in Figures 3.3-6 and 3.3-7.

5.0   BIT ERROR PROBABILITY

We now derive expressions for the bit error rate for the PSK and pMSK signals. This allows us to quantize the effect of the modulation angle on bit error rate. The probability of bit error for coherent demodulation is in general (Ref. 6),

$$P_E = \frac{1}{2} \, erfc \, \sqrt{(1-\rho)E_b/N_o}$$

where erfc (·) denotes the complementary error function, and ρ is the correlation coefficient between the waveforms $s_0(t)$ and $s_1(t)$, corresponding to a "0" and "1" bit, respectively.

$$\rho = \frac{1}{E_b} \int_{-\frac{T}{2}}^{\frac{T}{2}} \left[s_0(t) \, s_1(t) \right] dt$$

For the two cases considered, we find

$$\rho = \cos 2\theta \qquad \text{for PSK}$$

$$\rho = \frac{\sin \theta}{\theta} \qquad \text{for pMSK}$$

The lowest error probability for a given E_b/N_0 is achieved when PSK is used, with $\theta = 90°$ (i.e., $\rho = -1$). We are interested in comparing the increase in bit energy required to maintain the same minimum error probability when using PSK with $\theta < 90°$, or when using the pMSK signal. To have the same error probability, the quantity $(1 - \rho) E_b$ must stay at the value it takes for PSK, $\theta = 90°$, or $2E_b$. To accomplish this, the bit energy must be increased by the ratio

$$r(\theta) = \frac{2}{1 - \cos 2\theta} \cdot \frac{1}{\sin^2 \theta} \qquad \text{for PSK}$$

$$r(\theta) = \frac{2}{1 - \frac{\sin 2\theta}{2\theta}} = \frac{4\theta}{2\theta - \sin 2\theta} \qquad \text{for pMSK}$$

These ratios were used to find the E_b/N_0 values for constant bit error rate with varying modulation angles shown in Figures 3.3-6 and 3.3-7. $E_b/N_0 = 12$ dB for PSK with $\theta = 90^O$ was taken as a baseline.

6.0   PHASE VARIANCE DUE TO THERMAL NOISE

Previous results from this appendix are combined to give the thermal noise phase variance values of Figures 3.3-6 and 3.3-7. As stated earlier, the variance of the equivalent phase noise on the carrier due to additive noise is

$$ \sigma^2 = \frac{P_n}{2P_c} $$

where P_n is the noise power admitted by the filter and P_c is the carrier power. The noise power for a noise density of N_0 is simply $N_0 B$, and the carrier power is related to the total signal power P_t by:

$$ P_c = \cos^2\theta \; P_t \qquad \text{for PSK} $$

$$ P_c = \left(\frac{\sin\theta}{\theta}\right)^2 P_t \qquad \text{for pMSK} $$

Finally, noting that the bit energy $E_b = P_t T$, we have

$$ \sigma_q^2 = \frac{1}{2} \frac{1}{\cos^2\theta} \left(\frac{N_0}{E_b}\right) BT \qquad \text{for PSK} $$

$$ \sigma_q^2 = \frac{1}{2} \left(\frac{\theta}{\sin\theta}\right)^2 \left(\frac{N_0}{E_b}\right) BT \qquad \text{for pMSK} $$

A-6

including the relation found earlier between E_b/N_0 and θ for constant error rate,

$$\sigma_\varphi^2 = \frac{1}{2}\,\text{Tan}^2\theta\left(\frac{N_0}{E_b}\right)_0 BT \qquad\qquad \text{for PSK}$$

$$\sigma_\varphi^2 = \left(\frac{\theta}{\sin\theta}\right)^2 \frac{2\theta - \sin 2\theta}{8\theta} \left(\frac{N_0}{E_b}\right)_0 BT \qquad \text{for } \rho\text{MSK}$$

where the quantity $(N_0/E_b)_0$ is the reciprocal of the "baseline" value, taken as 12 dB in the plots of Figures 3.3-7 and 3.3-8.

A-7

APPENDIX B
PHASE MEASUREMENT TIMING

1.0   INTRODUCTICN

This Appendix presents the analyses on which the estimated times of Figure 3.3-8 are based. First, the transient responses of a phase-locked loop are examined. Expressions are then obtained for the phase variance of the tone containing the phase difference information after it is passed through the filter. Finally, the effect of integrating the phase measurement is determined.

2.0   PHASE-LOCKED LOOP TRANSIENTS

2.1   LOOP TYPE AND PARAMETERS

The type of loop is determined by the requirement to track signals that have a linear frequency variation with time. Of the conventional second-order loops (Ref. 4), one type exhibits a constant phase errcr when tracking a linear frequency variation, while other types have an increasing phase error. The type with constant error, which is the best loop in this application, has a loop filter with the following transfer function:

$$F(s) = \frac{1 + \tau_1 s}{\tau_2 s}$$

which is known as a perfect integrator with phase lead correction. This filter cannot be realized exactly, since it has infinite DC gain, but it can be approximated closely using active components. The time constants τ_1, and τ_2, along with the loop gain, determine two parameters that govern the response of the loop. These are the damping factor γ and natural (radian) frequency ω_n.

When this loop is suddenly presented with a linearly varying frequency, its phase error goes through a transient before reaching the steady state value. For small values of γ, there is an overshoot and oscillation about the final value. For large values of γ, the phase error slowly approaches the final value asymptotically. The final value is reached most quickly, without oscillation, for $\gamma = 1$. This value will be used.

The natural frequency and damping factor together determine the loop's noise bandwidth. When the damping factor is unity for this type of loop, the noise bandwidth $B_n = (5/8)\omega_n$, where ω_n is expressed in radians/sec and B_n is in Hz.

2.2 FREQUENCY ACQUISITION

When the loop is presented with a signal at a frequency different from the VCO quiescent frequency, cycle slipping occurs at the difference frequency until the VCO frequency reaches that of the input signal. The time from the application of the signal, until the cycle slipping stops, called here the frequency acquisition time, is approximated by the formula (Ref. 4)

$$T = \frac{(2\pi \Delta f)^2}{2 \gamma \omega_n^3}$$

where Δf is the initial frequency difference between the VCO and the signal. Using the values from the text (Section 3.3.4), $B_n = 500$ Hz, $\omega_n = 800$ rad/s, and $\Delta f = 256$ Hz, gives $T = 2.5$ ms.

2.3 PHASE ACQUISITION

The time required for the static phase error to reach a given value, θ, assuming it started at $90°$, is given by (Ref. 7)

$$T = \frac{1}{2 B_n} \ln (2/\theta)$$

where θ is expressed in radians.

The phase variance in the loop, after the transient has died out, is given by

$$\sigma_\phi^2 = (c/N_o)^{-1} B_n$$

where C/N_0 is the carrier to noise density at the input to the loop.

The maximum expected phase error in the loop at the time the bandwidth is narrowed is estimated from the above formulas. It is approximately the static phase error plus twice the standard deviation, σ_ϕ.

After the bandwidth is narrowed, the static phase error goes through another transient. The settling time for this one is estimated from the loop's phase step response. For the type of loop considered, the response to a phase step of magnitude θ is given by

$$\phi(t) = \theta e^{-\omega_n t}(1 - \omega_n t)$$

This passes through zero at time $T = 1/\omega_n$, and undershoots to a maximum negative value of -0.135θ at time $T = 2/\omega_n$. For the case considered in the text ($B_n = 15$ Hz, $\theta = 30°$), we assume that the undershoot (amounting to 4°) is tolerable, and consider the phase to be acquired in $1/\omega_n$ sec or about 10 ms.

2.4   PHASE MEASUREMENT

The phase measurement time is the sum of the settling time of the tone in the measurement filter and the integration time necessary to reduce the variance to the desired value.

2.4.1   Settling Time

The time required for the tone containing the phase information to settle in the measurement bandwidth is estimated by considering the transients occurring in a narrow-band filter when a noisy sinusoid is suddenly applied.

We approximate the narrowband filter by a network with a simple impulse response.

$$h(t) = e^{-\alpha t} \cos \omega_0 t$$

The 3-db bandwidth of this network is $W = \alpha/\pi$. When a sinusoid at frequency ω_0, plus noise with flat PSD $N_0/2$ is applied, we have

$$
\begin{array}{ccc}
x(t) \longrightarrow & \boxed{h(t)} & \longrightarrow y(t) \\
= s(t) + n(t) & & = s_0(t) + n_0(t)
\end{array}
$$

$$x(t) = s \cos \omega_0 t + n(t)$$

$$R_{xx}(t_1, t_2) = s^2 \cos \omega_0 t_1 \cos \omega_0 t_2 + \delta(t_1 - t_2) \frac{N_0}{2}$$

$$R_{yy}(t_1, t_2) = \left[R_{xx}(t_1, t_2) * h(t_2) \right] * h(t_1)$$

Carrying out the convolutions, we obtain an expression for $R_{yy}(t_1, t_2)$. Of particular interest is the case $t_1 = t_2$:

$$R_{yy}(t, t) = \sigma_y^2(t) + \eta_y^2(t)$$

$$= \frac{N_0}{2} \frac{1}{4} \left\{ \frac{1}{\alpha}(1 - e^{-2\alpha t}) + \frac{1}{\alpha^2 + \omega_0^2}\left[\alpha + e^{-2\alpha t}(\omega_0 \sin 2\omega_0 t - \alpha \cos 2\omega_0 t)\right] \right\}$$

$$+ s^2 \left[a(1 - e^{-\alpha t}) \cos \omega_0 t + b(1 + e^{-\alpha t}) \sin \omega_0 t \right]$$

where

$$a = \frac{\alpha^2 + 2\omega_0^2}{\alpha(\alpha^2 + 4\omega_0^2)} \quad , \qquad b = \frac{\omega_0}{\alpha^2 + 4\omega_0^2}$$

the mean, $\eta_y(t)$, is just the noiseless response:

$$\eta_y(t) = s A(t) \cos(\omega_0 t + \phi)$$

B-4

$$\text{with} \quad A(t) = \left[a^2(1-e^{-\alpha t})^2 + b^2(1+e^{-\alpha t})^2\right]^{1/2}$$

$$= \left[(a^2+b^2)(1+e^{-2\alpha t}) + 2(b^2-a^2)e^{-\alpha t}\right]^{1/2}$$

The phase noise of the output is approximately the output noise divided by the sinusoid envelope amplitude, so

$$\sigma_\varphi^2(t) \cong \frac{\sigma_y^2(t)}{s^2 A^2(t)}$$

$$= \frac{\frac{1}{4}\frac{1-e^{-2\alpha t}}{\alpha} + \frac{\alpha}{\alpha^2+\omega_0^2} + \frac{e^{-2\alpha t}}{\sqrt{\alpha^2+\omega_0^2}}\cos(2\omega_0 t + \cdots)}{s^2\left[(a^2+b^2)(1+e^{-2\alpha t}) + 2(b^2-a^2)e^{-\alpha t}\right]}$$

Replacing the sinusoidal part by its magnitude and making the high Q approximation, $\omega_0 \gg \alpha$, we get

$$\sigma_\varphi^2(t) \cong \frac{1}{s^2}\frac{N_0}{2}\alpha\frac{1-e^{-2\alpha t}}{1-2e^{-\alpha t}+e^{-2\alpha t}}$$

which, as expected, approaches the limit

$$\sigma_\varphi^2(t) \xrightarrow[t\to\infty]{} \frac{1}{s^2}\frac{N_0}{2}\alpha = \frac{1}{s^2}N_0\frac{\pi}{2}W$$

where $W\pi/2$ is the noise bandwidth. $\sigma_\varphi^2(t)$ reaches 110% of its steady state value after three $1/\alpha$ time constants. This should be sufficient to begin the phase measurement.

To apply this result, it is necessary to relate the measurement bandwidth to the simple filter bandwidth. The measurement filter is assumed to have sharp skirts and have a bandwidth B. Equating this with the noise bandwidth of the simple filter:

$$\frac{1}{2}\pi W = B$$

we get the equivalent time constant $1/\alpha = 1/2B$.

For the parameters in the text, $B = 0.175R$ and $R = 128$ b/s, the required settling time is $3(1/\alpha) = 70$ ms.

2.4.2 Integration Time

The signal plus noise out of the phase detectors is integrated to reduce the variance of the noise component. Integration must be done for a period longer than the reciprocal of the narrowband filter bandwidth, however, for it to do any good. (See Figure B-1.) Note that an integrator has a response with squared magnitude

$$|H(f)|^2 = T^2 \left(\frac{\sin \pi f T}{\pi f T} \right)^2$$

which has a frequency range of $2/T$ between its first zeroes. The noise variance at the output of the integrator is then

$$\sigma_o^2 = \int_{-\infty}^{\infty} S_n(f) \, |H(f)|^2 \, df$$
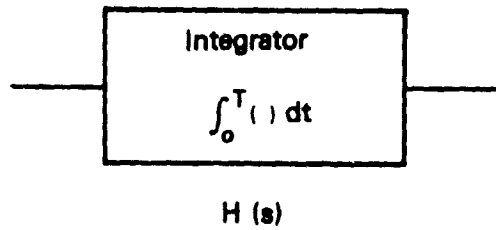
where $S(f) = \begin{cases} N_\rho & -B/2 \le f \le B/2 \\ 0 & \text{elsewhere} \end{cases}$

When the integration time is short, $1/T \gg B$, then

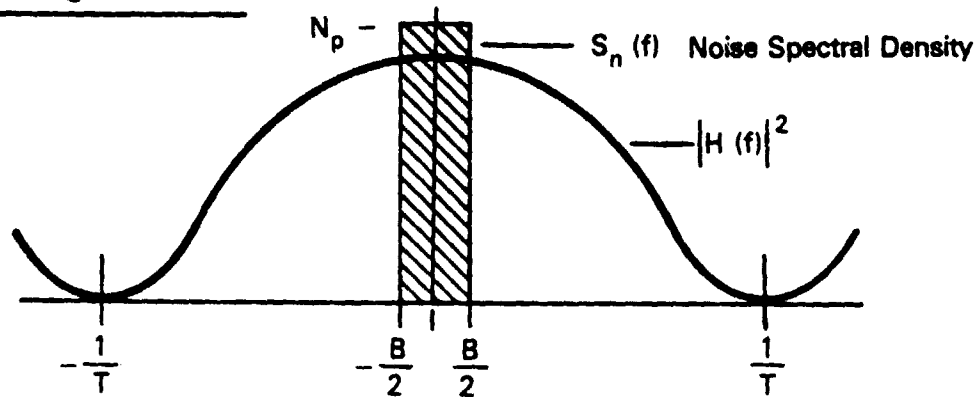$$\sigma_o^2 \cong T^2 B N_\rho$$

On the other hand, when the integration time is long, greater than about $4/B$,

$$\sigma_o^2 \cong N_\rho \int_{-B/2}^{B/2} T^2 \left(\frac{\sin \pi f T}{\pi f T} \right)^2 df$$

B-6

Integrator

$$\int_o^T (\ ) \, dt$$

H (s)

$$|H\,(f)|^2 = T^2 \left(\frac{\sin \pi fT}{\pi fT} \right)^2$$

Short Integration Time:

N_p — S_n (f)   Noise Spectral Density

$|H\,(f)|^2$

$-\frac{1}{T}$ $-\frac{B}{2}$ $\frac{B}{2}$ $\frac{1}{T}$

Integral Variance $\sigma_o^2 = $ ////// Area

Long Integration Time:

$|H\,(f)|^2$

N_p —

S_n (f)

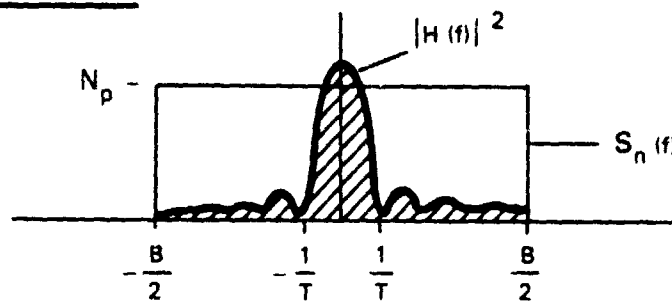$-\frac{B}{2}$ $-\frac{1}{T}$ $\frac{1}{T}$ $\frac{B}{2}$

FIGURE B-1. EFFECT OF INTEGRATION

$$\cong N_p \int_{-\infty}^{\infty} T^2 \left(\frac{\sin \pi f T}{\pi f T} \right)^2 df = N_p T$$

Now we compare the two cases relative to the power of the integrated signal $S = p^2 T^2$, where p is the phase voltage.

- Short integration time:

$$\frac{S}{\sigma_o^2} \cong \frac{p^2 T^2}{B N_p T^2} = \frac{p^2}{B N_p} \qquad \text{(same as no integration)}$$

- Long integration time:

$$\frac{S}{\sigma_o^2} \cong \frac{p^2 T^2}{N_p T} = \frac{p^2}{N_p} T$$

The improvement then is approximately BT when $T \gtrsim 4/B$.

APPENDIX C
NUMBER OF DATA EXTRACTION CHANNELS REQUIRED

We select the number of data extraction channels so that the probability that there are more simulataneous signals than the number of channels is less than a chosen value.

The number of simultaneously present signals is assumed to be Poisson distributed:

$$Prob [k \; signals] \; = \; e^{-r} \frac{r^k}{k!}$$

with rate $r = N\tau/T$

When a signal arrives while there are no others present, there is no possibility of a processor not being available. Therefore, the probabilities must be conditioned on the fact that at least one signal is present. Then we have:

$$P = Prob \left[signal \; lost \; due \; to \; no \; channel \; available \right]$$

$$= 1 - Prob \left[processor \; available \; \middle| \; at \; least \; one \; signal \; in \; progress \right]$$

Where Prob $[x|y]$ denotes the probability of x conditioned on y. Let k be the number of simultaneous signals in progress and M be the number of data extraction channels (DECs). Then

$$P = 1-Prob \left[k \le M \; \middle| \; k \ge 1 \right]$$

$$1-P = Prob \left[1 \le k \le M \right] / Prob \left[k \ge 1 \right]$$

$$1-P = \frac{1}{1-e^{-r}} \sum_{k=1}^{M} \frac{r^k}{k!} e^{-r}$$

Figure 3.4-1 shows the solutions to this equation.

APPENDIX D
EFFECT OF PLATFORM OSCILLATOR STABILITY
ON INTERFEROMETER ERROR

We show herein that the frequency stability of the platform oscillator has only a negligibly small contribution to the error in the interferometer estimate of position.

The phase of the platform signal received in one interferometer antenna is the integral of its frequency from some arbitrary starting time t_0 up to the time of measurement, t. The frequency of the received signal is that of the oscillator at r/c seconds earlier in time, where r is the range to the platform and c is the speed of propagation. Letting $f_p(t)$ be the platform oscillator frequency, the received phase $\phi_1(t)$ is thus given by

$$\phi_1(t) = 2\pi \int_{t_0}^{t} f_p(\tau - r/c) d\tau$$

The phase of the signal received at a second antenna, at range r + Δr, is the same as that at the first antenna, except delayed by Δr/c:

$$\phi_2(t) = \phi_1(t - \Delta r/c) = 2\pi \int_{t_0}^{t - \Delta r/c} f_p(\tau - r/c) d\tau$$

The measured phase difference is therefore

$$\Delta\phi(t) = \phi_1(t) - \phi_2(t) = 2\pi \left[\int_{t_0}^{t} f_p(\tau - r/c)d\tau - \int_{t_0}^{t - \Delta r/c} f_p(\tau - r/c)d\tau \right]$$

$$= 2\pi \int_{t - \Delta r/c}^{t} f_p(\tau - r/c)d\tau$$

For a constant frequency f_p, this gives the expected result

$$\Delta\phi(t) = 2\pi(\Delta r/c) f_p = 2\pi \Delta r/\lambda$$

If the platform oscillator is f_0 at time $t = 0$, and has a constant frequency drift of rate R Hz/sec:

$$f_p(t) = f_0 + Rt$$

then the measured phase difference is

$$\Delta\phi(t) = 2\pi \int_{t - \Delta r/c}^{t} f_0 + R(\tau - r/c)d\tau$$

$$= 2\pi \left[f_0 \frac{\Delta r}{c} + \frac{R}{2}\left(\frac{\Delta r}{c}\right)^2 + R\frac{\Delta r}{c}(t - r/c) \right]$$

$$= 2\pi \frac{\Delta r}{c} f_p(t - r/c) + \pi R \left(\frac{\Delta r}{c}\right)^2$$

The oscillator drift causes an error in the measured phase difference directly proportional to the drift rate and the square of the range difference. To see the magnitude of the error, we assume a very large range difference and find what drift rate is required to cause a phase difference error of 0.01°.

$$\Delta r = 100 \text{ m}$$

$$\Delta r / c = 3.33 \times 10^{-7} \text{ s}$$

$$\frac{\pi}{180}(0.01°) = \pi R (3.3 \times 10^{-7})$$

$$R = 510 \text{ MHz/s} \quad !$$

We may conclude that no reasonably-sized drift rate can cause a noticeable error.

APPENDIX E
ERROR DISTRIBUTION

The figures presented in Section 2.2 relate the quantities "Location Error" and "Velocity Error" to the various parameters under evaluation. This Appendix defines what is meant by these terms, and provides the mathematical basis and assumptions for its determination.

One of the major results of utilizing the method of least squares to estimate position and velocity from a sequence of measurements is the covariance matrix of errors in these estimated parameters for unit variance of some measured quantity, e.g., phase difference. As a result of the coordinates employed for the analysis, the covariance matrix includes the variance of two components of position and the variance of two components of velocity in the east and north directions. However, if the distribution of the measurement errors can be assumed to be gaussian, then the distribution of location/velocity errors is also gaussian. This allows the following:

With the gaussian assumption, the two dimensional probability density of east and north position errors (for example) is

$$f(E, N) = \frac{e^{-G/2}}{2\pi \, \sigma_E \, \sigma_N \sqrt{1-r^2}}$$

where

$$G = \frac{1}{1-r^2}\left[\left(\frac{E}{\sigma_E}\right)^2 - \frac{2r\,EN}{\sigma_E\,\sigma_N} + \left(\frac{N}{\sigma_N}\right)^2\right]$$

E-1

E,N = the east and north errors respectively

σ_E^2, σ_N^2 = the east and north error variances, respectively

γ = the correlation coefficient of E and N (defined by the covariance of the E and N errors divided by the product of their standard deviations)

However, by defining a position error radius, P, and a direction ω by

$$E = P\cos\omega$$
$$N = P\sin\omega$$

G may be rewritten as

$$P^2 = G(1-r^2) \bigg/ \left[\left(\frac{\cos\omega}{\sigma_E}\right)^2 - \frac{r\sin 2\omega}{\sigma_E \sigma_N} + \left(\frac{\sin\omega}{\sigma_N}\right)^2 \right]$$

This expression then defines an equal probability error ellipse as a function of direction measured positively north of east. Also, by integration of $f(E,N)$ over the area contained by this equal probability ellipse, ellipses can be defined within which the location error is less than some predetermined value. For example, with G set equal to 1.3853, the resulting error ellipse is the 50 percent probability ellipse. Other values of G give the following probability ellipses:

P	G
.25	.5753
.50	1.3853
.75	2.7722
.90	4.6053
.95	5.9921
.99	9.2112

A complete description of either position or velocity errors, therefore, requires not only the specification of some level of probability but also requires a two-dimensional description of the error ellipse. To avoid this in presenting the errors in the body of the report, the following definition of "Location Error" (or "Velocity Error") has been adopted.

- the 50 percent probability ellipse is assumed throughout

- the error rate presented corresponds to the direction giving rise to the maximum value of P.

In this regard, the maximum value of P can be shown to occur when the angle ω satisfies the following relationship

$$\tan 2\omega = \left(\frac{2r}{\sigma_E \sigma_N} \right) \bigg/ \left(\frac{1}{\sigma_N^2} - \frac{1}{\sigma_E^2} \right)$$

LOCATION/VELOCITY ALGORITHM

In Figure 2.2-1, the concept of the interferometer is shown in terms of an angular measurement indicating platform direction relative to the baseline. However, in developing the algorithm for utilizing range difference measurements, the angle itself need not be determined explicitly. Instead, the geometry between a platform and the interferometer is completely described in terms of three mutually orthogonal cartesian coordinates centered at the earth's center and fixed to the earth itself.

The range vectors describing LBI- platform geometry is indicated in Figure F-1. These vectors are defined as follows

$\vec{R}_p$ - location vector of platform

$\vec{R}_s$ - location vector of c.g. of satellite

$\vec{R}_{sp}$ - range vector between platform and satellite

$\vec{R}_i$ - range vector between platform and i^{th} receiver of the LBI

$\vec{R}_j$ - range vector between platform and j^{th} receiver of the LBI

$\vec{r}_i$ - location vector of ith receiver relative to c.g. of satellite

$\vec{r}_j$ - location vector of jth receiver relative to the c.g. of the satellite

With these definitions, the quantity measured by two receivers on a baseline is the difference in magnitudes of $\vec{R}_i$ and $\vec{R}_j$. In terms of cartesian components, this measurement may be written as

$$R_{ij} = |\vec{R}_i| - |\vec{R}_j| = \sqrt{R_{i_x}^2 + R_{i_y}^2 + R_{i_z}^2} - \sqrt{R_{j_x}^2 + R_{j_y}^2 + R_{j_z}^2}$$

where, for example

$$R_{i_x} = R_{s_x} - R_{p_x} - r_{i_x}$$

By taking differentials of this expression, a small change in R_{ij} can be related to corresponding changes in position coordinates of the platform.
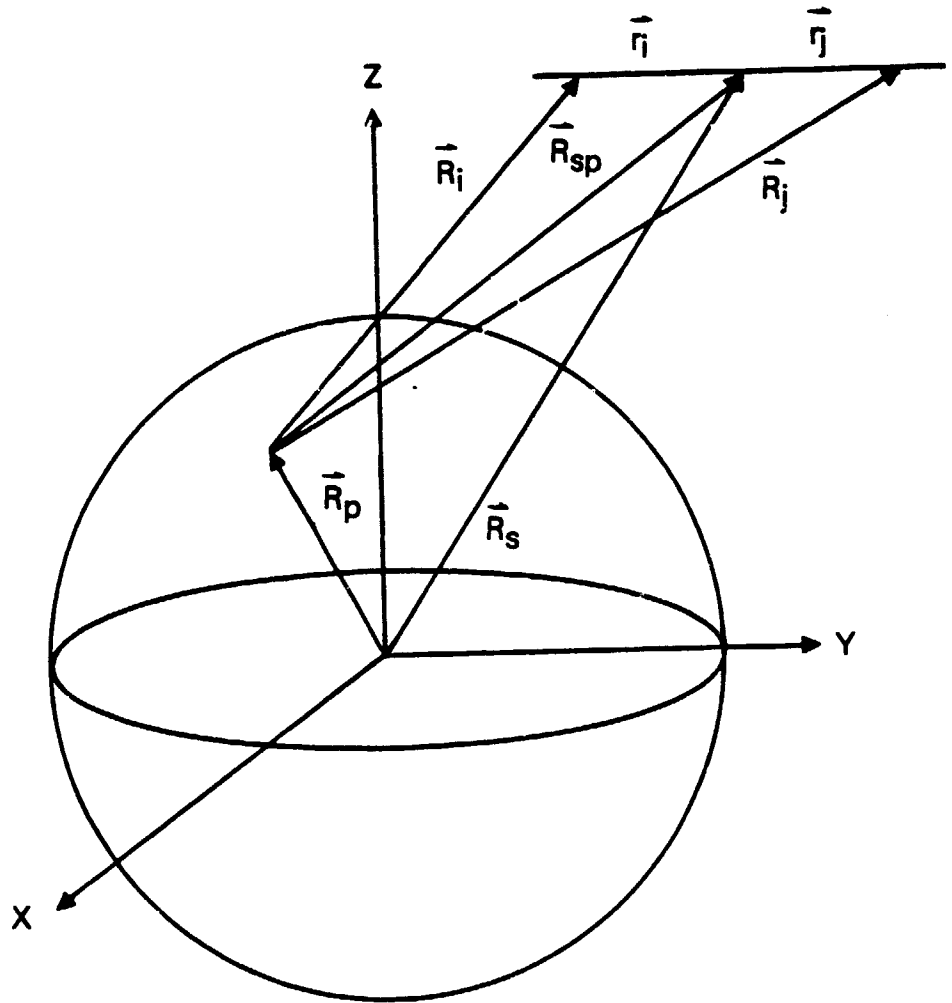
FIGURE F-1.   INTERFEROMETER - PLATFORM GEOMETRY

$$\delta R_{ij} = \left(\frac{R_{jx}}{R_j} - \frac{R_{ix}}{R_i} \right) \delta R_{P_x} + \left(\frac{R_{jy}}{R_j} - \frac{R_{iy}}{R_i} \right) \delta R_{P_y} + \left(\frac{R_{jz}}{R_j} - \frac{R_{iz}}{R_i} \right) \delta R_{P_z}$$

However, if the assumption is made that the altitude of the platform above the earth's surface is known -- i.e. $|\vec{R_p}|$ then this constraint reduces δR_{ij} to

$$\delta R_{ij} = \left[\left(\frac{R_{ix}}{R_i} - \frac{R_{jx}}{R_j} \right) \frac{R_{P_y}}{R_{P_x}} - \left(\frac{R_{iy}}{R_i} - \frac{R_{jy}}{R_j} \right) \right] \delta R_{P_y} + \left[\left(\frac{R_{ix}}{R_i} - \frac{R_{jx}}{R_j} \right) \frac{R_{P_z}}{R_{P_x}} - \left(\frac{R_{iz}}{R_i} - \frac{R_{jz}}{R_j} \right) \right] \delta R_{P_z}$$

This relationship is the basis for estimating platform position coordinates on a given altitude sphere from range difference measurements. The process is one of assuming a position for the platform (R_{P_y} and R_{P_z}) and using this relationship to correct position estimates until measured range differences correspond to computed range differences.

A similar relationship may also be derived for estimating platform position when the measured quantity is assumed to be the time rate of change of range difference. In this case,

$$\dot{R}_{ij} = |\dot{\vec{R_i}}| - |\dot{\vec{R_j}}|$$

from which

$$\delta \dot{R}_{ij} = \left[\left(\frac{\dot{R}_{jx}}{R_j} - \frac{\dot{R}_{ix}}{R_i} \right) + V_{R_i} \frac{R_{ix}}{R_i^2} - V_{R_j} \frac{R_{jx}}{R_j^2} \right] \delta R_{P_x} + \left[\quad \right] \delta R_{P_y} + \left[\quad \right] \delta R_{P_z}$$

where V_{R_i} is the range rate between the platform and the ith receiver.

By imposing the altitude sphere constraint, this relationship again reduces to $\delta \dot{R}_{ij}$ as a function of two position coordinates of the platform.

By similar differential analyses, δR_{ij} and $\delta \dot{R}_{ij}$ may be related to platform velocity components. In this case, the assumption is made that the platform's velocity is horizontal which leaves two components of velocity to be estimated from measurements.

APPENDIX G

ALDCS SYSTEM REQUIREMENTS DEFINITION

1.0 OVERALL SYSTEM DESCRIPTION

The overall ALDCS system concept is illustrated by Figure 1.

Surface data acquisition platforms located within the NOSS field of view will transmit to the NOSS satellite for several short time periods during each overpass. The transmissions will be received aboard the spacecraft by two antennas located approximately three meters apart with their line of separation orthogonal to the satellite direction of motion.

A combination of Doppler frequency measurement and interferometer phase difference measurement instruments are located on the spacecraft. The instruments measure the frequency of each received signal burst and the difference in phase sensed at the two antennas.

Sensor data contained in the transmissions are recovered and formatted along with the frequency and phase measurements and are re-transmitted through the NOSS communications subsystem and the Tracking and Data Relay Satellite (TDRS) to the NOSS Primary Processing Facility (PPF). The data will be stripped in the PPF and forwarded to the System Assessment and Research Facility (SARF).

The locations of the surface platforms are determined from the ALDCS data after recovery, conditioning and quality screening at the SARF. The
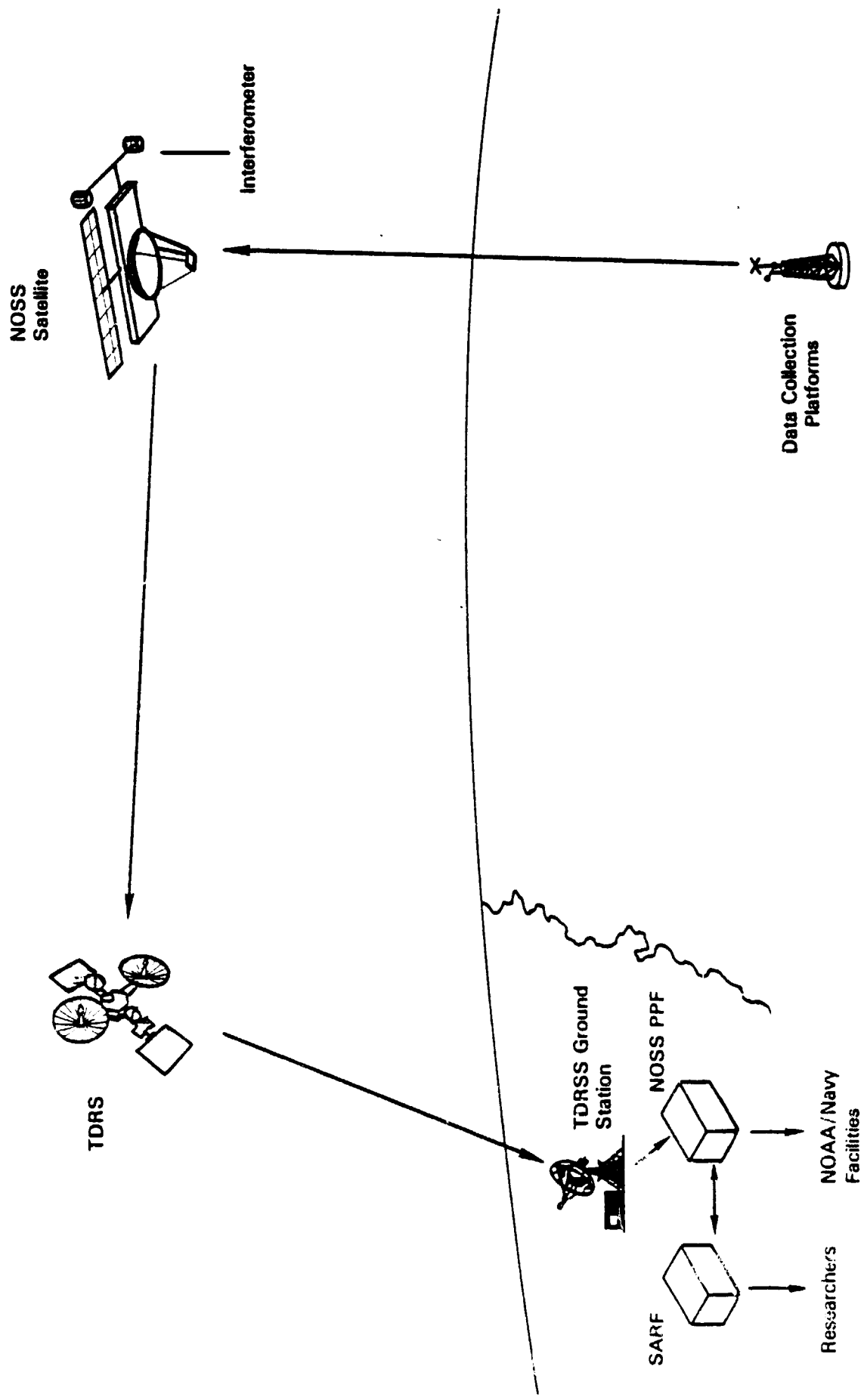
FIGURE 1. NOSS ADVANCED LOCATION/DATA COLLECTION SYSTEM

platform data and platform positions are then placed in on-line storage for use in remote sensor system assessment functions within the SARF and are simultaneously delivered to researchers and returned to the PPF for delivery to the NOAA and Navy user facilities.

The in situ surface data and platform locations will be made available for use concurrently with remote sensor data by the process described above.

Surface platform transmissions are not time synchronized with respect to each other which can cause loss of some transmissions due to mutual interference. This potential loss is overcome by using redundant transmissions. This transmission technique was successfully used on several previous data collection systems, including the currently operating TIROS/ARGOS system, and reduces transmitter costs. Table 1 lists expected ALDCS performance.

2.0   SURFACE PLATFORM SEGMENT

The system is designed to accommodate a variety of data collection platforms, including simple low-cost drifting buoys and complex fully-instrumented platforms. These platforms were characterized into two classes, according to the number of data bits each transmits to the space segment during each transmission burst.

Low-Cost Drifting Buoy

The Low-Cost Drifters are intended to be non-recoverable and will be designed for absolute minimum cost. They will carry no instrumentation (though simple instruments could be added) and will provide location only. Their function is to aid in mapping ocean currents and are expected to be deployed in large numbers. The platforms will consist of a simple buoy hull with integral antenna, a crystal oscillator, modulator, power amplifier and minimum timing and control logic. The timing and control logic activates the oscillator and power amplifier at regular intervals and impresses a digital identification code on the transmitted frequency via the modulator. A simple

TABLE 1

ALDCS SYSTEM PERFORMANCE SUMMARY

Position Location Error:	1) Stationary Platform: better than 1 km
	2) 20 Knot Platform: 2 to 5 km
Data Message Error Probability:	0.01%
Data Message Capacity:	40 to 1200 bits (5 to 150 measurements)
Number of Platforms in Field of View· (Nominal Mix):	1) Low-cost (no data): 300
	2) Minimum Message Length: 250
	3) Maximum Message Length: 50
Transmitter Frequency:	TBD (near 400 MHz)
System Bandwidth:	50 kilohertz
Transmitter Power:	1 watt
Max. Allowable Frequency Drift:	± 10 kilohertz in ten minutes (linear), otherwise remain in system bandwidth.
Transmitter Duty Cycle:	One second transmission each 90 seconds (nominal).
Data Bit Rate:	128 bits per second
Transmitter Modulation:	Biphase Continuous Shift, Manchester signalling.
Antenna Patterns:	Hemispherical (nominal), both space and surface platform.

monopole or printed circuit antenna is used to omnidirectionally radiate the signal toward the NOSS.

Instrumented Buoys and Ship Platforms

These platform transmitters will differ from the low-cost drifters in that instrument interfaces and data formatting electronics are required. Integrated circuit analog-to-digital converter sensor interfaces and microprocessors will be used for data manipulation. Message lengths of zero, 40 bits, 80 bits, and 1200 bits may be used to transmit up to 2400 bits per satellite pass to accommodate the variety of buoy configurations expected.

Carrier Preamble (25 ms)	Bit Sync (8 bits)	Frame Sync (12 bits)	Platform ID (14 bits)	Platform Type (2 bits)	Error Code (2 bits)	Mode Code (2 bits)	Sensor Data (0,40,80,1200 bits)

	Transmission Times (sec)	Interval (sec)
Low-Cost Drifters	0.353	90
Instrumented Platforms	0.681-9.744	90-180

FIGURE 2.   MESSAGE FORMATS AND TIMING

Message Formats and Timing

Figure 2 shows the general message formats.

The initial carrier segment is used by the on-board system for signal recognition and acquisition and to begin frequency and phase measurements. Frequency and phase measurements continue during the fixed part of the message prior to the sensor data block. The bit-sync and frame-sync allow the data recovery circuits on the spacecraft to acquire, process and format platform identification and sensor data.

The type code identifies the type of platform and the mode code specifies the length of data message to expect to the spacecraft data extraction unit. An error control "word" is included which consists of a collection of parity bits that apply to the platform ID and mode code.

3.0   SPACE SEGMENT

Functional elements of the ALDCS space segment are shown in Figure 3. Included are two wide-angle antennas spatially separated by three meters, radiofrequency preconditioning and distribution circuits, and circuits for measuring transmitter frequency, relative phase of the signals arriving at the two antennas, and for recovery of the surface platform sensor data. Additional elements are included for timing, calibration and interfacing with the NOSS spacecraft.

Signals received simultaneously by the two antennas are down-converted in frequency, amplified and distributed to a bank of twelve data extraction units. One antenna's output is processed by a signal detection unit which detects signal presence and estimates frequency. When a transmission is detected, one data extraction unit is directed to lock onto two representations of the signal (one from each antenna), measure its frequency, detect the phase difference between the two input signal representations and extract surface platform instrument data.

Frequency and phase measurements are digitized and supplied along with sensor data and platform identification to the data formatter/buffer, which in turn supplies it to the NOSS data handling system for transmission to the ground processing facility via the Tracking and Data Relay Satellite (TDRS).

Calibration signals of accurately controlled frequency and phase are periodically injected into the system to detect biases in the phase measurement system. This bias reading is transmitted to the ground for use in data processing corrections. In addition, a number of high quality calibration platforms will be dispersed on the surface in accurately known locations to aid in detection of system biases and errors. Table 2 lists spacecraft bus requirements for the ALDCS space segment.
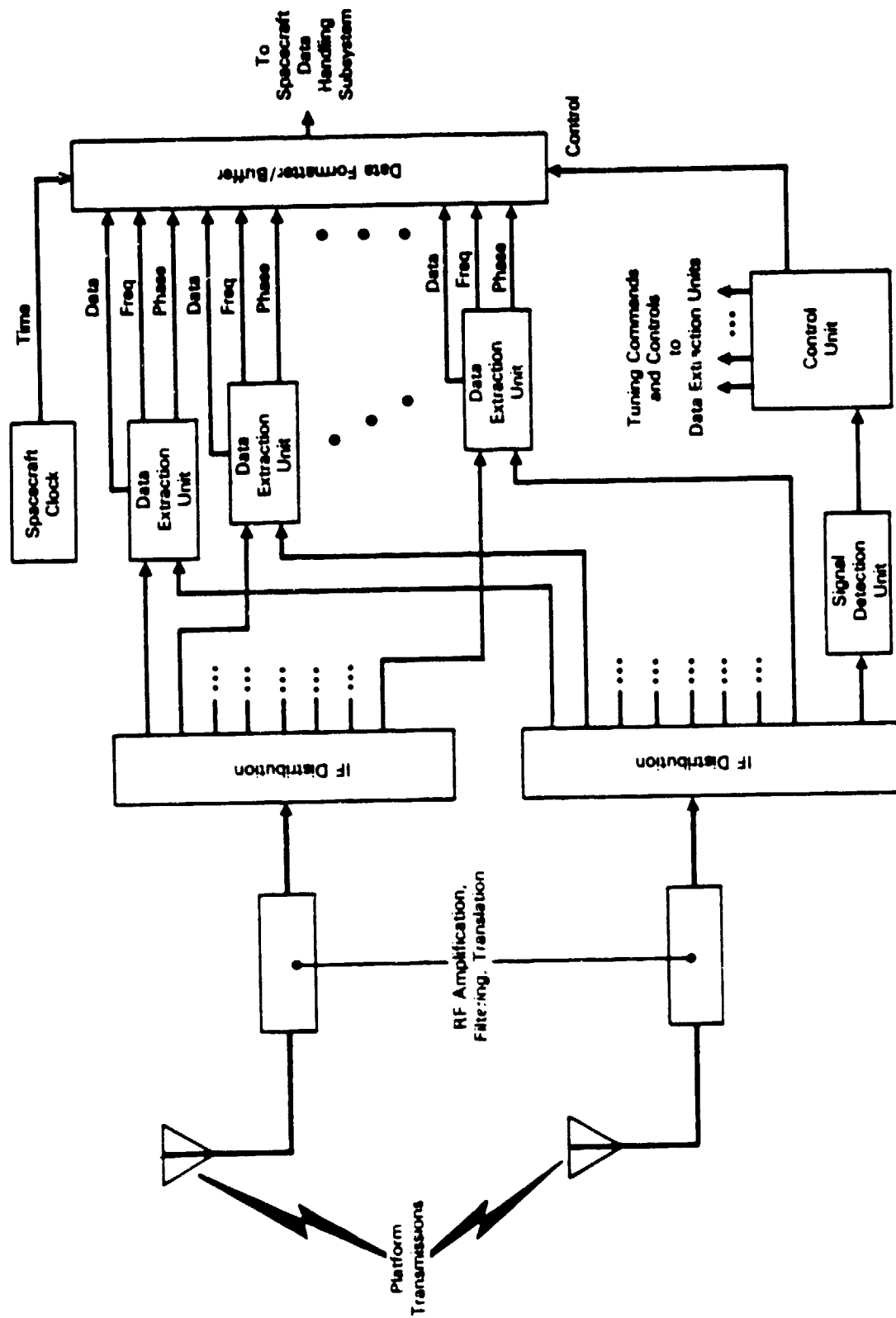
FIGURE 3. ALDCS SPACE SEGMENT BLOCK DIAGRAM

G-7

TABLE 2
SPACECRAFT BUS REQUIREMENTS

Orbit:	700 Kilometers, Circular, Sun-Synchronous (nominal)
Attitude:	Earth Pointing, ± 2° each Axis (non-critical)
Attitude Rate:	0.1 Degree per Second
Antenna Separation:	3-5 Meters (maximum without deploying booms)
Antenna Mechanical Excitation:	To Be Determined
Thermal:	Electronics Baseplate — +5 to +30°C
Commands:	12 Equivalent On-Off Commands
Telemetry:	12 Bytes for System Monitoring
Data Transfer Rate to S/C:	1230 bps (max.)
Antenna Volume (each):	1200 cc
Electronics Volume:	15,143 cc
Antenna Weight (each):	0.7 kg
Electronics Weight:	18.4 kg
Electronics Power:	44.4 watts

Antennas and Phase Detection

The two wide-angle antennas sweep out the same surface swath, nearly horizon to horizon, as the spacecraft moves over the earth. On succeeding orbits sufficient overlap is provided so that no surface area remains uncovered.

Figure 4 illustrates the difference in phase sensed at the two antennas from a single arriving signal. The signal angle of arrival, θ, may be determined from the electrical phase difference measurement, ϕ, the antenna separation distance, L, and the wavelength λ:

$$\theta = \arcsin \frac{\phi \lambda}{2 \pi L}$$

Knowledge of the angle of signal arrival in one plane and the spacecraft's height and position allows plotting a line of possible transmitter positions (LOP) on the surface. Several measurements may be made during the satellite overpass, yielding several LOP's whose crossing point represents an unambiguous estimate of the surface platform location.

Signal Detection Unit

The spectrum is constantly monitored by the detection unit for the presence of signals. The spectrum analysis is performed by means of a chirp-Z transformation mechanized through the use of charge-coupled transversal filters (Figure 5). The chirp-Z transform involves heterodyning the input signal with a signal that has linearly varying frequency and putting the resultant through transversal filters. The output of the transformer is a periodic "sweep" of the spectrum. When the presence of a signal is detected, its frequency is estimated to an accuracy of approximately 250 Hz. This information is used by the control unit to command a data extraction unit to acquire and process the signal.

Data Extraction Units

Figure 6 is a block diagram of the data extraction unit. Upon signal detection, the Voltage Controlled Oscillator (VCO) of an available data
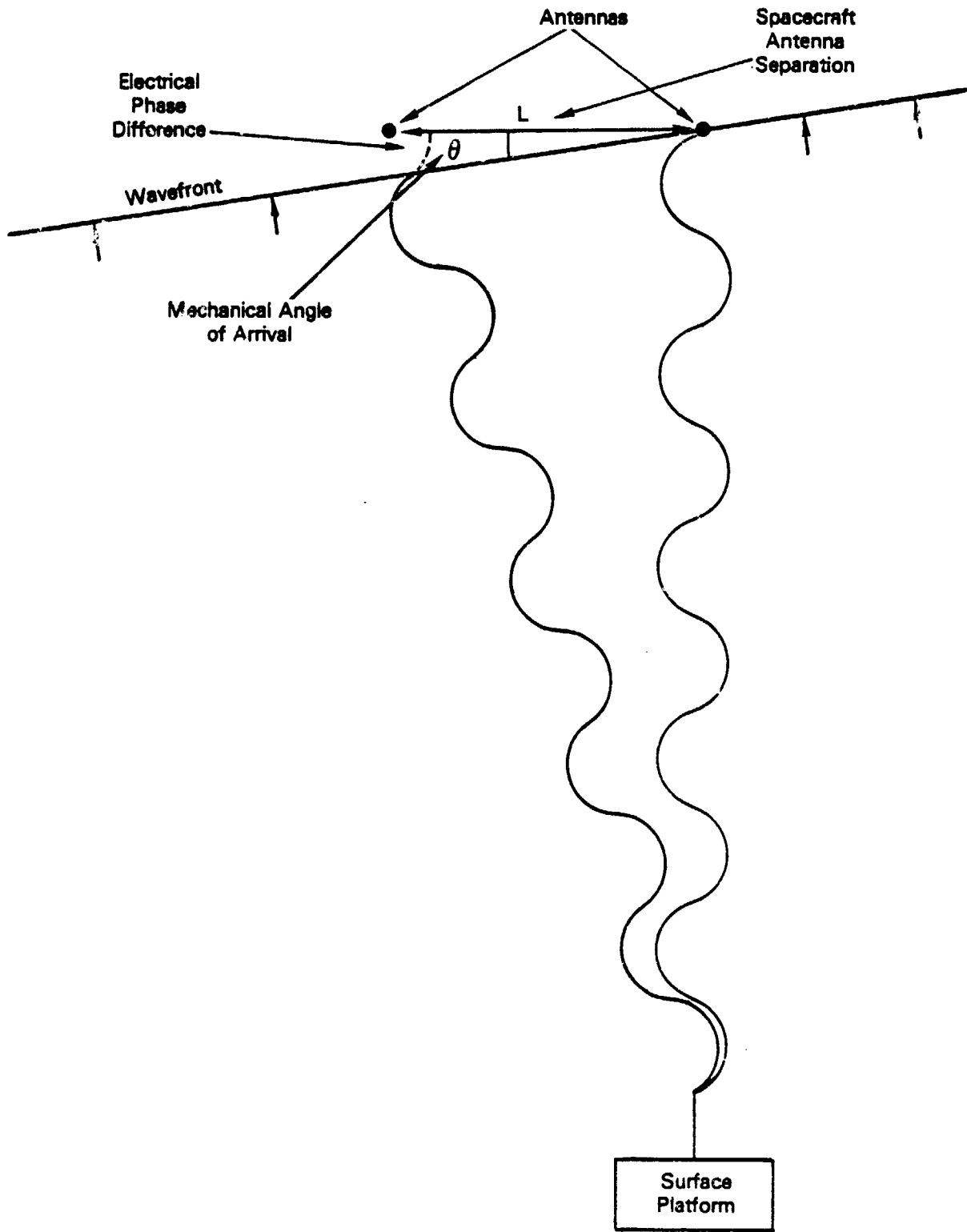
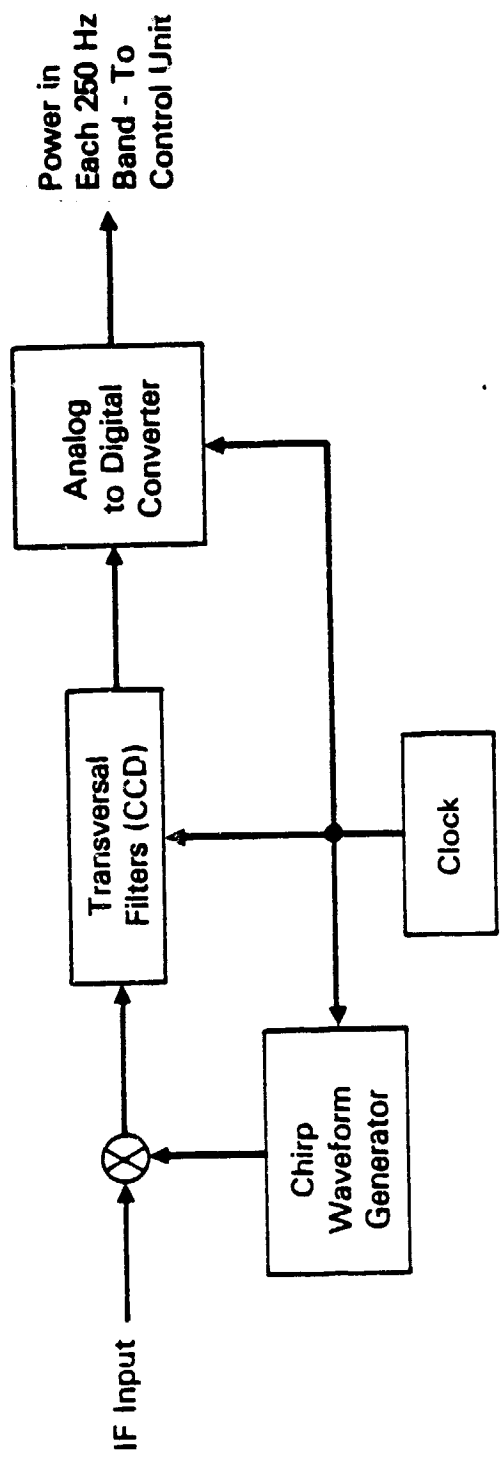FIGURE 4.   INTERFEROMETER LOCATION PRINCIPLE
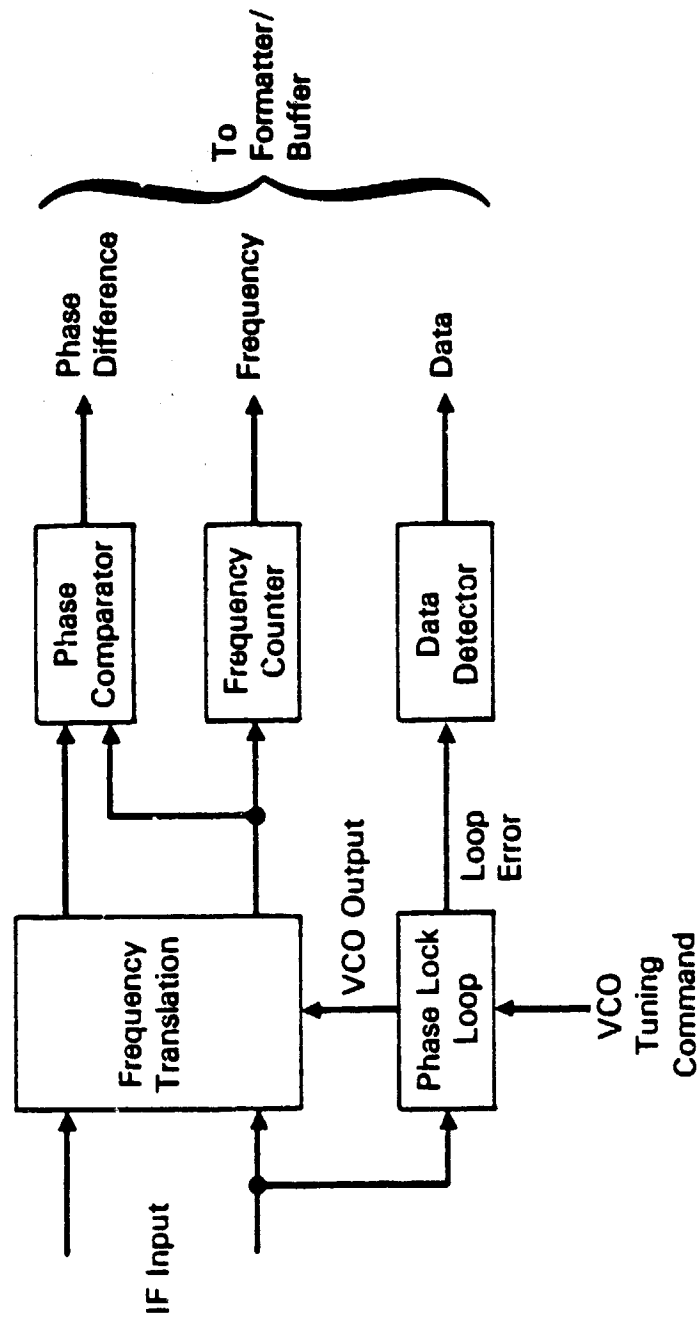
FIGURE 5. SIGNAL DETECTION UNIT BLOCK DIAGRAM

FIGURE 6. DATA EXTRACTION UNIT BLOCK DIAGRAM

extraction unit is tuned near the signal's frequency and the unit acquires the signal. When sufficient signal power is detected in the phase locked loop, the bandwidth is narrowed and phase lock is achieved. The loop error voltage (the input to the loop filter) thereafter is a filtered replica of the carrier phase modulation. This signal is supplied to the data demodulator and bit synchronizer for final data extraction.

The IF inputs from both antennas are down-converted by a shifted version of the VCO output. The resulting constant frequency signals are applied to a linear phase detector which measures the phase difference. The measurement is integrated over many cycles to reduce noise induced error.

The frequency of the VCO, when locked on the incoming carrier, varies in frequency according to the carrier's Doppler shift. The VCO signal is heterodyned down by a fixed frequency signal to increase the fractional frequency shift, and the frequency of the resultant signal is determined. The frequency measurement and phase difference measurement are supplied to the data multiplexer which combines them with platform data. This combined message is transferred to the NOSS data handling subsystem.

Control Unit

A microprocessor-based control unit directs the operation of the space segment. It performs the following functions:

- Monitors the status and controls the assignment of data extraction units.

- Decodes the mode word in received message, detects interference in the signal detection unit and releases data extraction units at message conclusion or when reception is not possible.

- Controls the transfer of phase and frequency measurements and platform data from the data extraction units to the multiplexer.

• Periodically performs self-check and calibration procedures.

4.0 GROUND PROCESSING SEGMENT

The ground processing segment is part of the System Assessment and Research Facility (SARF). It performs all handling, storage and retrieval of recovered ALDCS data and computes platform locations from the Doppler and phase measurements. It utilizes approximately the equivalent of 30% of the capacity of a PDP VAX 11/780 class CPU and a dedicated medium-sized disk storage facility.

Figure 7 shows the functions of the ground processing segment. The ALDCS data is recovered from the NOSS spacecraft return link data stream at the PPF and transmitted to the SARF where it is demultiplexed into two separate streams. One contains platform identification, data, and spacecraft equipment status, and is routed directly to on-line storage facilities. The other data stream contains platform identification, signal frequency, phase measurements, and interferometer calibration data. Data from multiple transmissions of the same platform are sorted and accumulated. Calibration data is used to determine correction factors, which are applied to the measured phase differences.

After the available Doppler and phase measurements for an overpass of a platform have been accumulated and corrected, they are used in one of three location algorithms. The first algorithm is applied to stationary reference platforms with known locations, such as the laser ranging stations. The location computed for these reference platforms is used to determine correction factors for the orbit, spacecraft attitude, and interferometer antenna phase center separation. These corrections are used by the other location and velocity algorithms. The second computes position only, when the platform is essentially stationary. The third algorithm computes position of platforms that are known to be moving at substantial rates.

Measures of the quality of the location estimates, such as error variances, are computed and appended to the data. The platform sensor data, which was stripped out initially, is then re-combined with the location and
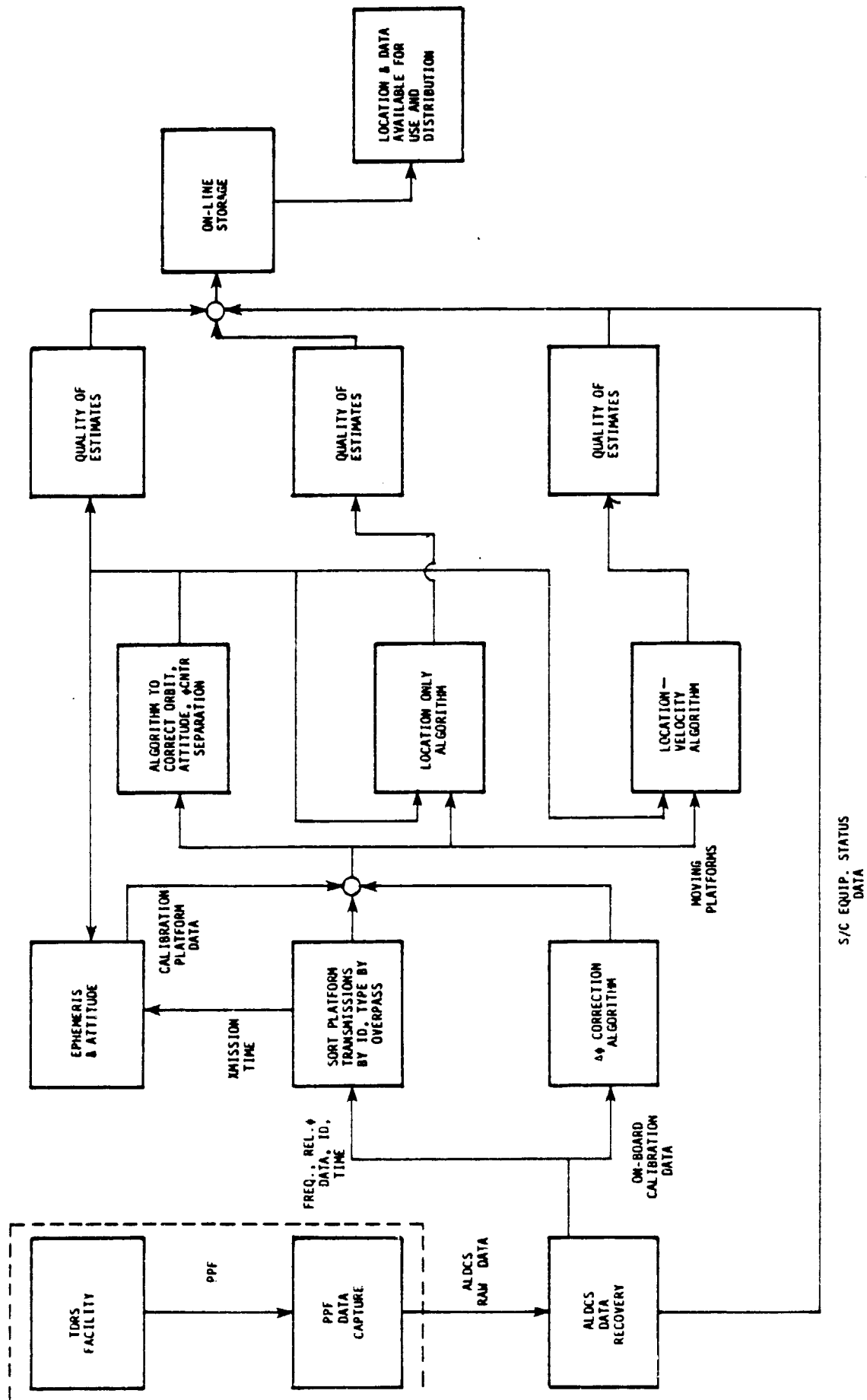
FIGURE 7. GROUND PROCESSING SEGMENT FUNCTIONAL BLOCK DIAGRAM

velocity estimates and with the quality measures and put in on-line storage. Here it is accessed for dissemination directly to users and NOSS remote sensor system performance assessment.

5.0   ESTIMATED SYSTEM PERFORMANCE

Estimation of platform position and velocity during an overpass is derived from a series of two distinct measurements of each signal received from a platform. One of these measurements is the received frequency. The other is the relative RF phase received at two antennas separated by approximately three meters. The line between these two antennas is perpendicular to the orbit plane of the satellite.

The phase and frequency measurements could be used independently to locate surface platforms. However, it is advantageous to combine their complementary characteristics as indicated by Figure 8. Two conditions are presented: the upper condition corresponds to a platform significantly removed from the satellite's sub-track, and the lower condition a platform located near the satellite's sub-track. Assuming that several signals are received from the platforms, the frequency measurements enable Doppler lines-of-position (LOP) for the platform to be drawn on the earth's surface. The intersection of these LOP's is the estimated position of the platform. Similarly, the relative phase or interferometric measurements also generate two LOP's from which platform position can also be estimated.

The upper sketch of Figure 8 illustrates that, for a platform located some distance from the satellite subtrack, the lines of position cross at an angle approaching the orthogonal for both the Doppler and interferometer techniques. In this case, the accuracy of the derived position is good, even in the event of slight line placement errors. Both techniques, therefore, provide accurate positions for the off-track platforms.

The lower sketch shows that the lines of position become more nearly parallel near the satellite subtrack. The crossovers become ambiguous, yielding low accuracy position estimates for either techniques alone.

SATELLITE
SUB-TRACK

Platform Removed
from Sub-Track

—— Doppler LOP
— — Interferometer LOP
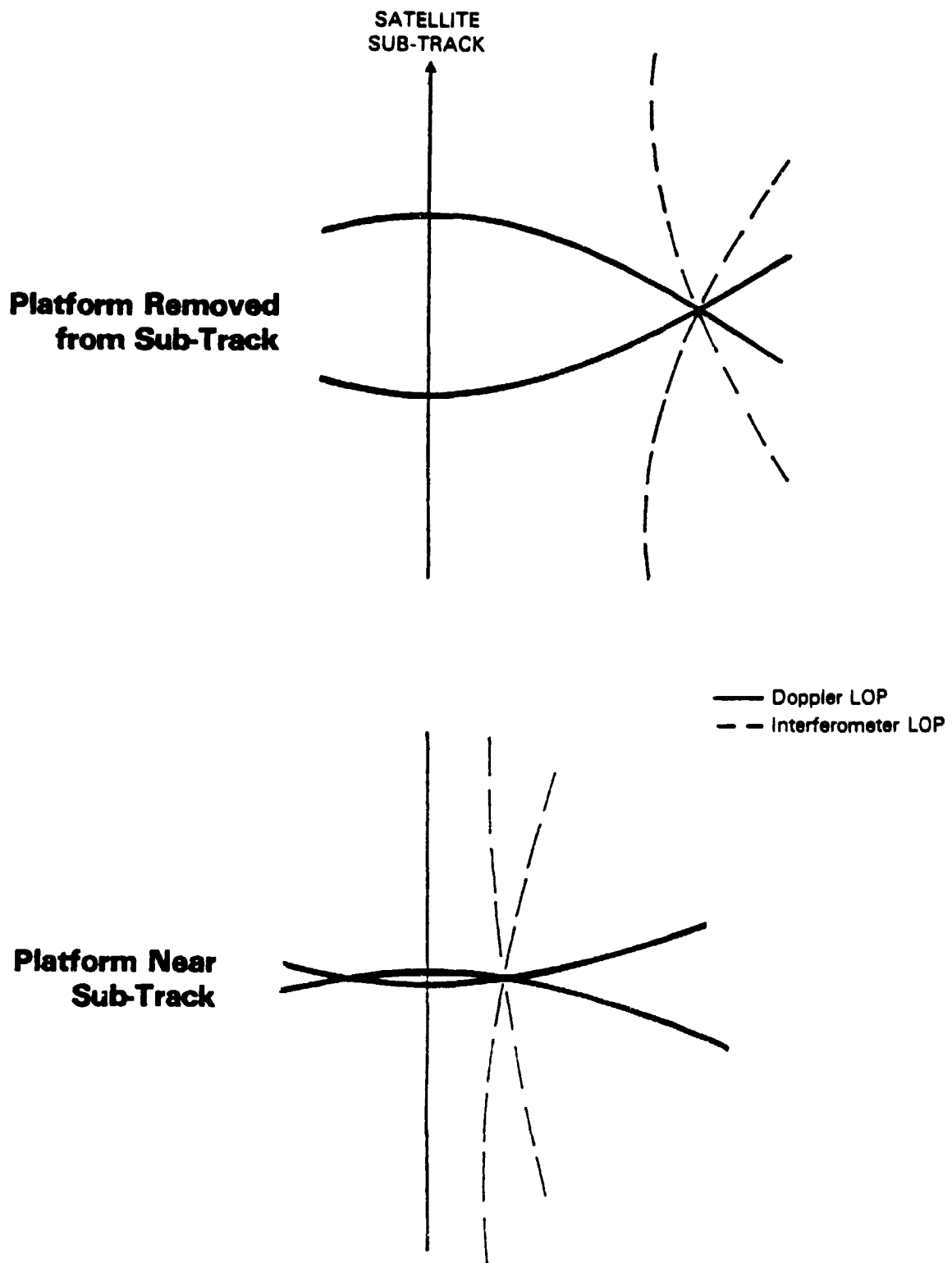
Platform Near
Sub-Track

FIGURE 8. DOPPLER VERSUS INTERFEROMETER PERFORMANCE

It is apparent from Figure 8 that the increased errors are in the along-track dimension for the interferometer and in the cross-track direction for the Doppler method. When used together, these techniques provide high quality positions near the subtrack and everywhere in the NOSS field of view.

Figure 9 compares expected ALDCS performance with the Doppler-only technique. The difference in performance near the subtrack previously described is clearly indicated.

It should be noted that the ALDCS performance allows large drifts in platform transmitter frequency while current Doppler systems limit transmitter drift to less than 10 Hz during the satellite overpass.
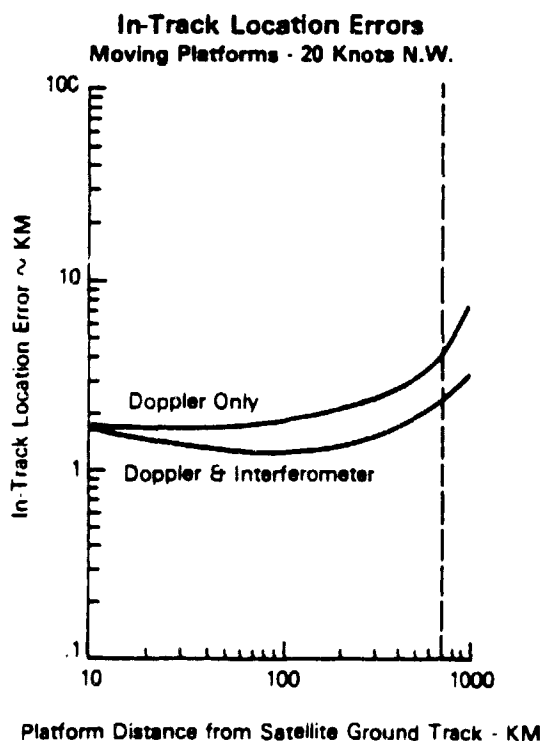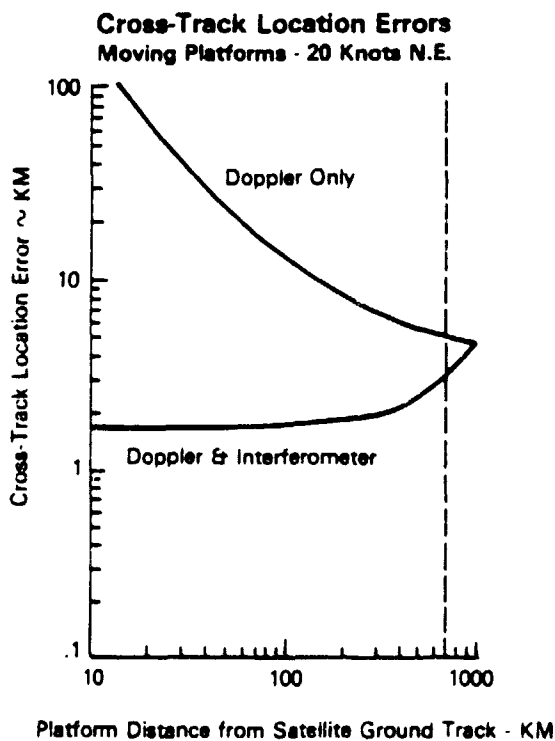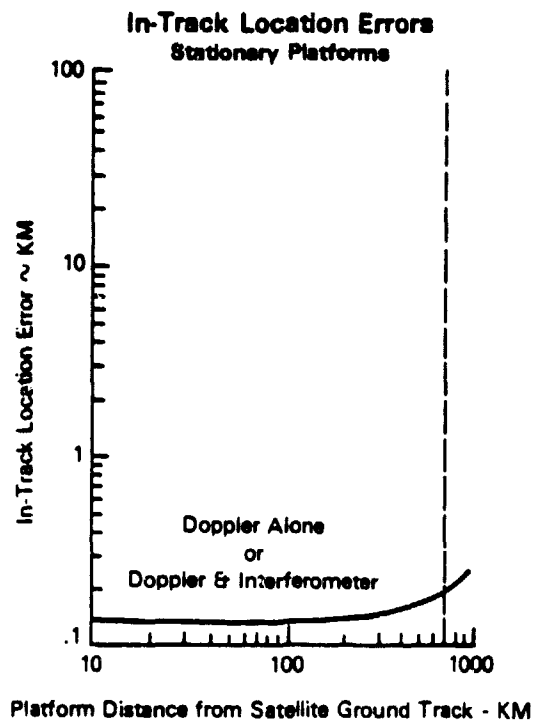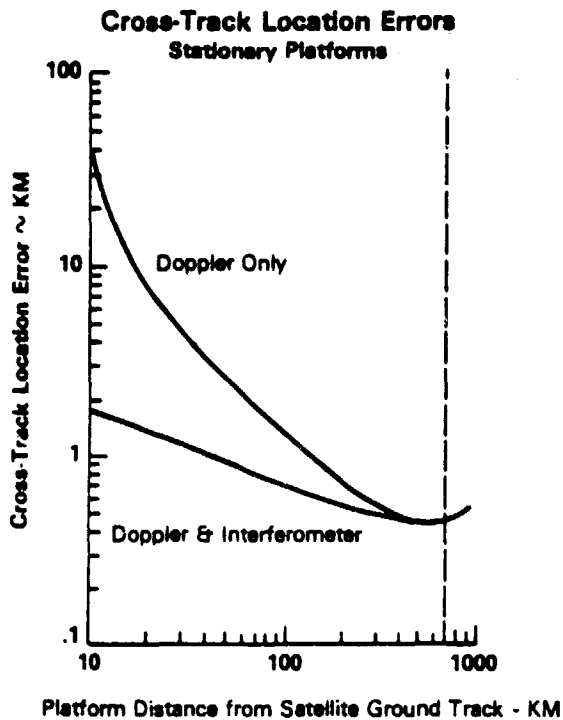
FIGURE 9.   EXPECTED ALDCS POSITION LOCATION PERFORMANCE VS. DOPPLER SYSTEM

REFERENCES

1. Reed, D.L., <u>On-Board Satellite Processing Study - Final Report</u>, ORI Technical Report 771, NASA GSFC Contract NAS5-21645, May 1973.

2. Papoulis, A., <u>Probability, Random Variables, and Stochastic Processes</u>, McGraw-Hill, New York, 1965, Chapters 12, 15.

3. Kilgus, C.C., "Shaped-Conical Radiation Pattern Performance of the Backfire Quadrafilar Helix," <u>IEEE Trans. on Ant. and Prop.</u>, May 1975, p 392.

4. Blanchard, A., <u>Phase-Locked Loops</u>, John Wiley and Sons, Inc., New York, 1976, Chapters 5, 7, 10, 12.

5. Bennett, W.R. and J.R. Davey, <u>Data Transmission</u>, McGraw-Hill Book Co., New York, 1965.

6. Viterbi, A.J., <u>Principles of Coherent Communication</u>, McGraw-Hill Book Co., New York, 1966, Chapter 7.

7. Spilker, J.J. Jr., <u>Digital Communications by Satellite</u>, Prentice-Hall, Inc. Englewood Cliffs, N.J., 1977, Chapter 12.